Modelling of Natural Attenuation

in Soil and Groundwater

Dissertation
zur Erlangung des Grades eines Doktors der Naturwissenschaften

der Geowissenschaftlichen Fakultät der
Eberhard -Karls- Universität Tübingen

vorgelegt von
Uli Maier
aus Göppingen

2004

Herausgeber: Institut für Geowissenschaften der Universität Tübingen
Sigwartstraße 10, D-72076 Tübingen

Schriftleitung der Reihe C: Zentrum für Angewandte Geowissenschaften (ZAG)
Lehrstuhl für Angewandte Geologie
Prof. Dr. Peter Grathwohl & Prof. Dr. Georg Teutsch

Redaktion: Dipl.-Geol. Björn Sack-Kühner

ISSN 0935-4948 (Print)
ISSN 1610-4706 (Internet)

All we see and all we seem

Is just a dream within a dream

E.A. Poe

Tag der mündlichen Prüfung: 9. Juli 2004

Dekan: Prof. Dr. Dr. hc. M. Satir

1. Berichterstatter: Prof. Dr. P. Grathwohl

2. Berichterstatter: Prof. Dr. U. Mayer, University of British Columbia, Vancouver (Canada)

TGA	Reihe C	Nr. 73	81 S., 47 Abb., 13 Tab.	Tübingen, Juli 2004

Summary

Contaminated land poses a serious problem with respect to soil quality and the risk of spreading of pollutants into other compartments of the environment such as groundwater. Under certain conditions, groundwater contamination remains restricted to a tolerable extent because of Natural Attenuation processes. In this study the size of these so called steady state plumes is evaluated by 2D and 1D modelling of homogeneous aquifers. For simplified conditions, if longitudinal mixing is negligible, scenarios can be modelled using a 1D domain in the direction vertical to flow. Sensitivity of the plume length on biodegradation kinetics, flow velocity, transverse vertical dispersivity α_t, the source and aquifer geometry and reaction stoichiometry was analysed. It was found, that for many readily biodegradable compounds, mixing due to transverse dispersion rather than reaction kinetics are the overall limiting factor for Natural Attenuation. If α_t and aquifer- and source geometry of a contaminant plume are known, the length of the steady state plume can be predicted.

Numerical simulations were performed in order to assess the diffusive spreading of volatile fuel constituents from a spill in the unsaturated zone and their biodegradation for the Værløse field experiment, Denmark. Sensitivity analyses illustrate that the net attenuation rates depend mainly on partitioning parameters such as Henry's Law constant of the fuel constituents, on the biological degradation rate constant, the depth of the source above the water table and to a lesser extent on soil water content and temperature. The measured field data of 14 NAPL compounds, oxygen and reaction products were reproduced by the model MIN3P. However, agreement was significantly enhanced if temporal variations of temperature and water content were implemented. By fitting measured soil gas concentrations in the unsaturated zone using the numerical models, estimates of aerobic biodegradation rate constants were obtained. The mass balance of the field site model indicates that most of the contaminant mass degasses to the atmosphere. Biodegradation was found to be important for compounds with low Henry's law constant (BTEX) and for heavier n-alkanes which showed very high degradation rate constants. The emission into groundwater could be determined after the processes in the unsaturated zone were quantified. Compared to measured pollutant concentrations in groundwater, which were detectable in a small area below the emplaced source, the model yielded qualitative agreement when vertical dispersivity in the capillary fringe was in the range of centimetres. A risk of groundwater contamination was found for compounds which show both, low Henry's law constant and low biodegradation rate constant. Quantification of biodegradation appears to be the most crucial task for risk assessment in the unsaturated zone.

Zusammenfassung

Die Verschmutzung von Böden und Grundwasser stellt in der heutigen Zeit ein gravierendes Problem dar. Unter bestimmten Bedingungen sind natürliche Rückhalteprozesse (Natural Attenuation) in der Lage, Verschmutzungen des Grundwassers auf ein akzeptables Maß zu beschränken. Das Ausmaß sogenannter stationärer Grundwasserfahnen biologisch abbaubarer Schadstoffe wurde durch die Modellierung homogener Aquifere in 2D und 1D ermittelt. Für vereinfachte Bedingungen, insbesondere wenn longitudinale Mischung keinen Einfluß auf die Fahnenlänge hat, können szenario-spezifische Modellierungen in 1D quer zur Grundwasserströmungsrichtung für die Abschätzung der Schadstofffahnenlänge eingesetzt werden. Die Sensitivität der Fahnenlänge auf biologische Abbaukinetik, Grundwasser Fließgeschwindigkeit, vertikale Querdispersion α_t und Aquifer- und Schadensherdgeometrie sowie die Reaktionsstöchiometrie wurde ermittelt. Als kritischer Faktor für die Ausbreitung aerob abbaubarer Schadstoffe im Grundwasser wurde die Querdispersivität α_t identifiziert, wohingegen die biologische Abbaukinetik in den meisten Fällen nicht den limitierenden Faktor darstellt. Bei bekannter Querdispersivität α_t, Schadensherdgeometrie und Ausgangskonzentration kann das Ausmaß stationärer Schadstoffahnen im Grundwasser vorhergesagt werden.

Für Abschätzung des von einem Herd organischer Schadstoffe in der ungesättigten Bodenzone ausgehenden Risikos für das Grundwasser wurden numerische Simulationen durchgeführt. Das Feldexperiment Værløse Airforce Base in Dänemark lieferte dazu hervorragend geeignete Meßdaten. Die Modellierung beinhaltete die diffusive Ausbreitung der Schadstoffe in der Bodenluft, nicht stationäre, gemessene Wetterdaten vom Standort und eine Abschätzung des biologischen Abbaus. Sensitivitätsanalysen zeigten, daß die Gesamtabbauraten in erster Linie von den Verteilungskoeffizienten der Schadstoffe wie der Henrykonstante, den biologischen Abbauratenkonstanten, der Tiefe des Schadenherdes und außerdem von Temperatur und Bodenwassergehalt abhängen. Die im Gelände gemessenen Konzentrationen der aus einem Gemisch von 14 Kerosinbestandteilen ausgasenden Schadstoffe konnten mit dem numerischen Modell MIN3P nachvollzogen werden. Die Übereinstimmung konnte deutlich verbessert werden, wenn zeitliche Schwankungen von Bodentemperatur und in geringerem Maße des Bodenwassergehalts berücksichtigt wurden. Durch die Anpassung mit MIN3P simulierter Konzentrationen an die gemessenen Daten konnten die biologischen Abbauratenkonstanten erster Ordnung abgeschätzt werden. Die Massenbilanz des Modells zeigt an, daß der Großteil der Schadstoffmasse in die Atmosphäre ausgast. Biologischer Abbau war von großer Bedeutung für Stoffe mit niedriger Henrykonstante wie die BTEX und für die langkettigen n-Alkane, denen sehr hohe Ratenkonstanten zugeordnet wurden. Der Transport ins Grundwasser konnte nach der Bestimmung der Massenbilanz in der ungesättigten Zone abgeschätzt werden. Gemessene Konzentrationen im flachen Grundwasser konnten für Querdispersivitäten α_t in der Größenordnung von Zentimetern qualitativ reproduziert werden. Das Risiko einer Grundwasserkontamination ergibt sich demgemäß für Stoffe, die sowohl eine niedrige Henry Konstante als auch niedrige biologische Abbauratenkonstante aufweisen. Im Gegensatz zur gesättigten Zone muß in der ungesättigten Zone geschlußfolgert werden, daß die Quantifizierung des biologischen Abbaus die wichtigste Aufgabe zur Abschätzung des Risikos einer Grundwasser-Beeinträchtigung darstellt.

Danksagung

Für die Vergabe des Themas und die umfangreiche fachliche Betreuung und Unterstützung danke ich Herrn Prof. Dr. P. Grathwohl und Herrn Prof. Dr. U. Mayer.

Für die Finanzierung der Arbeit sei dem DAAD (Deutscher Akademischer Austauschdienst) und dem EU Projekt GRACOS-EVK1-CT1999-00029 (Groundwater Risk Assessment at Contaminated Sites) großer Dank ausgesprochen.

Für die hervorragende Zusammenarbeit, viele Anregungen und den Austausch von Daten aus Labor und Geländeversuchen danke ich ganz besonders unseren internationalen GRACOS-Projektpartnern Patrick Höhener, Peter Kjeldsen, Mette Broholm, Mette Christophersen, Petros Gaganis, Vasilis Burganos, Hrissi Karapanagioti, Karin Kaufmann, Celine Duwig, Nathalie Dakhel, Gabriele Pasteris, David Werner, Trine Bjerne und Lone Holtegard.

Für fachliche Hilfe und Anregungen in mathematischen Fragen danke ich Herrn Dr. habil Rudi Liedl, in Fragen der Bodenkunde und Bodenphysik Herrn Dr. Dietrich Halm. Ganz besonders wichtig war die Kameradschaft und fachliche Anregung und Diskussion mit meinen Kollegen Bernd Susset und Åsa Olsson, denen ich an dieser Stelle ein großes Dankschön aussprechen möchte.

Nicht vergessen möchte ich Anett, Ingo und Detlef, mit denen ich die überwältigenden Eindrücke der Sonnenfinsternis in Afrika teilte und danke meinen Kollegen, Freunden und WG, Rainer, Iris, Andrea, Till, Guohui, Susanne, Pia, Katia, Séverine, Andrea, Angela, Annette, Eva, Martin, Thomas, Sanna, Sarah und ganz besonders Riccarda, die mich in manchmal nicht einfachen Zeiten unterstützt haben.

Contents

List of abbreviations

C_G: concentration in the gas/air phase [mg l^{-1}]
C_S: concentration in the solid/sorbed phase [mg l^{-1}]
C_W: concentration in the aqueous phase [mg l^{-1}]
D_{app}: apparent diffusion coefficient [m^2 s^{-1}]
D: apparent diffusion coefficient in a particular equation [m^2 s^{-1}]
D_{eff}: effective diffusion coefficient [m^2 s^{-1}]
D_p: pore diffusion coefficient [m^2 s^{-1}]
f_g: fraction of specific compounds present in the gaseous phase [-]
f_s: fraction of specific compounds present in the solid/sorbed phase [-]
f_w: fraction of specific compounds present in the aqueous phase [-]
H: Henry's law constant [-]
K: reaction equilibrium constant
k_{air}: kinetic reaction rate constant with respect to the soil air phase [s^{-1}]
k_{app}: apparent kinetic reaction rate constant [s^{-1}]
k_{aq}: kinetic reaction rate constant in the aqueous phase [s^{-1}]
k_{bulk}: kinetic reaction rate constant for the bulk soil [s^{-1}]
k: first order kinetic rate constant for a particular equation [s^{-1}]
κ: second order kinetic rate constant for a particular equation [s^{-1} mg^{-1} l]
K: zeroth order kinetic rate constant for a particular equation [mg l^{-1} s^{-}]
K_d: equilibrium sorption distribution coefficient solid-aqueous phase [l kg^{-1}] = [mg kg^{-1}/mg l^{-1}]
K_f: hydraulic conductivity [ms^{-1}]
n: total porosity [-]
n_g: gas/air filled porosity [-]
Q: source/sink-term due to biogeochemical reaction in the porous medium [mg l^{-1} bulk s^{-1}]
R: reaction rate of specific reaction, attributed to the aqueous phase [mg l^{-1} aqueous phase s^{-1}]
R_d: retardation factor for transport in a porous medium [-]
S_g: saturation of the gaseous phase [-]
S_w: saturation of the aqueous phase [-]
x: horizontal spatial coordinate in groundwater flow direction [m]
y: horizontal spatial coordinate perpendicular to groundwater flow direction [m]
z: vertical spatial coordinate [m]
ΔG: Gibbs free enthalpy of a reaction [kJ/mol]
ΔH: reaction enthalpy [kJ/mol]
ΔS: reaction entropy [J/mol/K]
α: capacity factor of porous medium [-]
α_t: transverse vertical dispersivity [m]
α_l: (or α_x) longitudinal dispersivity [m]
s: stoichiometric coefficient for a specific compound of a chemical reaction [-]
θ: volumetric soil water content [-]
ρ: soil bulk density [kg l^{-1}]
ρ_s: solid phase/grain density (Quartz: 2.65 g/cm^3)
A: mass balance contribution of total volatilisation to the atmosphere as % of degassed mass
B: mass balance contribution of total biodegradtion as % of degassed mass
G: mass balance contribution of total outflux in groundwater as % of degassed mass
N: mass balance contribution of mass remaining in NAPL as % of initial mass
BTEX: aromatic compounds (benzen, toluene, xylene, ethyl-benzene)
VOC: volatile organic compounds

1. Introduction

1.1 Problem

Contaminated land poses a serious problem with respect to soil quality and the risk of spreading of pollutants into other compartments of the environment. The major concern at most contaminated sites is the risk of groundwater pollution by organic and inorganic compounds. Since the remediation of all of the contaminated sites is economically not feasible, groundwater risk assessment procedures are needed for the ranking of sites, decision making on further use and remedial actions. Especially interesting because of its low monetary and engineering costs is the method of Monitored Natural Attenuation (Wiedemeier et al., 1999), which requires detailed knowledge about the site and contaminant situation and a long-term monitoring campaign. Tools to predict the long term processes at a site, such as numerical reactive transport models, are essential for risk assessment decisions.

1.2 Scope of this work

Theoretical concepts of environmental science relevant for this work will be discussed in § 2, and a short sketch of modelling strategies will be given. A brief introduction of the modelling tools applied is delineated in § 3. § 3 also shows the development of a simpler 1D model used in this study. Modelling of Natural Attenuation as predictive measure was elucidated in two example studies: a theoretically based scenario specific modelling approach to predict lengths of steady state groundwater plumes under aerobic conditions (the saturated zone, § 4). This approach was later used to predict applicability of Natural Attenuation for a contaminated field site. § 5 provides a modelling study for a well controlled field experiment about an artificial "spill" of kerosene in the unsaturated soil zone. Sensitivity analyses and reproduction of measured field data are included. A brief summary of the thesis is listed below (§ 1.2.1 and 1.2.2).

1.2.1 Saturated zone

In this study numerical simulations in homogeneous model domains were performed in order to determine the size of steady state plumes as a function of the biodegradation kinetics, flow velocity, transverse vertical dispersivity α_t, the source and aquifer geometry and reaction stoichiometry.

Main objective was to develop empirical relationships for the prediction of the length of stagnant plumes. The aim is to clearly identify the controlling factors for a range of representative contamination scenarios and to establish a simple relationship between the factors influencing Natural Attenuation. The base case scenario considered consists of an aquifer contaminated with an aerobically degradable compounds and the delivery of electron acceptors such as oxygen by transverse dispersion from the water table. A completely contaminated aquifer thickness (landfill or boundary source) is presumed. For

other scenarios such as partially contaminated aquifer thickness and pollution by groundwater recharge, qualitative relationships are developed.

1.2.2 Unsaturated zone

To my knowledge, the validation of numerical reactive transport models on a field experiment with a complex mixture of hydrocarbons in the vadose zone has not been conducted before. At the Værløse Airforce Base, Denmark, a well controlled field experiment on the diffusive spreading of volatile fuel constituents and their biodegradation in the unsaturated zone was performed. Experimental design and measurement strategies as well as NAPL phase evolution are described in publications of (Christophersen et al., 2003,Broholm et al., 2004). Numerical simulations were performed using the numerical model MIN3P (Mayer et al., 2002) in order to account for the relevant processes and governing factors for the field site. The objective was to validate the model MIN3P with the field data to allow future predictions for groundwater risk assessment at a variety of other sites.

The Værløse field experiment offered the opportunity to quantify transport processes across the capillary fringe at the field scale. The contribution of dispersive processes to mass transfer between the unsaturated and the saturated zone, as well as the magnitude of groundwater contamination could be investigated by numerical modelling based on the field data. Characterisation of processes as well as model accuracy concerning mass transfer across the capillary fringe, however, are still subject to uncertainty and require further research.

2 Basic Theory

2.1 Pollutants in the subsurface

Contaminated groundwater causes a serious risk for drinking water supplies. A huge number of locations with contaminated soil and groundwater exists in the industrialised countries. According to EU reports, some 750 000 potentially contaminated sites exist in Western Europe (CARACAS, 1998). For example, sites in the Netherlands alone will cause estimated costs for site remediation in excess of 13 billion €. Active remediation like pump and treat or excavation of all these sites will not be economically feasible, however, Natural Attenuation can help to mitigate the situation. Preconditions to apply naturally occurring attenuation processes as a remediation strategy are detailed knowledge about the site and attenuation processes and control by a long-term monitoring campaign (Wiedemeier et al., 1999). To support tools that have predictive capabilities, compilation of experience from already known sites combined with forward numerical modelling is useful. Adding both together, scenario specific modelling can provide a scheme for decision-makers to assess the risk for groundwater at contaminated sites (Prommer et al., 2000,Prommer et al., 2003).

At sites where petroleum products are handled or stored, contamination of the unsaturated soil zone is frequently found. The volatile organic contaminants (VOC) of the fuel are released from the spill by vaporisation and spread by gas migration in the unsaturated zone. The volatile contaminants cause contamination of the subsurface environment including the groundwater both in lateral and vertical directions. As a fuel phase migrates downward through the unsaturated zone following a spill, some of it will become trapped in the pore space at residual concentrations. Volatilisation of this residual fuel phase will result in the formation of a vapour phase contaminant plume in the unsaturated zone. The plume will spread by vapour diffusion and, potentially, by density-induced advection of the soil gas mixture. As it spreads, the vapour plume will also cause contamination of the pore water and soil as a result of phase distribution. Contamination of the underlying groundwater can ultimately occur by way of vapour migration downward to the capillary fringe, a rise of the groundwater table into the contaminated zone, or infiltration of groundwater recharge through contaminated areas. Conversely, partitioning from underlying ground water VOC plumes can contaminate soil gas (Grathwohl et al., 2003).

Investigations on the detection of unsaturated zone contamination and their implication on groundwater risk assessment have been performed for more than one decade (Marrin, 1988,Schlender, 1989). The detection of VOC vapour was complemented by survey of natural soil gas compounds like oxygen or reaction products such CO_2 or methane which provide integral information of Natural Attenuation of the VOC contamination (Maier, 1998). Based on soil gas surveys, numerical models have been used to quantify the rates of biodegradation and volatilisation at contaminated sites (Lahvis, 1996). Even the tracing of groundwater contamination by vadose zone concentration anomalies was attempted (Rivett, 1995). Ongoing from

delineation of unsaturated zone distribution of VOCs, prediction of groundwater risk assessment at contaminated sites is aimed for. As the water table is generally considered as the point of compliance for groundwater risk, transport of VOC's across the capillary fringe is of particular interest. Since these processes are highly site-specific, besides on site and laboratory testing methods, robust and reliable as well as efficient models for predictions are demanded.

2.1.1 Legal limits

For the contamination pathway from soil to groundwater, trigger values are defined in the German Federal Soil Protection Law (BBodSchV, 1999). If these are exceeded at the point of compliance, (i.e., the water table) of a suspected contaminated site, detailed investigations have to be conducted and decisions about remedial action have to be made. Such trigger values and supporting information are listed in tab. 1.1 for organic compounds.

Tab. 1.1 Trigger values for the assessment of the pathway soil - groundwater pursuant to § 8 paragraph 1 sentence 2 No. 1 (Federal Soil Protection Law - BBodSchV, 1999).

organic substances	trigger value [µg/l]
mineral oil hydrocarbons [1)]	200
BTEX [2)]	20
benzene	1
high-volatile halogenated hydrocarbons [3)]	10
DDT	0.1
aldrin	0.1
phenols	20
PCB, total [4)]	0.05
PAH, total [5)]	0.20
Naphthalene	2

1) n-alkanes (C10 C39), isoalkanes, cycloalkanes and aromatic hydrocarbons

2) high-volatile aromatic hydrocarbons (benzene, toluol, xylols, ethylbenzene, styrene, cumene)

3) high-volatile halogenated hydrocarbons (sum of the halogenated C1 and C2 hydrocarbons)

4) PCB, total: sum of the ploychlorinated biphenyls; as a rule, determination by way of the 6 congeners according to Ballschmiter pursuant to Used Oil Ordinance (DIN 51527) muliplied by a factor of 5; if applicable, for example in case of a known substance spectrum, simple formation of the sum of all relevant individual substances (DIN 38407- 3-2 or 3-3).

5) PAH, total: sum of the polycyclic aromatic hydrocarbons without napththalene and methylnaphthalene; as a rule, determination by way of the sum of 15 individual substances according to the list of the US Environmental Protection Agency (EPA) without naphthalene; if applicable, in consideration of other relevant PAH (e.g. quinolene).

2.2 Natural Attenuation

Investigation of a great number of sites has shown that contaminant plumes may, after initial spreading, reach a steady state (so called steady state plumes) as a result of attenuation - mainly biodegradation – processes (Wiedemeier et al., 1999) and finally shrink because of source depletion. Thereby, the extent of contaminant plumes depends on both, hydrogeological and hydrogeochemical site conditions as well as contaminant characteristics. Typical plume lengths for specific chemical compounds were evaluated by (Schiedek, 1997). Plumes of easily degradable compounds such as fuel hydrocarbons and aromatic compounds (benzene, toluene, ethyl-benzene and xylene: BTEX), e.g., are often found to be restricted to a reasonable distance from the contaminant source. Those are especially compounds that are readily degradable under aerobic conditions.

Biodegradation and volatilisation act as a combined mechanism for the mass removal of volatile and semivolatile organic compounds from the unsaturated zone. In the best case these processes can restrict the contamination to the vadose zone. Although the effectiveness

of this combined pathway has been well documented, little information is available on actual rates of aerobic and anaerobic biodegradation, volatilisation, and their variability among different compounds and different subsurface geologic settings.

Reactive transport in groundwater is described by the advection-dispersion-reaction partial differential equation (PDE) with respect to the aqueous concentration C of a specific compound in a saturated porous medium.

$$\frac{\partial C}{\partial t} = -v\nabla C + \nabla \cdot (D\nabla C) - sR \qquad \text{eq. 2.1}$$

where v denotes groundwater flow velocity, D the dispersion tensor and s the stoichiometric ratio for the compound. The reaction rate R, in general, is a non-linear term depending on concentrations of the compounds involved and can be described using different kinetic formulations (Prommer et al., 2003).

2.2.1 Biogeochemical reaction kinetics

Biodegradation as the other important attenuation process takes place in the aqueous phase of the soil, driven by microorganisms either free in the pore water or attached to surfaces. If detailed knowledge about microbial metabolism and population dynamics is not available, first order rate constants k can act as bulk measures for the degradation kinetics. A problem is given by convertibility of reaction rates obtained from measurements of vapour phase concentration to apply in the aqueous phase. Biodegradation rate constants measured in the pore air can be transformed to aqueous phase rates by using

$$\theta\, k_w/H = k_g \qquad \text{eq. 2.2}$$

with θ as the volumetric water content, k_w the rate constant in the aqueous phase, H Henry's law constant and k_g the rate constant with respect to the gaseous phase (Pasteris et al., 2002). Biodegradation also depends on temperature under field conditions. Often a maximum can be observed around 25°C. This effect, however, depends on a great number of soil, site and microbiological conditions and is thus hard to quantify.

If high soil water saturation restricts oxygen delivery and anaerobic conditions establish, other possible degradation scenarios can be considered: (1) degradation by atmospheric electron acceptors such as Nitrate and Sulphate, (2) reduction of iron oxide or manganese oxide containing minerals present in the soil and (3) methanogenesis. Generally, anaerobic biodegradation is much less efficient than aerobic (Schlesinger, 1997).

Bioenhancement of source phase depletion was previously reported from laboratory work (Yang, 2000,Seagren et al., 2002) and also theoretical modelling studies (Reitsma, 2001) and could be proven at the field scale for the Værløse field experiment (Broholm et al. 2003).

Aerobic degradation in the presence of oxygen is the most efficient way of attenuation for BTEX, gasoline hydrocarbons and also inorganic contaminants, such as ammonium, which can be biologically transformed. That way, the pollutants will be mineralised to anorganic compounds such as CO_2 and H_2O or nitrate in the case of ammonium. For mathematical formulation of biogeochemical reactions, different kinetic approaches can be used.

In zeroth order kinetics, the reaction rate does not depend on the compound concentration. This condition is often given for a rapidly growing microbial population without nutrient limitation (Meckenstock, 2001)

$$R = -K \qquad K: [\mathrm{M\ L^{-3}\ T^{-1}}] \qquad \text{eq. 2.3}$$

The rate constant K for only this case is attributed the same unit as the reaction rate R itself. In first order kinetics there is a linear relationship between concentration and reaction rate:

$R = -k\, C_A$ $\quad k$: [T^{-1}] eq 2.4

In the second order formulation (for two compounds) the reaction rate becomes dependent of two concentrations and therefore is non-linear:

$R = -\kappa\, C_A\, C_B$ $\quad \kappa$: [$M^{-1}\, L^3\, T^{-1}$] eq. 2.5

Monod kinetics provide a more sophisticated model for biotransformation of a compound *A* (electron donor) and an electron acceptor *B* (Cirpka, 1997)

$$R = -\mu_{\max} C_M \frac{C_A}{C_A + K_{1/2,A}} \frac{C_B}{C_B + K_{1/2,B}}$$

μ_{max}: [$M\, L^{-3}\, T^{-1}\, (M_M\, L^{-3})^{-1}$] eq. 2.6

where A is the concentration of contaminant *A,* B is the concentration of an electron acceptor, μ_{max} is the maximum utilisation rate of the reaction, C_M is the microbial population density (microbial concentration) and $K_{1/2}$ is the half utilisation rate of the reaction for each compound. Note that μ_{max} has the unit of concentration of contaminant per concentration of microbial mass M_M. If $K_{1/2}$ is high compared to A, the border case of a first order degradation is approximated with a linear dependency of contaminant concentration. If $K_{1/2}$ is very small compared to A, the reaction will shift to zeroth order kinetics, and the total rate becomes independent of concentration. Microbial population dynamic itself can also be described using a Monod-approach:

$$\frac{\partial C_M}{\partial t} = -\mu_{\max} C_M Y_M \frac{C_A}{C_A + K_{1/2,A}} \frac{C_B}{C_B + K_{1/2,B}} - dC_M$$

eq. 2.7

where Y_M is the microbial yield (microbial growth rate as a fraction of consumed substrate) and d is the microbial mortality rate (first order, [T^{-1}]). As the majority of bacteria thrives on surfaces and are only subject to very slow transport, microbial community can be assumed to be immobile in most cases (Griebler and Mösslacher, 2003).

2.2.2 Transport and mixing

A precondition for the occurrence of biogeochemical transformations is the simultaneous availability of the reaction partners (e.g. organic contaminant as substrate and oxygen as electron acceptor) at the same time and at the same place. In the absence of interphase mass transfer (e.g. dissolution of mineral phase electron acceptors such as Fe3+-bearing minerals or sorption), dispersion is the only process that transports external electron acceptors into contaminant plumes and enables biotransformation processes (Cirpka, 2002). Consequently, in the case of "fast" reaction kinetics, Natural Attenuation is restricted to thin mixing zones and the dispersivity can become the controlling factor for the length of steady state plumes (Grathwohl et al., 2000). Steady state conditions (i.e. stagnant plumes) establish only if the reaction rate matches the input flux of the contaminant in groundwater. Dispersive mixing in flowing groundwater, i.e. hydrodynamic dispersion, consists of two different processes: molecular diffusion and mechanical dispersion (Domenico and Schwartz, 1998). The combination of both is termed hydrodynamic dispersion. The transverse hydrodynamic dispersion coefficient D_T in a porous medium is commonly expressed as the sum of the pore diffusion coefficient D_p and a coefficient of mechanical mixing (Domenico and Schwartz, 1998)

$$D_T = D_p + \alpha_t v_a \qquad \text{eq. 2.8}$$

where α_t is the vertical transverse dispersivity and v_a the linear groundwater flow velocity.

Diffusion is caused by random molecular motion due to kinetic energy of the molecules and tends to even out any concentration gradients independently of directional flow. Its mathematical description usually is based on Fick's laws (Fick, 1855).

In the unsaturated zone, vapour phase diffusion in many cases represents the most efficient transport process because gaseous diffusion coefficients are about four orders of magnitude

greater than aqueous diffusion coefficients. If the surface layers of the soil are sufficiently permeable, volatilisation to the atmosphere can be a significant sink to soil contamination by VOC's.

In porous media, diffusion is decelerated due to the restricted area available for transport and prolonged pathways (tortuosity). Empirical relationships for the calculation of effective diffusion coefficients in a porous medium are described in (Grathwohl, 1998) and (Wang, 2003).

Mechanical dispersion, on the other hand, is caused by advective transport of dissolved compounds in flowfields with spatially different velocities (differential advection or longitudinal dispersion), or by the mass exchange between different flowlines occurring transverse to flow direction as well as changes in flow direction of streamlines (transverse dispersion). Differential advection in aquifers is mainly caused by variations in hydraulic conductivity and therefore increases with the groundwater travel distance (Cirpka, 1997). Nevertheless, Fickian approaches are commonly used to describe mechanical dispersion in longitudinal direction as well.

While diffusion inherently causes dilution (mixing) of solutes, mechanical dispersion leads to mixing of compounds as well as undiluted spreading of contaminants parallel to the flow direction. The amount of mixing or dilution of concentrations at the pore scale is called local dispersion. Differential advection due to spatially varying velocities keeps solute mass in the same streamtube but separates masses from before adjacent streamtubes (spreading). This effect will be observed in conservative tracer tests with depth averaged sampling and increases with the scale of investigation (macroscale-dispersion). However, if dispersion coefficients determined that way are used to predict reactive transport, the amount of mixing and therefore bioattenuation can be significantly overestimated (Cirpka et al., 1999). Only mass movement between streamtubes contributes to mixing. An effective dispersion coefficient can therefore be defined to account for mixing in the macroscale (Dagan, 1990). This coefficient will be somewhat higher than the one that represents local dispersion, because spreading (differential advection) creates greater surfaces accessible for mixing processes (Cirpka, 1997). For continuous sources as in several decades old contaminated sites quasi steady state or steady state conditions establish and reaction rates depend solely on α_t.

α_t is often linked to the grain size of the porous medium. Assuming complete mixing of solutes in pore canals due to molecular diffusion (De Josselin de Jong, 1958) reports the following relationship between α_t and the characteristic length d in a porous medium.

$$\alpha_t = \frac{3}{16} d \qquad \text{eq. 2.9}$$

d is related to the mean grain size. (Carvalho and Delgado, 2000) found that α_t depends on the flow velocity or the Peclet number, respectively.

$$\alpha_t = \frac{1}{12} d \quad \text{(for Pe} < 80\text{) and } D_t = 0.5 Pe^{0.57} \quad \text{(for } 80 < \text{Pe} < 1400\text{)} \qquad \text{eq. 2.10}$$

where d is the medium grain size and D_t is the coefficient of transverse mechanical dispersion, defining $Pe = v\ d/D_{aq}$ as the dimensionless Peclet number of the porous medium. For Pe > 80 D_t does not increase linearly with flow velocity.

The mass transfer of volatile compounds from the unsaturated zone to groundwater across the capillary fringe is governed by the two processes dispersion and diffusion. It has been subject to recent research activity to determine which process is dominant for mass transfer, either dispersion or diffusion depending on groundwater flow velocities soil and physico-chemical characteristics of the compounds (McCarthy, 1993,Nielsen and Perrochet, 2000,Klenk and Grathwohl, 2002).

Laboratory experiments on this issue (McCarthy, 1993,Klenk and Grathwohl, 2002) confirm that mass exchange between saturated and unsaturated zone is restricted due to low aqueous diffusion coefficients and weak vertical dispersion. Entrapped air in the quasi saturated zone of the capillary fringe can enhance mixing because they intoduce additional tortuosity to the water flowpaths and to some extent lead to higher diffusion coefficients (Klenk and Grathwohl, 2002). Water table fluctuations, on the other hand, can enhance mass transfer significantly (Werner, 2002).

2.2.3 Phase distribution

In multicomponent organic liquids the more volatile compounds evaporate first resulting in changing composition of the mixtures Raoult's law, § 2.3.3). To predict this ageing of the phase during the diffusion dominated volatilisation process physico-chemical properties of the compounds involved have to be considered. A compilation of carefully selected physico-chemical properties from the literature relevant for this work *(ρ, MW, p_0, H, K_{OW}, S_W)* is given in Tab. 5.1.

Besides physico-chemical properties of the contaminants, a number of soil as well as climatic conditions affect contaminant behaviour such as the geological characteristics of the soil (grain size distribution, permeability and organic matter content) or temperature, water saturation and groundwater recharge. An increase in soil water content decreases the available space for gas phase diffusion, elongates the path lengths for gas phase diffusion (tortuosity) and, especially for compounds with low Henry's law constants, enhances the fraction of the compound dissolved in pore water, all together resulting in decelerated gaseous phase transport.

The efficiency of biodegradation reactions depends on the distribution of a compound between the phases of the soil (gaseous, aqueous and solid, and, if present, NAPL). Microorganisms live in the aqueous phase, adhered to mineral surfaces or free in the pore water, and feed on dissolved chemical compounds. Sorbed compounds, e.g., are not accessible to microorganisms in most cases. Gaseous compounds, on the other hand, are subject to rapid transport due to gas phase diffusion and can only be accessed by microorganisms if they dissolve in pore water. NAPL phase compounds may dissolve in water or volatilise to the soil gas phase. If the NAPL phase itself is immobile (residual saturation), partitioning into the other compartments of the soil is a prerequisite for compound transport. Only compounds that are present in the aqueous phase may be available to microbial transformations.

Dissolution as well as volatilisation of NAPL constituents are described by Raoult's law. The solubility of a compound from the phase is proportional to its aqueous solubility times its mole fraction in the mixture.

$$C^R_{Sat} = C^W_{Sat}\, \chi_i\, \gamma_i \qquad \text{eq. 2.11}$$

Where C^R_{Sat} is the solubility from the mixture, C^W_{Sat} the total aqueous solubility χ_i the mole fraction in the organic mixture and γ_i the activity coefficient which is considered equal one for an ideal mixture. A kinetic formulation can be met as well, describing the dissolution rate R_{dis} as a function of a dissolution rate constant k_{dis} (first order)

$$R_{dis} = -k_{dis}\,(\chi\, \gamma_i\, C^W_{Sat} - C) \qquad \text{eq. 2.12}$$

Air-water phase partitioning is generally considered as an equilibrium process, which is described by Henry's law, using either a dimensionless Henry's law constant $H^{[-]}$, if both, aqueous and gaseous concentrations are measured in mg/l or mol/l, or $H^{[atm\ l/mol]}$, if gaseous concentration is defined as partial gas pressure. Using Henry's law, gaseous concentration C_g or partial gas pressure p, respectively, can be calculated from the aqueous concentration C_w.

$C_g = C_w H^{[-]}$

$p = C_w H^{[atm\ l/mol]}$ eq. 2.13

The two forms of H can be converted into each other using absolute temperature T and universal gas constant R (8.31434 J mol^{-1} K^{-1}, Reisinger and Grathwohl, 1996).

$H^{[atm\ l/mol]} = H^{[-]} RT$ eq. 2.14

Note that 1 atm is 1013 hPa (=1.013 x10^5 J m^{-3}), so the transformation factor is 24.47 for a temperature of 298.15 K (25°C). Volatilisation of an organic phase to pore air can be easily described by superimposing both, Raoult's and Henry's law, underlying the assumption that local equilibrium prevails between NAPL, aqueous and gas phase at the pore scale. The gaseous concentration and partial gas pressure then become

$C_g = C_w^{Sat} \chi_i \gamma_i H^{[-]}$

$p = C_w^{Sat} \chi_i \gamma_i H^{[atm\ l/mol]} = C_w^{Sat} \chi_i \gamma_i H^{[-]} RT$ eq. 2.15

If sorption to the solid phase of the soil (in most cases to natural organic matter) is significant, the easiest description of linear equilibrium sorption is

$C_s = K_d C_w = K_{OC} f_{OC} C_w$ eq. 2.16

Where K_d denotes the sorption coefficient, K_{OC} the sorption to organic carbon coefficient and f_{OC} the fraction of organic carbon in the soil.

Biodegradation rates of volatile organic compounds in the unsaturated zone are commonly estimated regarding measurements of gas phase concentrations (Pasteris et al, 2002). It should be noted that those, depending on aqueous and gaseous saturation of the pore space and distribution coefficients, will be different from the actual rate constants in the pore water, as biodegradation takes place only in the aqueous phase of the soil. To formulate biodegradation rate constants in soil depending on distribution coefficients, it is useful to define apparent biodegradation rate constants which apply to the bulk phase of the soil, similar to the definition of apparent diffusion coefficients (Grathwohl, 1998). Starting from the definition of the bulk phase source/sink-term Q as the sum of all intra-aqueous reaction rates R_i affecting a given compound of interest (Mayer et al., 2002), here for simplicity considering a single reaction with aqueous phase rate R and a stoichiometric coefficient of unity,

$Q = \theta R$ eq. 2.17

For the case of first order reaction this can be formulated by substituting $k_{app} C_{bulk} = Q$ and $k_W C_W = R$:

$k_{app} C_{bulk} = \theta\ k_W C_W$ eq. 2.18

The bulk concentration C_{bulk} equals the aqueous concentration C_W times capacity factor α with respect to the aqueous phase

$k_{app} C_W\ \alpha = \theta\ k_W C_W$

C_W can be cancelled, leading to

$k_{app} = k_W \theta \alpha^{-1}$ eq. 2.19

That way, the apparent rate constant k_{app} (first order) can be defined as the product of the rate constant in the aqueous phase times the fraction of the compound in the aqueous phase $f_W = \theta \alpha^{-1}$, where the reaction takes place (Valsaraj, 1995,Werner, 2002):

$$k_{app} = k_w f_w = k_w \frac{\theta}{\rho_b K_d + \theta + n_g H}$$

$$= \frac{k_w}{R_d}$$ eq. 2.20

where ρ_b denotes the bulk density of the soil, θ the water filled porosity, n_g the air filled porosity and R_d the retardation factor. $\alpha = K_d \rho_b + \theta + n_g H$ is also referred to as the capacity factor of the soil with respect to compounds dissolved in the aqueous phase.

2.2.4 Temperature dependence of distribution coefficients

Soil temperature influences vapour pressure and diffusion coefficients of chemical

compounds and thus accelerates both degassing and gas phase transport. These relationships can be quantified using thermodynamic equations. The temperature dependence of p_0 and H is significant and listed in tab. 5.2, applying the thermodynamic relation according to the Van't Hoff equation. Temperature dependence of aqueous solubility S_W, however, was only available for benzene and is generally insignificant compared to that of p_0 and H (Reisinger and Grathwohl, 1996) and was therefore neglected.

The temperature dependence of distribution coefficients can be derived from the basic laws of thermodynamics. Given the Gibbs free enthalpy ΔG driving a reaction, depending on the quotient Q of reactants involved according to the law of mass action (1) and the reaction enthalpy ΔH_0, temperature T and entropy ΔS (2)

$$\Delta G = \Delta G_0 + RT \ln Q \qquad \text{eq. 2.21}$$

$$\Delta G = \Delta H_0 - T\Delta S \qquad \text{eq. 2.22}$$

Where ΔG_0 denotes the Gibbs free enthalpy at standard state conditions. In the state of equilibrium Q shifts to the equilibrium constant K, setting eq. 1.21 = eq. 1.22 => eq. 1.20 we obtain:

$$\Delta G_0 = \Delta H_0 - T\Delta S_0 = -RT \ln K$$

rearranged: $$-\frac{\Delta H_0}{RT} + \frac{\Delta S}{R} = \ln K \qquad \text{eq. 2.23}$$

Subtracting this equation formulated twice accounting for two different temperatures from each other will lead to the Van't Hoff equation.

$$\ln K = \ln K_0 - \frac{\Delta H_0}{R}\left(\frac{1}{T} - \frac{1}{T_0}\right) \qquad \text{eq. 2.24}$$

It is convenient to set T_0 = 25°C (standard temperature), then equilibrium constants for other temperatures can be calculated based on the knowledge of T_0 and ΔH_0.

2.2.5 The Damköhler number

Natural Attenuation in the case considered depends on two processes: the biological reaction itself and the transport of the two reactants to the bacterial population at the plume fringes. Depending on how fast either process is, the slower one will be the limiting factor. The ratio of time scale of biogeochemical reaction to the transport process is expressed by the dimensionless Damköhler number

$$Da = \frac{t_T}{t_R} \qquad [-] \qquad \text{eq. 2.25}$$

with t_T denotes time scale of transport [T] and t_R: time scale of reaction [T], (Damköhler, 1936,Mayer, 1999).

Generally, the time scale of transport equals $t_T = L/v$ for advective transport and $t_T = L^2/D$ for dispersive transport, where L represents a characteristic length of the system or a distance to a given point of interest, respectively. The time scale of reaction $t_R = C/R$ where R denotes the reaction rate and C a characteristic concentration.

In systems with Da >> 1 the reaction dominates, transport processes will be limiting mass transformation and quasi equilibrium conditions can be assumed. On the other hand, when Da << 1 reaction kinetics will be limiting. Generally, Damköhler numbers range over several orders of magnitude. (Jennings and Kirkner, 1984) investigated reversible chemical reactions in groundwater contamination problems and found that the equilibrium assumption becomes valid at Da > 100.

2.2.6 Example of a 1D diffusion-reaction experiment

A short example how Damköhler numbers can help to describe the behaviour of a system shall be given here. Consider a unsaturated column

experiment with length *L*, constant concentration C_0 boundary of volatile organic compounds at the lower side and atmospheric concentrations (zero) at the upper boundary. Within the column, the presence of oxygen supports an overall constant biodegrading microbial community. After a steady state is established, an analytical solution for first order biodegradation can be applied given in (Pasteris et al., 2002)

$$C/C_0 = \frac{\sinh(\sqrt{\frac{k}{D}}x)}{\sinh(\sqrt{\frac{k}{D}}L)} \qquad \text{eq. 2.26}$$

Where *D* denotes the apparent diffusion coefficient and *k* the apparent reaction rate constant. Assuming zeroth order degradation, which shall be discussed here, the PDE becomes:

$$\frac{\partial C}{\partial t} = D\frac{\partial^2 C}{\partial x^2} - k = 0$$

$$k = D\frac{\partial^2 C}{\partial x^2} \qquad \text{or} \qquad C'' = k/D$$

eq. 2.27

Integrating in the spatial dimension yields

$C' = k/Dx + C_1$

$C = ½\ k/D\ x^2 + C_1 x + C_2$

With C_1 and C_2 as integration constants. By evaluation of the boundary conditions BC 1 and BC 2 we can eliminate these constants:

BC 1: $C(0) = C_0$

$\Rightarrow\ C_2 = C_0 \Rightarrow C(x) = ½\ k/D\ x^2 + C_1 x + C_0$

BC 2: $C(L) = 0$

$\Rightarrow C(L) = ½\ k/D\ L^2 + C_1 L + C_0 = 0$

$\Rightarrow C_1 = -C_0/L - 1/2\ k/D\ L$

As solution we obtain:

$$C(x) = ½\ k/D\ x^2 - x(C_0/L + ½\ k/D\ L) + C_0 \qquad \text{eq. 2.28}$$

A more generalised equation can be formulated if we define *Da*,

$$Da = \frac{L^2 k}{DC_0} \qquad \text{eq. 2.29}$$

as the dimensionless Damköhler number which provides a relation of zeroth order kinetic reaction to diffusive transport rate. Also, $x/L = X$ can be substituted by the dimensionless length proportion *X* and *C* by C/C_0 as relative concentration. The dimensionless solution is given by

$$C/C_0 = ½\ X^2\ Da - X\ (1 + ½\ Da) + 1 \qquad \text{eq. 2.30}$$

The null of the quadratic equation is encountered within the model domain ($X_0 \leq 1$) if $Da \geq 2$. Then degradation exceeds the supply of the compound at the influx and the breakthrough out of the column as well as concentrations at $X > X_0$ equal zero. Exactly half of the influx will be degraded before leaving the column if Da = 2/3.

In the first order kinetics solution, a finite breakthrough out of the column remains for any degradation rate. If eq. 1.23 is also substituted to dimensionless numbers $Da = L^2 k D^{-1}$ and $X = x/L$ it becomes

$$C/C_0 = \frac{\sinh(\sqrt{Da}X)}{\sinh(\sqrt{Da})} \qquad \text{eq. 2.31}$$

Because it is somewhat more complicated, the *Da* numbers which lead to 50 %, 90 % and 99 % degradation within the domain were evaluated numerically, Tab. 1.2 shows Damköhler numbers required for certain amounts of degradation for this theoretical column experiment.

Tab. 2.2 Damköhler number and resulting efficiency of degradation (first order)

Da 1st [-]	Da 0th [-]	% of degradation
1.73	0.67	50
8.33	1.64	90
28	2	> 99

Obviously, the zeroth order Da are somewhat lower than the ones representing similar condition in first order.

An example of concentration profiles is shown in Fig. 2.1. For compounds with low degradation rates like cyclo-pentane, first and zeroth order degradation looks similar, but for high rates (decane) significant differences in the concentration profiles can be seen, even though total rates for both kinetics are similar in this example.

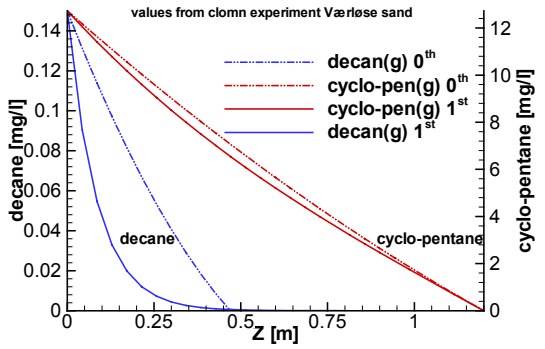

Fig. 2.1 Comparison of 2 concentration profiles in a 1D column experiment: cyclo-pentane with low, decane with high reaction rates.

For this simple scenario, the exact ratio of transport and reaction kinetics can be defined easily, but it is obvious that conditions differ significantly between the two types of kinetics applied. For more complex, 2D or 3D real world applications which will be subject in the scope of this thesis, the Damköhler number can only be referred to as a rough estimate of the contaminant behaviour. However, as indicated in previous investigations (Jennings and Kirkner, 1984), for Da > 100 a system can be credited as reaction dominated or close to equilibrium.

2.3 Scenario specific modelling at the field scale

Scenario specific modelling of contamination scenarios in the subsurface helps to gain knowledge about the importance of factors affecting contaminant behaviour and allows for predictions of the risks at contaminated sites and their potential of Natural Attenuation (Grathwohl et al., 2003). In the given scope, models that account for the saturated zone as well as the vadose zone have to be considered.

Numerical modelling is a field of vastly growing importance for risk assessment in environmental sciences due to growing computational capabilities and advances in modelling tools. An overview of unsaturated zone public domain codes is given in (Karapanagioti et al., 2003).

Numerical models can act as powerful tools for prediction even at large scales, however, they need to be validated. Laboratory experiments generally account for only a limited number of relevant processes and their smaller dimension makes results less conferrable to the field scale. Real spills, on the other hand, are mostly uncertain in size, age and constitution and therefore provide an uncertain basis for model validation.

Well controlled field experiments, which provide an opportunity to validate models on and allow for exact calculation of contaminant mass fate, have mostly focussed on the saturated zone (LeBlanc, 1991,Rivett et al., 2001). Field experiments that were performed in the unsaturated zone considered only single compounds and chlorinated hydrocarbons which undergo only minor biodegradation under aerobic conditions (Rivett, 1995,Hughes-Conant, 1996,Jellali et al., 2003).

Many authors have measured transverse dispersivities at the lab scale which are in the order of millimetres (Susset, 1998,Klenk and Grathwohl, 2002) or below (Eberhardt and Grathwohl, 2002). Moreover, also field studies (Garabedian, 1991,Gelhar, 1992,Rivett et al., 2001) and theoretical modelling investigations (Cirpka and Kitanidis, 2000) imply that α_t is very small and undergoes only limited enhancement on larger spatial scales. Those reported values are considerably smaller than the values that are commonly used in reactive transport modelling studies which are based on the assumption that α_l/α_t is generally some

factor around 10 (Domenico and Schwartz, 1998).

A challenge for numerical codes is to achieve the necessary numerical accuracy in heterogeneous media or transient flow conditions with standard reactive transport models at acceptable computational cost (Prommer et al., 2002). Discretisation in a dimension of millimetres or streamline oriented grids may be achieved in the lab scale but are not feasible for field conditions (Cirpka et al., 1999). If coarser grids are applied, artificial mixing occurs in the direction of flow (Frind, 1999) and can lead to overprediction of mixing and rates of Natural Attenuation (Cirpka et al., 1999).

According to geostatistical theory of flow in heterogeneous media, the Central Limit Theorem applies, i.e. solute distribution for the large scale limit approaches a Gaussian distribution (Gnedenko and Kolmogorov, 1968,Dagan, 1989). This state is also referred to as ergodicity, and Fick's law applies to describe dispersion. Although the absolute travel distance required for this behaviour cannot be easily defined (Trefry et al., 2003), effective dispersion coefficients were shown to guarantee correct mass balances for reactive mixing when applied in equivalent homogeneous domains (Cirpka, 2003).

Such effective (and also macrodispersion-) coefficients in heterogeneous aquifers, e.g., can be determined by comparing conservative tracer tests to analytical models or numerical dispersion free particle tracking simulations. The dispersivities obtained will henceforth allow the use of nowadays very powerful reactive transport models (Mayer et al., 2002,Molson et al., 2002,Prommer et al., 2003) in equivalent uniform model domains to predict Natural Attenuation unaffected of numerical inaccuracy.

3 Numerical Methods

A great numbers of numerical models for the simulation of soil- and groundwater processes have been developed in recent times (Frind et al., 1999,Steefel, 2000,Mayer et al., 2002,Prommer et al., 2003). Selected for the current task were the models BIONAPL for simulating groundwater plumes and the model MIN3P for simulating both, groundwater as well as unsaturated zone reactive transport. MIN3P was chosen because of its capability to combine variably saturated flow in soil and groundwater with an unlimited number of geochemical reactions and compounds. BIONAPL, on the other hand, has the advantage to account for microbial population dynamics.

For the given problem of a steady state groundwater plume caused by dissolved and aerobically degradable pollutants, the additional development of a simple and easily applicable model in 1D to reproduce the governing equations of coupled transport and biogeochemical reaction, their dimensionality and the evolution of reaction fronts was found to be of advantage.

3.1 The model MIN3P

The numerical model MIN3P allows for the calculation of vapour phase transport and unsaturated flow in the vadose zone. Groundwater transport processes and mass transfer across the capillary fringe can be simulated as well (Mayer et al., 2002) in one, two or three dimensions. MIN3P uses two sets of governing equations, one for groundwater flow under variably saturated conditions (Richard's equation) and the other for multicomponent reactive transport in variably saturated media. Diffusion coefficients in the are implemented using the approach of Millington (Millington, 1959). The dissolution or degassing of organic compound mixtures is simulated using Raoult's law, whereas Henry's law is applied to aqueous and gas phase partitioning. Biogeochemical reactions and transport processes are coupled by a global implicit solution method and solved using a finite volume algorithm. A variable number of geochemical compounds and reactions, such as biodegradation processes, can be handled based on an external database derived from the geochemical equilibrium model MINTEQ (Allison et al., 1991). All the physical and chemical properties of the compounds are defined in this external database. Transient boundary conditions and time and depth dependent soil temperature profiles can be applied in the simulations.

3.2 The model BIONAPL

BIONAPL can be used as a one, two, or three-dimensional numerical model for simulating multicomponent non-aqueous phase liquid (NAPL) dissolution and biodegradation in a porous aquifer. It includes a transient groundwater flow model coupled with an advective-dispersive multicomponent transport model. The governing equations are solved using a Galerkin finite element approach with a rectangular mesh. The nonlinear dissolution and decay terms are handled using a Picard iterative scheme with central time-weighting (Molson, 2000). Microbial growth is

implemented as a Monod kinetic approach (eq. 2.7).

3.3 Development of the 1D diffusion-reaction code DR

3.3.1 Governing PDE

The advection-dispersion-reaction differential equation affecting a dissolved compound with concentration C in a water saturated porous medium is given by

$$\alpha \frac{\partial C}{\partial t} = D_{eff} \frac{\partial^2 C}{\partial x^2} - q \frac{\partial C}{\partial x} + Q$$

[M T^{-1} L^{-3} porous medium] eq. 3.1

where α denotes the capacity term of the porous medium and reduces to the porosity n if the medium is saturated and sorption is neglected, D_{eff} is the effective dispersion coefficient and q is the specific discharge due to moving aqueous phase. The source/sink term due to intra-aqueous reactions Q is defined by

$$Q = -s\,\theta R \qquad [\text{M T}^{-1}\ \text{L}^{-3}\ \text{porous medium}] \qquad \text{eq. 3.2}$$

With s as the stoichiometric coefficient of the compound, θ the water filled porosity and R the reaction rate. If the medium is saturated and sorption is absent, both, α and θ equal n. R is defined in DR by second order kinetics depending on the reaction rate constant κ and the concentrations of two compounds involved.

$$R = \kappa C_A C_B \qquad [\text{M T}^{-1}\ \text{L}^{-3}\ \text{H}_2\text{O}] \qquad \text{eq. 3.3}$$

Assuming the medium being saturated and sorption being absent, dividing eq. 3.1 by n leads to the PDE that applies to the aqueous phase

$$\frac{\partial C}{\partial t} = D \frac{\partial^2 C}{\partial x^2} - v \frac{\partial C}{\partial x} + sR$$

[M T^{-1} L^{-3} H$_2$O] eq. 3.4

where D equals the sum of pore diffusion coefficient D_p and contribution of mechanical dispersion $v_x \alpha_x$, defining α_x as the longitudinal dispersivity (direction of the model orientation equals the flow direction x) and v_x the groundwater flow velocity.

$$D = D_p + v\,\alpha_x \qquad \text{eq. 3.5}$$

3.3.2 Numerical formulation

The method of finite differences requires to discretize the continuous differential equation by defining values only for certain nodes within the boundaries of the model domain. In the case of groundwater flow or transport this denotes points in space. It can be shown by Taylor expansion of the approximation of the derivatives, that uniform spatial discretisation Δx provides a more accurate solution than variable discretisation (Frind, 1999). As computational demand in 1D simulations is relatively small, variable grid spacing is not required and a uniform grid spacing is obliged in DR due to its simplicity. A set of linear or non-linear algebraic equations is obtained which then can be solved using a variety of numerical solution strategies.

$$\frac{\partial C}{\partial x} \approx \frac{C_i - C_{i-1}}{\Delta x} \qquad \text{eq. 3.6}$$

$$\frac{\partial^2 C}{\partial x^2} \approx \frac{C_{i+1} - 2C_i + C_{i-1}}{\Delta x^2} \qquad \text{eq. 3.7}$$

Using this discretisation scheme, a concentration C at node i and time t can be calculated by the discretised approximation of the differential expressions.

$$C_t = C_{t-1} - \Delta t(D \frac{\partial^2 C}{\partial x^2} - v \frac{\partial C}{\partial x} + s\,R) \qquad \text{eq. 3.8}$$

At this stage, it is of advantage to define the mass contribution MC for a given node as

$$MC = (D \frac{\partial^2 C}{\partial x^2} - v \frac{\partial C}{\partial x} + s\,R) \qquad \text{eq. 3.9}$$

If only the mass contribution from the previous timestep is used to gain the solution, the method is called explicit, if only the mass contribution from the current timestep is used, the procedure is called implicit. For most applications a centred time weighting using 50% implicit and 50% explicit proportion is providing the most accurate solution. This technique is called Crank-Nicholson method and was further applied.

$C_t = C_{t-1} - \Delta t(½\ MC_t + ½\ MC_{t-1})$ eq. 3.10

3.3.3 Boundary conditions

Essential for solving partial differential equations (PDEs) is an appropriate formulation of boundary conditions. Three different types of boundary conditions can be distinguished: first type (Dirichlet-type), second-type (Neumann) or third type (Cauchy-boundary condition). In the model DR, the spatial distribution of concentration C is assigned as boundary values at the first and last node, but boundary conditions at internal areas are also possible.

For the temporal distribution of concentration C, a boundary condition is defined as an initial concentration distribution before the start of the computation. However, the term 'boundary condition' is unusual for temporal behaviour of physical properties and rather referred to as an initial condition.

A first type boundary condition is simply the external definition of the physical property of interest at the boundary, which is the concentration C in this scope. Numerically, the boundary condition has to be read from an external input file. In general, it can be defined time-dependent.

First type: $C(x=0) = C_0$

$C(x=L) = C_L$, respectively

$C_1(t) = C_{BC}(t)$ eq. 3.11

In a second type boundary condition, the first derivation of C is defined at the boundary location. The most common one is the special case of a simple zero gradient boundary condition, i.e. the boundary is considered impermeable.

$$\frac{\partial C}{\partial x}(x=0) = 0 \qquad \text{eq. 3.12}$$

In this case the value at the boundary location is kept equal to the adjacent value to prevent any mass flux across the boundary, for the example of the first node

$C_1 = C_2$

For a given nonzero boundary flux the boundary condition becomes:

$$-D_{eff}\frac{\partial C}{\partial x}(x=0) = F_0 \qquad \text{eq. 3.13}$$

Then the boundary equation is defined by (considering the node i as the boundary node):

$F_{BC} = -D_{eff}\,\Delta C/\Delta x$ eq. 3.14

$F_{BC} = -D_{eff}\,(C_i - C_{i+1})\,/(x_i - x_{i+1})$ eq. 3.15

Rearranging this eq., assuming F_{BC} time dependent, leads to a calculated boundary node concentration:

$C_i = C_{i+1} - F_{BC}\,(t)\,D_{eff}^{-1}\,(x_i - x_{i+1})$ eq. 3.16

Third type (Cauchy) boundary conditions were not applied in the current model.

3.3.4 Solution strategy

Transport and reaction are solved simultaneously. For the current problem, a Gauss-Seidel iteration scheme was employed. The reaction rate is updated in each iteration step and added as a contribution to the mass conservation equation.

3.3.5 Mass balance

The model must account for the conservation of mass within the system. A concentration unit of mgl^{-1} offers the simplest option because it equals gm^{-3} (SI units) and requires no transformations. The contributions of mass flux across the boundaries and the reactions within the system have to equal out the change of mass for each compound within the system for a given time interval. A time interval can be chosen as a single timestep from t_1 to t_2 or cumulative for the whole simulation from time = 0 to time of termination T:

$$A_n \alpha \left[\int_0^L C(x,T)dx - \int_0^L C(x,0)dx \right] + \int_0^T \int_0^L Q(x,t)dxdt + \int_0^T F_{BC}dt = 0$$

eq. 3.17

The area A_n perpendicular to the model dimension is considered equal unity (1 m^2) and can be dropped. If the porous medium is saturated and sorption is not considered, α equals n, eq. can be formulated in the discrete form by averaging over the node-centred grid:

$$M(t) = A_n \, \Delta x \, n \, (\sum_2^{n-1} C_{i,t} + ½ \, (C_{1,t} + C_{n,t}))$$

eq. 3.18

$$\Delta M = M(t_2) - M(t_1) \qquad [g] \qquad \text{eq. 3.19}$$

The source-sink term Q for the porous medium contributes

$$Q(t) = A_n \, \Delta x \, s \, n \, (\sum_2^{n-1} R_{i,t} + ½ \, (R_{1,t} + R_{n,t}))$$

$$[g \, s^{-1}]$$

with

$$R_{i,t} = k \, C_{i,t}^{Cont} \cdot C_{i,t}^{O_2} \qquad [g \, l^{-1} \, s^{-1}]$$

eq. 3.20

as the reaction rate around node i. Assuming a linear interpolation of the reaction rate between two timesteps yields a global source/sink contribution for the entire model domain between the timesteps:

$$\overline{Q} = \int_{t_1}^{t_2} Q(t)dt \qquad \text{eq. 3.21}$$

$$\overline{Q} = ½ \, \Delta t(Q(t_2) + Q(t_1)) \qquad [g]$$

eq. 3.22

The fluxes across the model domain boundaries for discrete time t can be calculated according to

$$F_0(t) = A_n \, D \, n \, (C_n - C_{n-1})/\Delta x \qquad [gs^{-1}]$$

$$F_L(t) = A_n \, D \, n \, (C_0 - C_1)/\Delta x \qquad [gs^{-1}]$$

eq. 3.23

and for the flux contribution during the timestep between t and $t-1$

$$F_0 = ½ \, \Delta t(F_{0,t} + F_{0,t-1}) \quad [g]$$

$$F_L = ½ \, \Delta t(F_{L,t} + F_{L,t-1}) \quad [g] \qquad \text{eq. 3.24}$$

The mass balance error is obtained by

$$E = \Delta M - Q - F_0 - F_L \qquad [g]$$

eq. 3.25

and can be defined either per timestep or cumulative as the sum over all previous timesteps. The mass balance error relative to total mass is

$$e = (\Delta M - Q - F_0 - F_L)/M \qquad [\%]$$

eq. 3.26

3.3.6 Detection of the reaction front.

The reaction front is defined as the location where the reaction rate reaches its maximum. If the reaction is sufficiently fast, both, the concentration of the substrate and its corresponding electron acceptor will have very low values at the reaction front. One side from the reaction front will be dominated by one of the compounds, the other to the corresponding. Thus, the reaction front can be encountered computationally where the condition holds:

$$C_{S,\,i} > C_{EA,\,i} \wedge C_{S,\,i+1} > C_{EA,\,i+1}$$

eq. 3.27

With C_S and C_{EA} as the substrate and electron acceptor concentration at node i and node i+1, respectively. The exact location of the reaction front then becomes

$X_{front} = (i - ½)\ \Delta x$ eq. 3.28

3.4 Verification of the numerical model DR

The numerical model DR includes advection and dispersion in one dimension coupled with chemical reaction. It was verified comparing results with analytical solutions of the governing differential equations. The three compartments dispersion/diffusion, advection/dispersion and chemical reaction were regarded separately.

3.4.1 Diffusion through a layer

The partial differential equation (PDE) for nonsteady state diffusion through a layer with uniform diffusion coefficient is described in Grathwohl (1998).

$$\frac{C}{C_0} = 1 - \frac{x}{L} - \frac{2}{\pi} \cdot \sum_{n=1}^{\infty} \frac{1}{n} \sin\left(n\pi \frac{x}{L}\right) \cdot e^{-n^2\pi^2 D \frac{t}{L^2}}$$

eq. 3.29

Results are shown in Fig. 3.1. The agreement is very good.

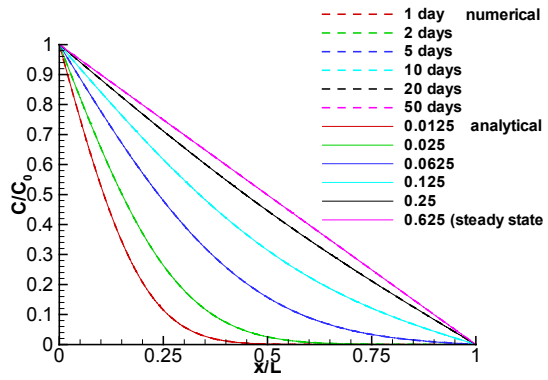

Fig. 3.1 Comparison of DR numerical results with the analytical solution for diffusion through a layer with a constant diffusion coefficient.

3.4.2 Advection – Dispersion

To prove the accuracy of the numerical model, its results were compared with the analytical equation of Ogata & Banks as well as with Bear et al. (1979), the latter one also considering first order biodegradation.

$$\frac{C}{C_0} = \frac{1}{2}\left(erfc\left(\frac{x - vt}{2\sqrt{Dt}}\right) + e^{\frac{vx}{D}} \cdot erfc\left(\frac{x + vt}{2\sqrt{Dt}}\right)\right)$$

eq. 3.30

Results for the Ogata-Banks solution of the advection-dispersion equation in 1D are shown in Fig. 3.2 and give a very good agreement. The flow velocity and dispersivity (flow direction) were 1 m/day and 0.0864 m, respectively.

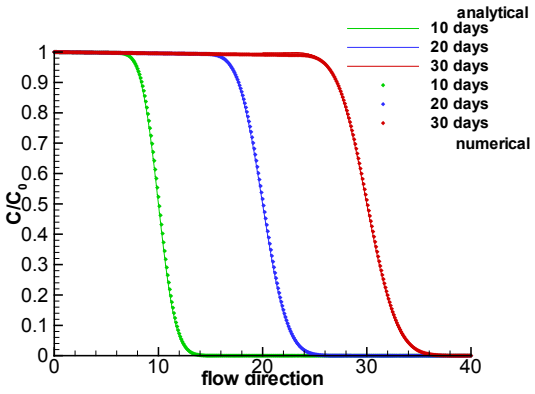

Fig. 3.2 Comparison of DR numerical results with the analytical Ogata-Banks solution of the advection-dispersion equation.

$$\frac{C}{C_0} = \frac{1}{2} \cdot e^{\frac{x}{2\alpha L}} \cdot \left(1 - \sqrt{1 + 4\lambda \frac{\alpha L}{v}}\right) \cdot erfc\left(\frac{x - vt\sqrt{1 + 4\lambda \frac{\alpha L}{v}}}{2\sqrt{\alpha L vt}}\right)$$

eq. 3.31

Results are given in Fig. 3.3 v_a = 1 m/day, λ = 0.01 [day^{-1}] and α_L = 0.5 m, which makes up a dispersion coefficient of 5.787 x 10^{-6} m^{2}s^{-1}.

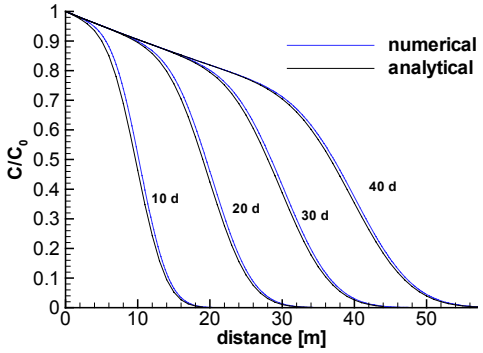

Fig. 3.3 Comparison of DR numerical results with the analytical solution of the advection-dispersion equation including first order decay from Bear (1979).

3.4.3 Kinetic chemical reaction

Consider a closed, well mixed batch system where compounds initially present react irreversibly to another one, with second order kinetics.

a.) The easiest example of a second order reaction uses the stoichiometry:

2 A → C eq. 3.32

leading to the PDE:

$$\frac{\partial A}{\partial t} = -kA^2 \qquad \text{eq. 3.33}$$

The analytical solution of the PDE is obtained by separation of variables:

$$\frac{\partial A}{A^2} = -k\partial t \qquad \text{eq. 3.34}$$

Integration: $$\int \frac{\partial A}{A^2} = -k\int \partial t$$

$$-\frac{1}{A} + C_1 = -kt + C_2$$

$$\frac{1}{A} = kt + C_1 - C_2$$

$$A = \frac{1}{kt + C_1 - C_2} \qquad \text{eq. 3.35}$$

If the initial condition is: $A(0)=A_0$

$$A_0 = \frac{1}{0 + C_1 - C_2}$$

$$C_1 - C_2 = \frac{1}{A_0} \qquad \text{eq. 3.36}$$

this will lead to the solution:

$$A(t) = \frac{1}{kt + \frac{1}{A_0}} = \frac{A_0}{A_0 kt + 1}$$

eq. 3.37

Test:

$$\frac{\partial A}{\partial t} = -\frac{1}{(kt + \frac{1}{A_0})^2} \cdot k = -kA^2$$

It is obvious that the relative concentration $\frac{A}{A_0} = \frac{1}{A_0 kt + 1} = f(A_0)$ depends on the initial concentration, this means a greater initial concentration of A_0 accelerates the reaction more than proportionally and leads to a faster depletion. Comparison of analytical and numerical solution for two different initial concentrations are given in Fig. 3.4. Very good agreement is visible.

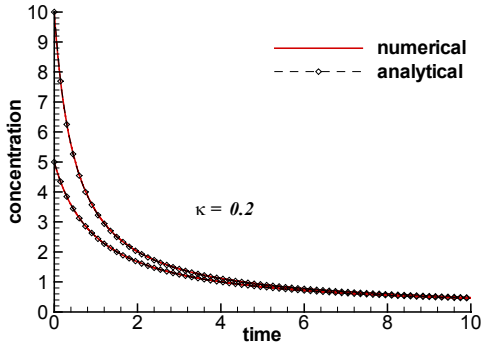

Fig. 3.4 Comparison of DR numerical results with the analytical solution of the second order kinetic reaction equation for 2 different initial concentrations (equal concentration for both compounds).

4 Steady state groundwater plumes

4.1 Methods to Predict the Size of Steady State Plumes

4.1.1 Conceptual model in 2D

Numerical simulations were performed to determine the lengths of stagnant plumes as a function of generally determined parameters, i.e. from field measurements and estimates of dispersivity. 2D numerical simulations were performed using the model BIONAPL (University of Waterloo, Canada;(Frind et al., 1999,Molson et al., 2002) and MIN3P (Mayer et al., 2002). A large number of simulations (80) was performed using the model BIONAPL due to simplicity, a smaller number of these were reproduced with the model MIN3P (about 10). It will be shown that once a steady state is achieved, longitudinal mixing can be neglected. This allows for a 1D model to be utilised to simulate the steady state which reduces computational time significantly and allows for a greater number (310) of different simulations. The 1D Finite Difference model development is described in § 2.3.

The base case scenario accounts for plumes extending over the entire thickness of the aquifer and a uniform concentration at the source (inflow boundary). In the model BIONAPL, only the saturated zone can be accounted for and a uniform flow field in an aquifer of constant thickness was assumed. Oxygen for biodegradation is delivered only by dispersion from a constant concentration boundary at the water table. For the aqueous contaminant NH_4^+, the water table is impermeable at realistic pH ranges and was reproduced by a zero gradient boundary condition. In BIONAPL, microbial growth was implemented by a Monod-term with a maximum concentration of microbial population of 0.5 g/l and a microbial yield of 0.4. That way an efficient microbial community establishes at the plume fringes, providing steep concentration gradients.

In the model MIN3P, an unconfined aquifer overlain by a thin vadose zone of one meter thickness was implemented. For this concept, the declaration of a boundary condition for the water table is not necessary, since it is implemented in the model. Atmospheric concentrations of oxygen were used as the top boundary condition, which complies with the ground surface. NH_4^+, in contrast, remains restricted to the saturated zone due to its geochemical behaviour. That way, the approximation of the water table as a constant concentration boundary in BIONAPL could be validated by comparing the two different models. Biotransformation in both models follows Monod kinetics with low half-utilisation rates of 0.1 mg/l for both, substrate and oxygen to achieve a close approximation to zeroth order kinetics as the most realistic approach (Meckenstock, 2001, personal communication). In MIN3P, however, microbial population dynamics are neglected and time invariant rate constants are implemented.

Simulations without groundwater recharge and with groundwater recharge of one millimetre per day were performed. The numerical experiments were run until the plume reached steady state conditions (due to biotransformation of NH_4^+ to NO_3^-), and for

this state the length of the plume was determined in concentration contour plots, regarding the legal limit isoline of 0.5 mg/l. The base case scenario was run with a 1 m/10 cm (x/z-direction) grid size, which was refined if necessary. Aquifer thickness and domain length were varied in the sensitivity analyses. The conceptual model in 2D is shown in Fig. 4.1 for transport and aerobic biotransformation of ammonium (NH_4^+) in a plume downgradient of a landfill for the base case scenario.

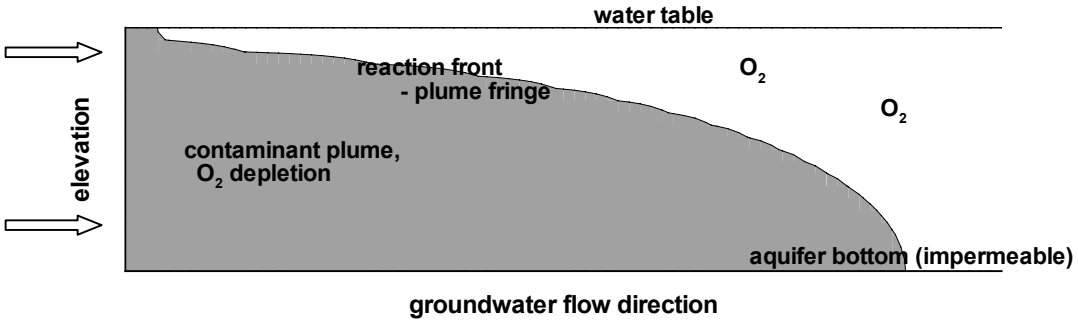

Fig. 4.1 Base Case scenario and conceptual model used for numerical simulation of a steady state NH_4-plume. Groundwater flow direction from left to right with a constant concentration (first type) boundary condition at the influx.

4.1.2 Accuracy Considerations – numerical dispersion

As outlined above, the transverse dispersivity is a sensitive parameter for the prediction of Natural Attenuation. The extremely small values of dispersivity, however, are a challenge for the accuracy of numerical modelling. Several strategies were applied to overcome this source of inaccuracy. A homogeneous model domain was applied and groundwater flow velocity was kept in x-direction parallel to the grid to avoid irregular flow fields with vertical components. That way, numerical dispersion can be minimised, because it is induced in the direction of flow (Frind, 1999).

Three different models were applied with different numerical solution strategies, BIONAPL: Finite Element Method (FEM), MIN3P: Finite Volume Method FVM and DR: Finite Difference Method (FDM) to allow for comparison of results with respect to plausibility. If necessary, grid spacing was refined.

To gain insight how modelling results respond to very small values of α_t, transverse dispersivities were gradually decreased from 8 cm to 0.01 mm. For α_t = 8 cm, which is in the order of the grid spacing, artificial mixing can be considered negligible. The penetration depth of the reaction front into the plume was correlated to transverse dispersivity. The numerical codes responded to the decrease of transverse dispersion to very small values, in the case of BIONAPL down to 0.1 mm for the chosen discretisation of Δz = 10 cm. Fig. 4.2 shows how concentration profiles change as α_t is sequentially decreased. Only at α_t = 0.01 mm, oscillations were observed. In the 1D Finite Difference code, which was somewhat more vulnerable to numerical dispersion, the grid was appropriately refined, with the resulting model run times remaining acceptable. Sensitivity analyses on α_t to evaluate an empirical relationship for plume length, were performed for values between 50 cm and 1 mm (see § Results). The results were consistent, which provides reason to allow for extrapolation to even smaller values of α_t.

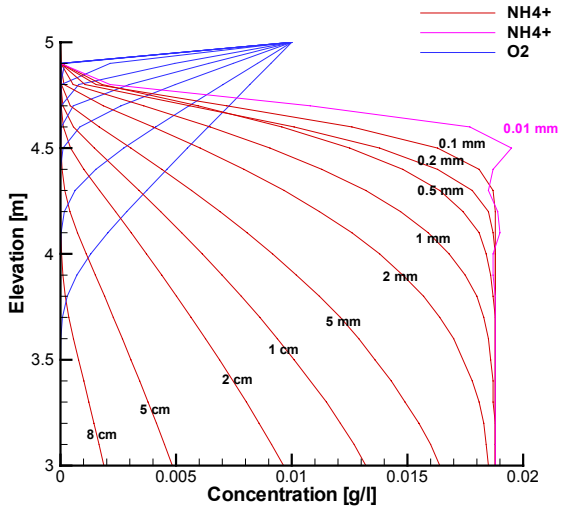

Fig. 4.2 Vertical concentration profiles of NH_4^+ and O_2 150 m downstream of the source (see Fig. 4) after 80 days (v = 2.7 m/day). The numerical model BIONAPL is stable down to values of α_t of 0.1 mm.

4.1.3 Influence of longitudinal dispersion

Generally, longitudinal dispersivities are assigned much larger values than vertical dispersivity (Domenico and Schwartz, 1998). Consequently, it is crucial to quantify to which extent longitudinal dispersion contributes to mixing of reactants and influences the plume size. This was tested in two ways: (i) varying α_l in the 2D base case model and assessing the impact on plume size, and (ii) evaluating the mixing and reaction rate in the same domain but allowing for no transverse influx of oxygen, leaving longitudinal dispersion as the only mixing process. The results are given in Tab. 4.1 and Tab. 4.2. It is shown that longitudinal dispersion even for very high α_l contributes only in a minor way to the reaction rates compared to transverse dispersion of relatively small α_t. Note that for the given parameters regarding Tab. 4.2, an α_t of 5 cm is sufficient to degrade the entire contaminant influx within the model domain (plume length 75 m). Biotransformed mass after 100 days in Tab. 2 is given as percentage of the total influx after 100 days. Influx is constant in time, the overall reaction rate, however, is decreasing with the power of ½, providing significant reactive mixing only for early times when steep gradients exist.

Tab. 4.1 Sensitivity of the base case scenario on longitudinal dispersivity with respect to plume size (α_t = 0.1 m, aquifer thickness M = 2 m).

α_l [m]	Plume length [m]
2.0	35,9
1.0	35,05
0.5	34.0
0.25	33,57
0.10	33,1

Tab. 4.2 Biodegraded mass in a 100 m domain of the base case scenario depending on longitudinal dispersivity if no transverse mixing occurs (α_t = 5 cm).

α_l [m]	Biodegraded mass [% of influx]
20	9.36%
10	7.57%
5	6.08%
2	4.07%
1	3.01%
0.5	2.11%

Analytical solutions for (ii), mixing due to longitudinal dispersion only in a 1D domain are described in (Valocchi et al., 2000,Cirpka, 2002). These also attest that reaction rates are proportional to $(Dt)^{-1/2}$ which implies that their contribution vanishes at the large time limit. It is obvious from this relationship, that longitudinal mixing is relevant only for initially steep concentration gradients. Furthermore, (Ham et al., 2004) derived an analytical solution for the length of a 2D steady state plume from a point source, where the plume length is independent of α_l, especially if $\alpha_l/\alpha_t < 10$, confirming the above findings.

Thus, the supply of electron acceptors for biotransformation of contaminant plumes is attributed to transverse dispersion mainly, and a simplification to 1D, which will be derived in

the next chapter, can be applied for the base case scenario.

4.1.4 A Simplification: 1D Modelling of 2D Scenario

To obtain empirical relationships from large numbers of numerical simulations, a major problem is the exhaustive computation time required. Therefore, simplifications that reduce computational effort are very helpful.

The 2D scenario can be reduced to a 1D model in vertical orientation once a steady state is achieved. Assuming steady state, the 2D reactive advection –dispersion equation becomes:

$$\frac{\partial C}{\partial t} = 0 = -v_x \frac{\partial C}{\partial x} + \alpha_l v_x \frac{\partial^2 C}{\partial x^2} + \alpha_t v_x \frac{\partial^2 C}{\partial z^2} - R$$

$[MT^{-1}L^{-3}]$ eq. 4.1

where C denotes the solute concentration, v_x the flow velocity, x and z the length parallel and normal (vertical) to flow direction, respectively, α_l and α_t longitudinal and transverse vertical dispersivity [m], respectively and R the reaction rate in [g m^{-3} s^{-1}]. If a uniform steady state flow field is applied, the x-dimension can be eliminated by substituting the travel distance $x = v_x \tau$ (travel time):

$$0 = -v_x \frac{\partial C}{\partial (v_x \tau)} + \alpha_l v_x \frac{\partial^2 C}{\partial (v_x \tau)^2} + \alpha_t v_x \frac{\partial^2 C}{\partial z^2} - R$$

eq. 4.2

Since v_x is a constant in the uniform flow field (homogeneous aquifer), it can be eliminated:

$$0 = -\frac{\partial C}{\partial \tau} + \frac{\alpha_l}{v_x} \frac{\partial^2 C}{\partial \tau^2} + \alpha_t v_x \frac{\partial^2 C}{\partial z^2} - R$$

$[MT^{-1}L^{-3}]$ eq. 4.3

For further simplification it is crucial that the contribution of term including longitudinal dispersion is insignificant for the scenario (see previous section) and can be eliminated. Then eq. 4.3 simplifies to

$$\frac{\partial C}{\partial \tau} = \alpha_t v_x \frac{\partial^2 C}{\partial z^2} - R$$

$[MT^{-1}L^{-3}]$ eq. 4.4

which equals the reaction-diffusion-equation in one dimension, but is vertically oriented, perpendicular to flow direction.

Regarding the contour lines of the steady state plume, the 2D model (isolines) and the 1D model reaction front (red line) show the same shape and depth of the reaction front (Fig. 4.3). Only in the length of the plume at its very dispersed forward edge some discrepancy can be observed. Physically this means that if only lateral mixing of electron acceptors to the plume from the water table is significant, the groundwater travel time (starting from the source) can be linked linearly to the time the plume was object to mixing with O_2 in vertical direction. When the groundwater velocity is considered as proportionality factor, a depth profile of a 2D model at a given location will fit a 1D model vertical profile of the corresponding time. That way, the length of the plume in flow direction can be calculated by a 1D model in vertical dimension. Applying the 1D model for predicting plume lengths (following section) allowed for a much greater number of simulations for different parameters (310) than using the 2D models only.

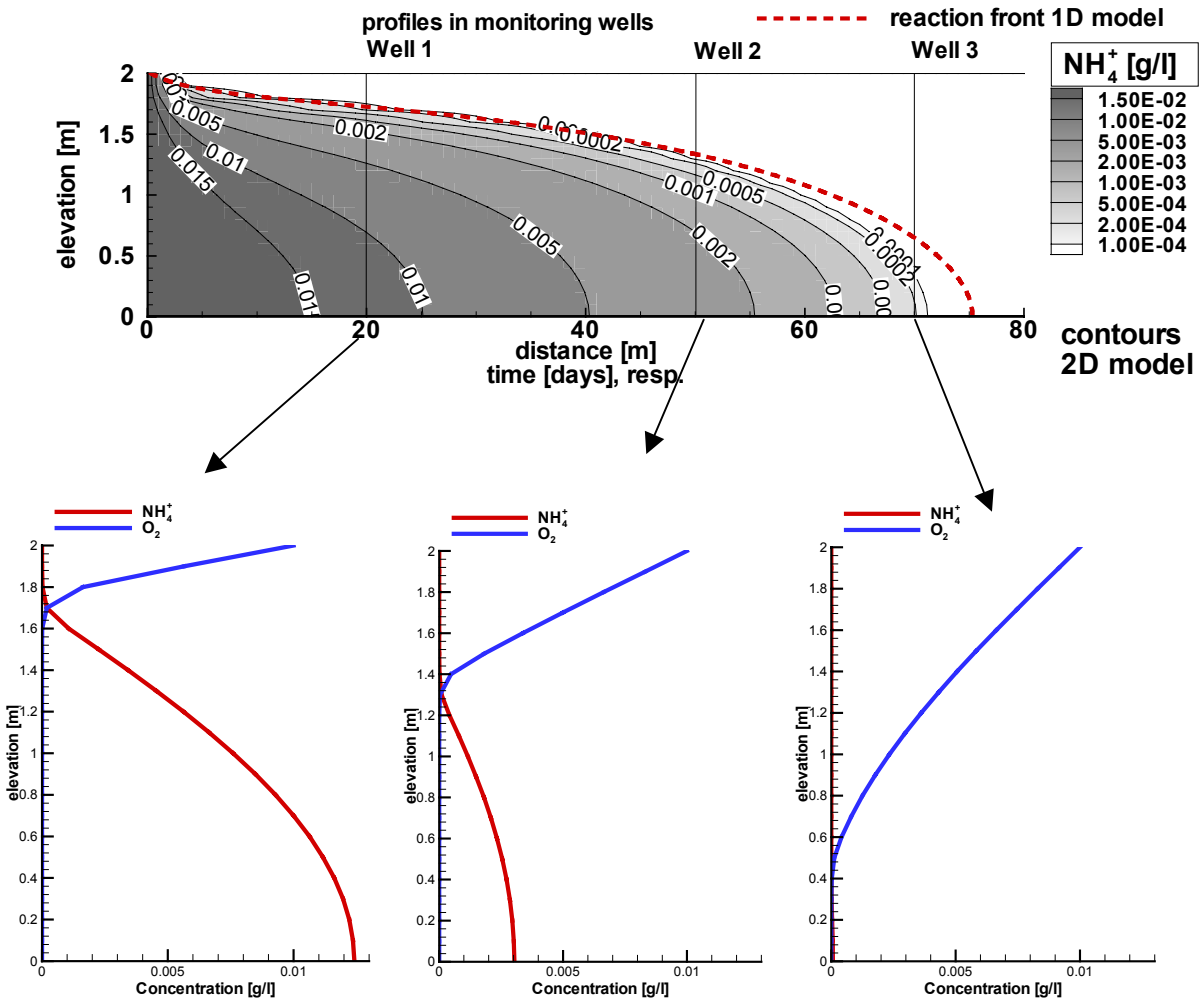

Fig. 4.3 Shape of a steady state plume for the base case scenario. A shows the correspondence of the 2D model contour lines and the propagation of the reaction front in the 1D model. B shows the vertical concentration profiles resulting from 2D simulations using BIONAPL for a steady state at wells 20 m, 50 m and 70 m, respectively, downgradient from the contaminant source.

4.2 Results for the Base Case Scenario

The shape of the steady state plume and the reaction front was already provided in Fig 4.3. Using the model BIONAPL, microbial population dynamics determine the time until a steady state is achieved. For low initial microbial density or slow growth, contaminants spread widely during early times and become mixed with oxygen and then retreat due to growing degradation capability. At steady state, steep concentration gradients establish at the plume fringes, especially close to the source, and oxygen within the plume becomes totally depleted. As described above, comparison of the 1D model and the 2D model BIONAPL yielded good agreement concerning the reaction front at steady state. Additionally, the model MIN3P was applied in 2D, with different conceptual assumptions implemented, concerning biodegradation kinetics and the boundary condition at the water table. Here, microbial population is neglected and time invariant reaction rate constants are used. Steady state conditions develop faster than in the population growth model, but result in good agreement with respect to the plume shape and lengths.

This also underlines that a first type top boundary condition (constant concentration) in

BIONAPL approves to represent the water table appropriately for a highly permeable porous medium.

As one factor included in the simulations, groundwater recharge had only minor influence on the plume length compared to the other factors. This may be explained by a short calculation. To compare the flux of oxygen F_D into a contaminant plume with the flux due to groundwater recharge F_{GWR} over a given length scale x,

$$F_D = D \frac{\Delta C_{O_2}}{\Delta z} b\, x = v\, \alpha_t \frac{C_{O_2}}{\Delta z} b\, x \qquad \text{eq. 4.5}$$

$$F_{GWR} = q_{GWR}\, b\, x \qquad \text{eq. 4.6}$$

Where q_{GWR} signifies the groundwater recharge to the aquifer, C_{O2} the oxygen concentration at the water table, and b the width of the aquifer. Setting both equal, b and x cancel out, and a minimum groundwater recharge $q_{GWR,\,lim}$ can be defined which would be required to provide the same contribution as the dispersive flux.

$$q_{GWR,\,lim} = v\, \alpha_t \frac{C_{O_2}}{\Delta z} \qquad \text{eq. 4.7}$$

Here, the vertical distance Δz becomes a critical value which depends on the length scale x, ranging from millimetres near the source area to eventually the whole aquifer thickness for the distant edge of the plume (Fig. 4.3). However, as shown in the previous consideration, very steep concentration gradients develop at the plume fringes, especially at the near source area, where the greater part of the mass transfer occurs. Thus, if Δz is in the range of cm or dm, a minimum groundwater recharge $q_{GWR,\,lim}$ of far beyond 1 mm/day, would result for most cases, which is not given under realistic conditions. This may also be explained intuitive arguments: a groundwater recharge of 1 mm/day (365 mm/year) would shift the plume *1/n* mm/year downwards or add 365 l of oxygen-rich water per m width to a plume of 365 m length, respectively. This input will be small compared to dispersive electron acceptor transport into the plume which is concentrated at steep gradients at the fringes. The minor influence of groundwater recharge is affirmed by the accordance of the water table aquifer in the model MIN3P to the first type boundary condition in BIONAPL.

As an example of the development of a steady state plume in a 2D model, Fig. 4.4 shows the propagation of concentration profiles in groundwater flow direction at the aquifer bottom (2 m below the water table). After 100 days the contaminant concentrations do not change anymore and the plume has reached a steady state. Note that the NH_4^+ concentrations drop slightly at earlier times because of the still growing microbial community. Microbial growth reaches a steady state somewhat before a stagnant plume has developed. However, bacterial population dynamics determine the time until establishment of steady state conditions, but do not affect the total length of the steady state plume.

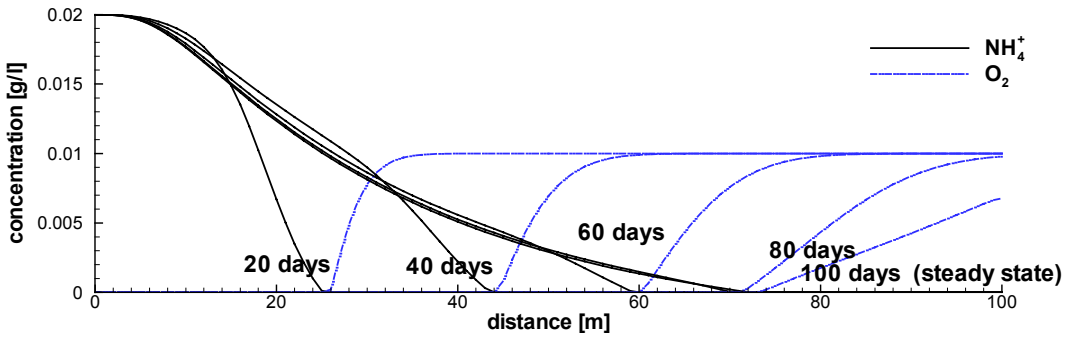

Fig. 4.4 Numerical modeling of the propagation of a NH_4^+ plume in groundwater. Between 80 and 100 days steady state conditions establish.

4.2.1 Sensitivity to biodegradation rate constant

For six different values of α_t (20, 10, 5, 2, 1 cm and 1 mm, respectively), sensitivity analyses were performed on the biodegradation rate constant in the 1D model (second order kinetics) and for α_t = 5 cm in the 2D model (zeroth order kinetics). To obtain a constant base for calculation of the biodegradation rate in the zeroth order microbial growth model (2D), the initial microbial concentration was set to 0.05 g/l and the microbial yield to zero to disable population change in space and time. This resulted in the same maximum rates as in the base case model.

Once the degradation rate would exceed the supply rate of electron acceptors to the plume by transverse mixing, reaction rates and thus the plume length does not depend on the biodegradation rate constant k anymore. In order to define a Damköhler number that gives information about how close the reaction is to mixing or reaction rate limitation, the characteristic time scales of both reaction and transport need to be defined. For dispersive transport the transport time scale is the characteristic length scale of dispersion squared over the dispersion coefficient: $t_T = L^2/D$. The aquifer thickness M is the distance that transverse dispersion has to cover and was therefore chosen as L, leading to $t_T = M^2/D_t = M^2 (v\alpha_t)^{-1}$.

In the case of first order degradation, the concentration cancels out when calculating the reaction rate. For second order kinetics, the concentration of the electron acceptor (oxygen) can be substituted by the fraction of its aqueous solubility. Then we obtain the same units for rate constant as using first order. As the oxygen concentration in the base case scenario is at saturation (about 10 mg/l at 13 °C (Truesdale, 1955), the factor equals one.

As a relation between transport and reaction kinetics, a Damköhler number can defined, accounting for the given scenario.

$t_T = \frac{M^2}{D_t} = \frac{M^2}{D_p + v\alpha_t}$, if D_p is small compared to mechanical dispersion $t_T = \frac{M^2}{v\alpha_t}$ eq.4.8

where M indicates the aquifer thickness [m], D_T the transverse vertical dispersion coefficient and D_P the pore diffusion coefficient. Depending on the reaction kinetic, the reaction time scale can be expressed as the ratio of contaminant mass to the mass consumption per time: $t_R = C\ R^{-1}$, then the Damköhler number becomes

$$Da = \frac{M^2 R}{v\alpha_t C} \qquad \text{eq. 4.9}$$

This can be further derived to functions of the rate constants for specific kinetic approaches:

Zeroth order: $t_R = C_{0,S}\ C_M^{-1}\ \mu_{max}^{-1}$

First order: $t_R = k^{-1}$

Second order: $t_R = (C_{0,EA}\ \kappa)^{-1}$ eq. 4.10

Where $C_{0,S}$ signifies the initial concentration of the substrate, $C_{0,EA}$ the initial concentration of the electron acceptor and C_M the microbial concentration (population density). It should be noted here, that modelling studies (Koussis et al., 2003) have shown that for most relevant cases of aerobic degradation of readily bioavailable compounds in groundwater the assumption of instantaneous reaction kinetics (or mixing limited conditions) is appropriate. Exception have to be considered for high flow velocities or steep gradients in near source areas.

$Da = \frac{M^2 \kappa}{v\alpha_t}$ for first or second order, and:

$Da = \frac{M^2 \mu_{\max} C_M}{v\alpha_t C_{0,S}}$ for zeroth order kinetics

eq. 4.11

To assess the critical value of the Damköhler number at which the reaction rate would exceed the rate of mixing, it was set into relation to the relative plume length, the multiple of the achievable minimum for the given conditions at high reaction rates (Fig. 4.5). Both kinetic approaches show similar results and mixing limited conditions were observed for biodegradation rate constants greater than about 0.1 per day (2^{nd} order kinetics, α_t = 5 cm) and 5 mg l^{-1} day^{-1} (zeroth order kinetics, α_t = 5 cm), respectively. It can be observed that for a Damköhler number (eq. 4.11) between 10 and 100, the plume size becomes independent of the reaction rate and the transverse dispersion will limit Natural Attenuation.

For field conditions where α_t can be expected in the scale of centimetres or below, this would apply to pseudo first order reaction rate constants with respect to substrate above 0.1 day^{-1}. Also included in the Damköhler- number described above is the role of groundwater flow velocity (Eq. 4.8 v = 1 m/day in Fig. 4.5). Groundwater flow velocity was varied as well (see eq. 4.8), but it has no influence on the plume size once the Damköhler number *Da* is above about 10. For naturally observed velocities in the field around or below 1 m/day the bacterial consumption remains high enough to compensate the higher mass flux due to high flow velocities. Only for very high flow velocities of more than 10 m/day observed in highly permeable aquifers such as in coarse gravel or large fractures, exceptions may have to be considered. Thus, for small transverse dispersivities in the order of 1 cm, as observed in the field, aerobic biodegradation kinetics will not be a limiting factor for Natural Attenuation.

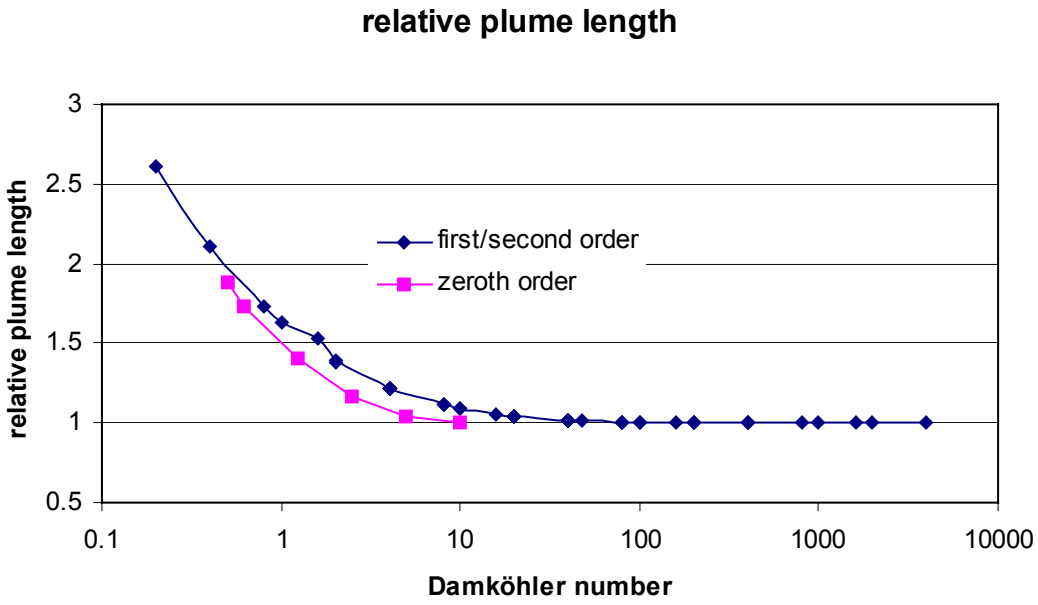

Fig. 4.5 Relative length of a steady state plume, relationship between dispersivity and dimensionless Damköhler number. n= 47 (2^{nd} order) and n= 6 (zeroth order).

4.2.2 Sensitivity on transverse dispersivity α_t

The plume length decreases linearly with increasing transverse vertical dispersivity α_t (Fig. 4.6).

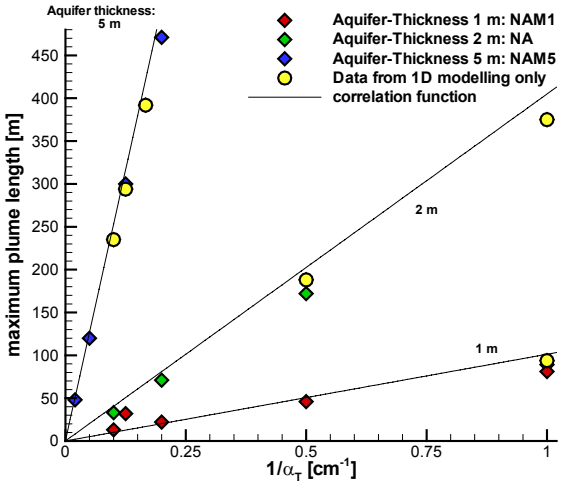

Fig. 4.6 Numerical modeling of the steady state length of a NH_4^+ groundwater plume. The maximum plume length increases linearly with decreasing α_t

4.2.3 Sensitivity on aquifer and plume geometry

The plume length of the base case scenario rises with the square of the aquifer thickness like in a simple diffusion approach according to $t \sim M^2$ Fig. 4.7).

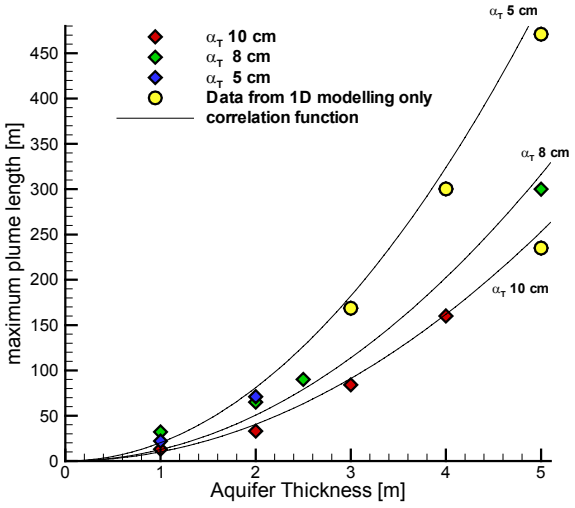

Fig. 4.7 Numerical modeling of the length of a steady state NH_4^+ plume as a function of the contaminated aquifer thickness

4.2.4 Sensitivity to reaction stoichiometry

The plume size in respect to the reaction stoichiometry, i.e. the initial concentrations of pollutant and electron acceptor, respectively, and the ratio of electron acceptor consumed by a specific mass of pollutant, shows a non-linear relationship. Within ranges that can be expected at the field scale, the best fit was found with an exponent of 0.3 (Fig. 4.8)

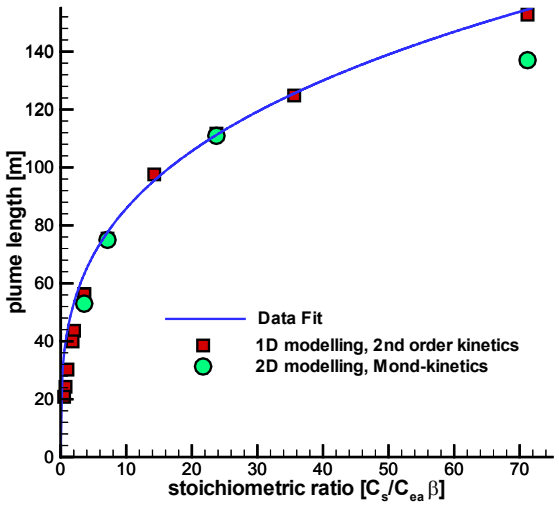

Fig. 4.8 Steady state plume lengths of NH_4^+ as a function of the stoichiometric ratio and initial concentrations in [g]. Realistic stoichiometric ratios range from 0.3 to about 60 ED/EA for the given scenario.

4.2.5 Correlation function for the plume size

Closed form solutions for related cases were developed by a number of authors.(Feeney et al., 1983) derived an analytical solution for semi-infinite conditions, (Ortoleva, 1994)for an infinite moving boundary condition including interphase transition (retardation) and (Valocchi et al., 2000) for an infinite longitudinal case with and without interphase transition. No applicable closed form solution, however, could be found for the given case of a plume confined within 2 finite boundaries. An empirical relationship was therefore complied from the simulations discussed above, accounting for the base case scenario. The correlation function for the length of steady state plumes is

$$pl \approx a \frac{M^2}{\alpha_t} \left(\frac{C_{cont} \beta}{C_{EA}} \right)^b \qquad [m]$$

eq. 4.12

pl, M, α_t, β, C_{cont}, C_{EA} denote the steady state plume length, the contaminated aquifer thickness, the transverse vertical dispersivity, the stoichiometric factor for the reaction, the concentration of the contaminant source, and the concentration of the electron acceptor, respectively. The best approximation was achieved for $a = 0.5$ and $b = 0.3$. This empirical relationship obtained by a large number of simulations (n = 310 for the 1D model; 80 for 2D model BIONAPL and 10 for the 2D model MIN3P) for dm to mm ranges of α_t may be used for the prediction of the plume size at dispersivities observed in experiments (eq. 4.9). It should be noted that these are minimum plume lengths which would be exceeded, e.g. if the compounds do not biodegrade easily, toxic effects limit the performance of the microorganisms or the availability of oxygen is restricted, in the vadose zone or due to consumption by other processes.

A theoretical reflection of the correlation function (eq. 4) shall be given as well. Consider an instantaneous or at least "fast enough" reaction. Underlying is the assumption, that a steady state plume is established once the advective influx of contaminant mass to the aquifer by groundwater flow is matched by the stoichiometrically equivalent dispersive influx of the electron acceptor (O_2) from the groundwater surface (upper boundary). The advective influx F_A is given by:

$$F_A = q\, C_S\, A_{in} = C_S\, b\, M\, n\, v \qquad \text{eq. 4.13}$$

where q signifies the specific discharge of the aquifer, C_S the initial contaminant concentration, b is the width of the aquifer (which may be normalised to unity), A_{in} the influx boundary area, M the aquifer thickness, n the porosity and v the groundwater flow velocity. The dispersive oxygen influx is:

$$F_D = -D_{eff} \frac{\Delta C_O}{\Delta M} A_{top} = - \frac{v \alpha_t}{n} \frac{C_O}{M} b\, x$$

eq. 4.14

where C_O signifies the boundary oxygen concentration, D_{eff} is the effective coefficient of dispersion and A_{top} the top boundary area.

Whereas the advective influx F_A can be determined exactly for a homogeneous aquifer, the dispersive influx F_D is concentration dependent and the variable x remains as an unknown 'characteristic length of interaction' in flow direction, which is related to the plume length. As for a steady state plume the contaminant consumption (right hand side) must match the advective influx from the source boundary F_A:

$$F_A = \frac{s_O}{s_S} F_D \qquad \text{eq. 4.15}$$

With s_O as the stoichiometric coefficient of oxygen, s_S as the stoichiometric coefficient of the substrate to the reaction and F_D the diffusive influx of oxygen from the water table (top boundary). A number of variables cancels out, leaving over:

$$x = n^2 \frac{M^2}{\alpha_t} \frac{C_S}{C_O} \frac{s_S}{s_O} \qquad \text{eq. 4.16}$$

Comparing eq. 4.16 with eq. 4.12 confirms the dimensions of the contributions of α_t and M to the plume size, whereas x appears to be non-linearly related to the plume length.

4.3 Model calibration for the landfill site "Osterhofen"

4.3.1 Site description

The landfill site "Osterhofen" is located in south-west Germany. The former gravel pit was filled with municipal waste between 1969 and 1977. The area is built up by moraine sediments and peri-glacial deposits from the latest alpine glaciation period. The contaminated gravel aquifer has a thickness between 2 and 5 m and a flow velocity between 2 and 3 m per day. In general, the regional aquifer is aerobic with concentrations of oxygen between 6 and 10 mg/l and elevated nitrate concentrations between 40 and 60 mg/l. Directly downgradient of the landfill anaerobic conditions prevail at a width of 150 m with zero concentrations of oxygen and nitrate as well as maximum ammonium (NH_4^+) concentrations of 25 mg/l, which is substantially above the legal limit of 0.5 mg/l according to state standards (Orientierungswerte, 1993). At a distance of 450 m downgradient in groundwater flow direction, however, only minor concentration of NH_4^+ were observed. This can be attributed to an aerobic biotransformation of NH_4^+ to nitrate (nitrification) which proceeds in two steps, driven mainly by the bacterial genus *Nitromonas* (step 1) and *Nitrobacter* (step 2) (Schachtschnabel et al., 1992):

$$NH_4^+ + 1.5\ O_2 \rightarrow NO_2^- + H_2O + 2\ H^+$$

$$\underline{NO_2^- + 0.5\ O_2 \rightarrow NO_3^-}$$

$$NH_4^+ + 2\ \ O_2 \rightarrow NO_3^- + H_2O + 2\ H^+$$

With an energetic balance for each reaction of:

$$\Delta H = -352\ \text{kJ/mol}$$
$$\underline{\Delta H = -74.5\ \text{kJ/mol}}$$
$$\Delta H = -426.5\ \text{kJ/mol} \qquad \text{eq 4.17}$$

Multilevel sampling with packers demonstrated that the whole thickness of the aquifer is contaminated by the ammonium plume. Detailed descriptions of the site, integral pumping tests and the assessment of monitored Natural Attenuation (MNA) as an appropriate contaminated land management option at the site are given in (Bayer-Raich et al., 2004,Rügner et al., 2004). An overview of the site is given in Fig. 4.9, demonstrating the groundwater flow direction in which the plume is extended and the two control planes where solute concentrations were measured. The second control plain is approximately 450 m downgradient of the landfill.

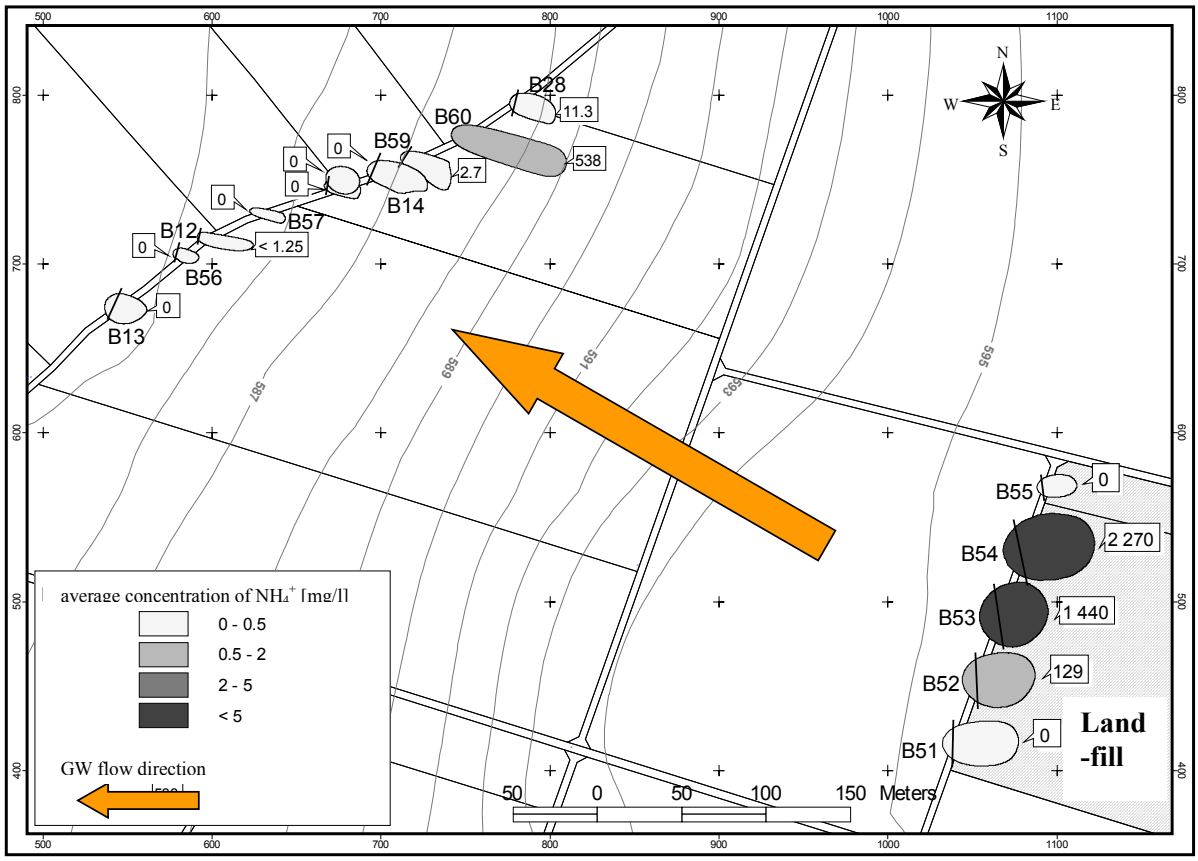

Fig. 4.9 Overview of the municipal landfill "Osterhofen", measured average concentrations of NH_4^+ and average groundwater flow direction (from (Rügner et al., 2004).

4.3.2 Modelling parameters

As the site consists of an aerobic aquifer which is assumed to be contaminated over its whole thickness, it serves as an ideal example of the base case scenario described above. The width of the contaminated plume is considerably larger than its thickness, providing a large surface area for transverse vertical dispersion. Lateral transport of oxygen into the plume will be of minor influence and 2D modelling in a vertical (xz)-plane is appropriate. As biodegradation parameters a microbial yield of 0.426, a maximum microbial concentration of 0.5 g/l and maximum utilisation rates of 0.1 $gl^{-1}day^{-1}$ per 1 gl^{-1} microbial mass was applied, with low half utilisation rates of 0.1 mgl^{-1} for both NH_4^+ and O_2. An average aquifer thickness of 4.5 m, groundwater flow velocity of 2.7 m/day, porosity of 35 %, an average influx concentration of NH_4^+ of 15 mg/l and an oxygen concentration at the water table of 8 mg/l were implemented in the model BIONAPL. A 1 m x 10 cm grid was applied in horizontal and vertical direction, respectively, together making up a model domain of 1000 by 450 elements. The aim was to reproduce the depth averaged concentration of NH_4^+ of 1.5 mg/l encountered at the control plane 450 m downgradient of the landfill by fitting α_t. Absolute plume length as well as transverse vertical dispersivity α_t was obtained by the procedure of calibration.

4.3.3 Calibration and results

Parameters for the fitting of α_t at the landfill site "Osterhofen" are given in Tab. 4.3. Such as plume length [m], depth averaged concentration 450 m downgradient of the landfill and aqueous mass of NH_4^+ [kg] of the plume for runs performed. Due to the previous knowledge of the plume behaviour for the base case scenario described, 5 runs were sufficient

to achieve an acceptable fit. The best fit with α_t of 3.2 cm resulted in the length of the plume of 570 m.

Tab. 4.3 Parameters obtained during the calibration procedure for the field site "Osterhofen"

α_t [cm]	Plume length [m]	Concentration 450 m [mg/l]	Aqueous mass [kg]
5	370	0	
3.2	571	1.411	3.299
3.1	592	1.6	3.399
3	611	1.834	3.5
2	900	5.175	4.87

Fig. 4.10 shows the concentrations the aquifer bottom of ammonium and oxygen for 250, 350, 500 and 600 days of simulation. After about 500 days, a steady state is achieved, providing clear evidence for a steady state of the already 25 year old plume at the field site.

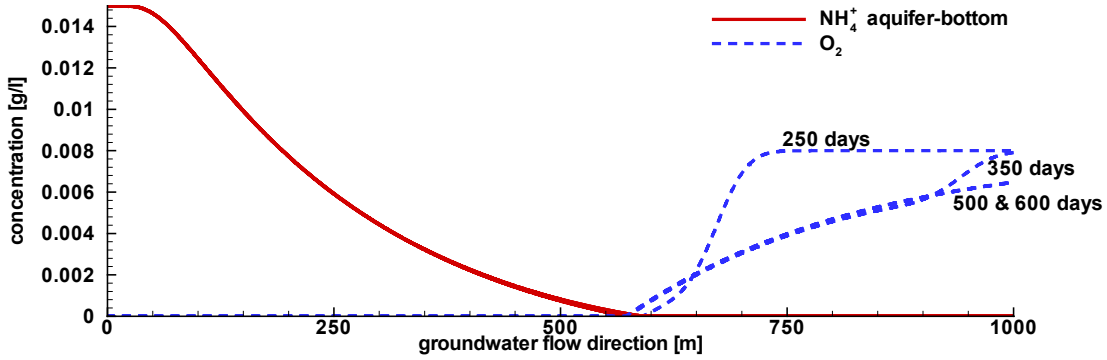

Fig. 4.10 Simulated concentrations at the aquifer bottom for the calibrated model landfill site "Osterhofen", SW Germany.

Fig. 4.11 provides simulated depth averaged concentrations at four (hypothetical) wells downgradient of the landfill at distances of 100, 200, 450 and 600 m respectively. As 600 m is already outside of the plume, the concentration is always zero. The monitoring well at 450 m, which is the distance of the monitoring plane installed at the field site, shows the averaged measured concentration of 1.5 mg/l. The breakthrough curves within the plume show higher concentrations, which after a slight peak concentration is visible before microbial community establishes, eventually reach a steady state. As a conclusion from site investigation and the numerical modelling performed Natural Attenuation could be proven as a suitable remediation strategy at the site, which enables to substitute cost extensive active cleanup procedure by a long term monitoring campaign (Rügner et al., 2004).

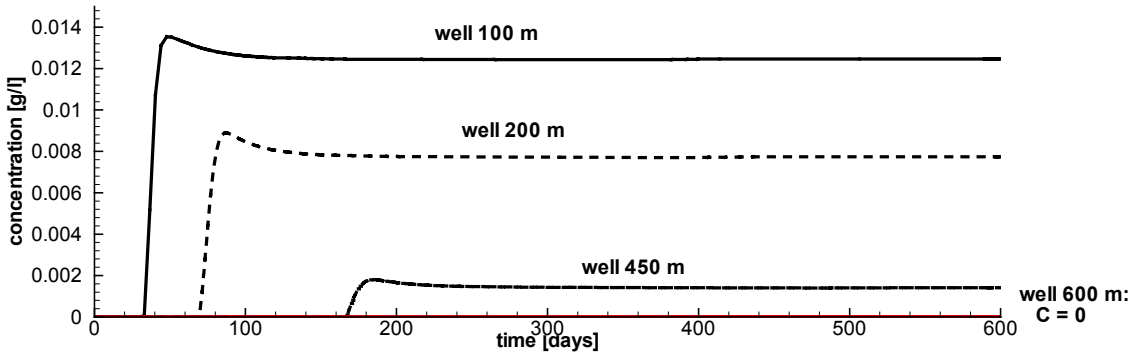

Fig. 4.11 Simulated depth average breakthrough curves for the calibrated model landfill site "Osterhofen", SW Germany, at two locations within the plume and at the monitoring plane (450 m).

4.4 Scenario of a partly Contaminated Aquifer

Up to here, the plume size was calculated for a scenario with fully contaminated aquifer thickness. In many cases, however, the contaminant source will only comprise a part of the aquifer, e.g. for gasoline spill or other LNAPL sources which remain at "smear zones" close to the water table (Wiedemeier et al., 1999).

The scenario of an aquifer contaminated in the upper part was evaluated, assuming oxygen saturation at the water table and also present oxygen in the part of the aquifer below the contamination. This was implemented as a first type (constant concentration) boundary condition. Concentrations of the contaminant, oxygen and the zone of microbial activity for an example with α_t = 8 cm and M = 5 m are shown in Fig. 10. Clearly present is a second reaction front developing below the plume. An analytical solution for a reaction-dispersion driven moving boundary front within infinite boundaries is given in (Cirpka, 2002). Considering the initial concentrations of two compounds as opposite heaviside functions *H* (in flow direction):

$C_A(t) = A_0\, H(t - x/v)$ and

$C_B(t) = B_0\, H(x/v - t)$, the location of the reaction front x_f is given by

$$x_f(t) = vt - 2\,\rho\,\sqrt{Dt} \qquad \text{eq. 4.18}$$

In our case, the propagation of the reaction front is oriented perpendicular (vertical) to flow, then the advective part *vt* of eq equals zero and the location of the front equals:

$$x_f(t) = -2\,\rho\,\sqrt{Dt} \qquad \text{eq. 4.19}$$

where $D = v\,\alpha_t$ is the (transverse) dispersion coefficient and $erf(\rho) = \dfrac{B_0 - A_0}{B_0 + A_0}$, with B_0 as the initial concentration times stoichiometric ratio of the compound in excess and A_0 the initial concentration times stoichiometric ratio of the compound entirely consumed. As can be seen in Fig. 4.12, this closed form equation can reproduce the lower front close to the source boundary. For later travel times, however, the aquifer bottom boundary begins to interact with the plume. As well, the correlation function in eq. for a fully contaminated aquifer does not hold for the upper reaction front in this case because a considerable mass fraction of the plume is already depleted due to the lower reaction front. Therefore, it is not possible to estimate the plume length for this more complex scenario as a superimposition of simpler analytical solutions.

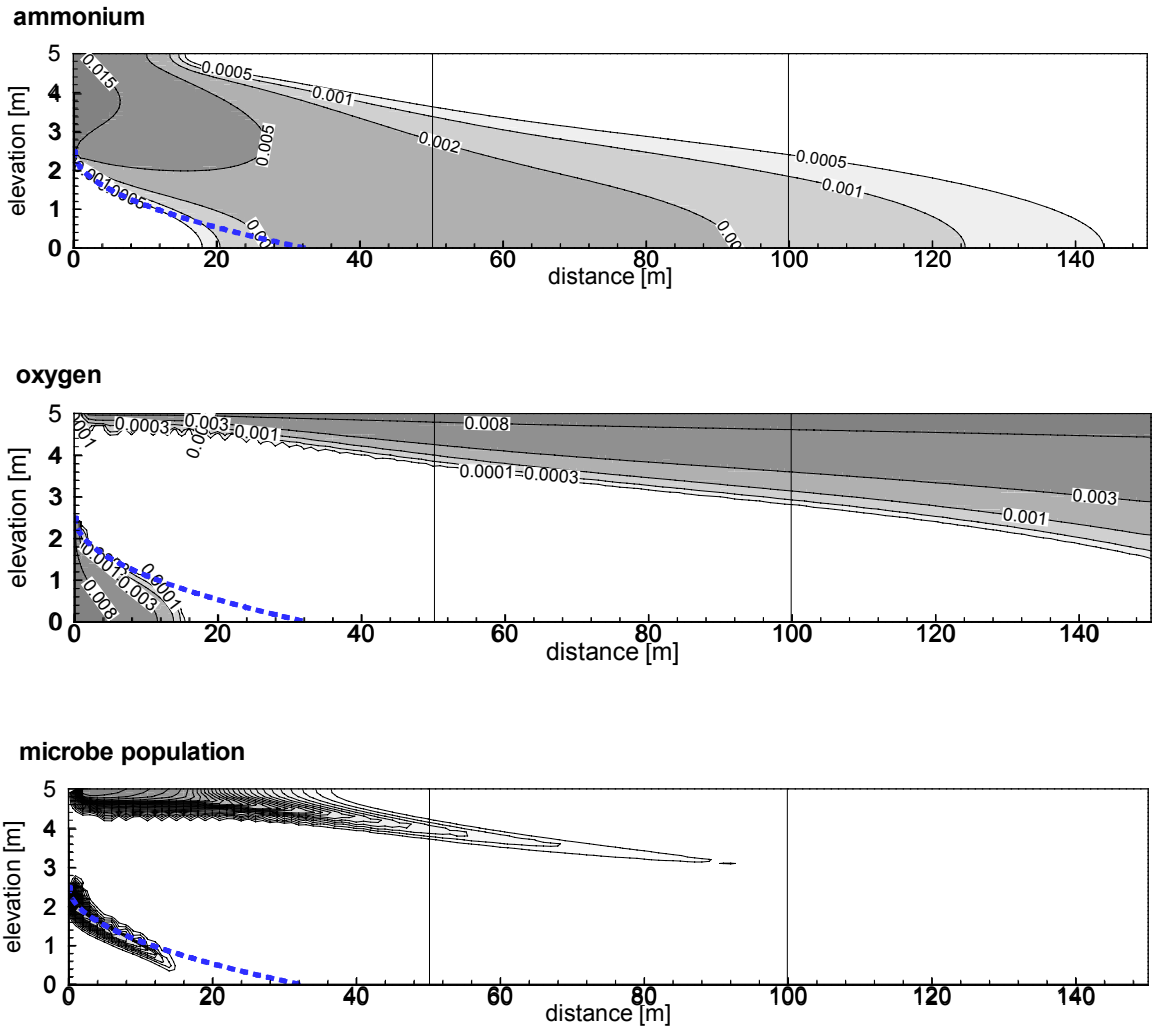

Fig. 4.12 contaminant plume (uppermost), zone of oxygen depletion (middle) and zones of microbial activity (lower) for a source comprising the upper half of the aquifer, concentration in [g/l]. Dashed line: analytical solution described in the text (eq. 4.19).

Five different correlations between the contaminated part of the aquifer M_{cont}/M_{tot} and the plume size, as a proportion pl/pl_{max} compared to the length for a fully polluted aquifer thickness with otherwise same condition, is given in Fig. 4.13. If only a thin fraction of the aquifer is polluted, the plume remains restricted to its upper part and the plume length is increasing squared with contaminated thickness (Fig. 4.14). Here, the agreement with the analytical solution fails. At a critical thickness the plume extents down to the aquifer bottom and the plume length increases rapidly at this stage. After more than one third of the whole aquifer thickness is polluted, the plume size increases almost linearly, eventually approaching the length given for the fully contaminated aquifer.

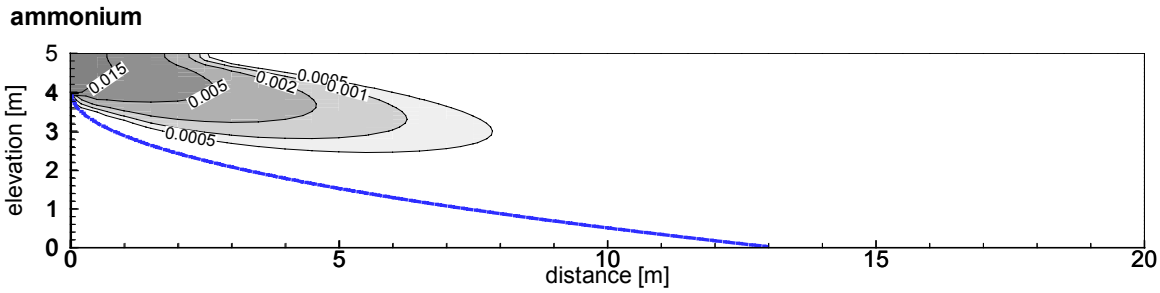

Fig. 4.13 Partly contaminated aquifer in a small zone close to the water table. α_t = 20 cm, α_l = 50 cm, lower oxygen concentration 3 mg/l. Dashed line: analytical solution described in the text (eq. 4.19).

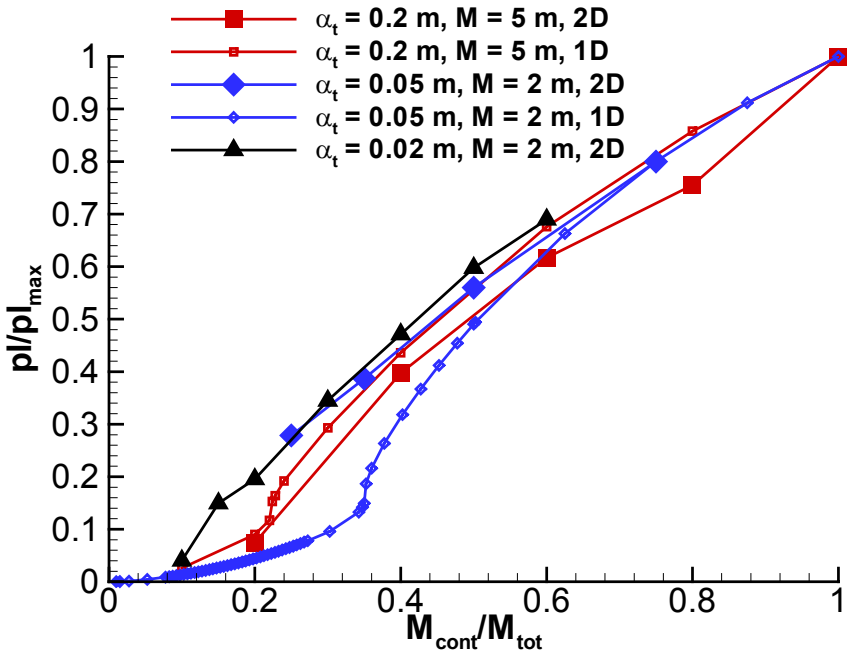

Fig. 4.14 Plume sizes for partly contaminated aquifers in relative proportions, n = 90

It should be noted that, for a partly contaminated aquifer, artificial mixing is more critical in this scenario than in the base case. As well, as indicated in Fig. 4.14, the agreement of the 1D and 2D models turned out to be less reliable and a stronger influence of longitudinal mixing on the plume size was observed. This indicates a further demand of model investigations for more complex scenarios including the assessment of applicability of simplifying assumptions.

5 Volatile organic pollutants in the unsaturated zone

5.1 Numerical model for Værløse field experiment

5.1.1 Strategy

Sketch of strategy:

Implementation of all available measured data

sensitivity of parameters - bandwidth of behaviour.

To reduce computational time: sensitivity analyses in 1D and 2D

3D model to reproduce field data (model validation:

1. unsaturated zone
2. groundwater

The model MIN3P (Mayer et al., 2002) was used applying a two step strategy: firstly, sensitivity analyses were performed evaluating the influence of parameters in the unsaturated zone and to identify the adjustable parameters to fit the field data. To assess the importance of soil, physico-chemical and meteorological parameters for the contaminant behaviour, sensitivity analyses on biodegradation rate constants k, Henry's law constant H for the different compounds, temperature T, groundwater recharge, soil water content θ and oxygen availability were conducted in 1D and 2D.

The trend of concentrations at certain locations differs depending on a great number of spatial and temporal circumstances and makes particularly sense to evaluate if a certain location of interest exists. A more general and steady view of a given situation, however, can be obtained from mass balance considerations, providing an integral information about the site or model domain. The focus of sensitivity analysis was therefore drawn on comparing results of the mass balance. An occasion to validate the use of MIN3P to predict Natural Attenuation of VOC in the unsaturated zone was given by comparing simulated to measured field data.

Results from the model MIN3P were evaluated with respect to mass balance contribution of diffusive outflux to the atmosphere (A), biodegradation (B), outflux from the domain to groundwater (G) and mass remaining in the NAPL (N). These compartments were chosen to provide an optimal base to assess the actual goal of the investigation, risk of groundwater contamination and the potential of Natural Attenuation. Whereas persistent NAPL phase represents a long term hazard and is desired to deplete fast, A and B act as the relevant mechanisms of Natural Attenuation for the unsaturated zone spill scenario. All the mass balance contributions of the kerosene compounds are expressed in percent using different modes. N is expressed as percent of initial mass present in the source, whereas A, B, and G are expressed as percent of mass that has been degassing from the source and that way denotes its fate once it has reached the pore air. This provides a better comparability between A, B and G.

Completing step one, biodegradation characteristics were identified as the only

fitting parameters which could not be derived from measurements at the site. Biodegradation rate constants were adjusted to reproduce measured vapour phase concentrations at sampling ports in the unsaturated zone. Then the mass balance for the unsaturated zone was quantified.

In a second step, starting from determined unsaturated zone situation, sensitivity of transverse vertical dispersivity was evaluated and adjusted to approach measured groundwater concentrations. The influence of relevant vadose zone parameters on contaminant transport to groundwater is also discussed in this context.

For the field site model, site characterisation with respect to grain size distribution, geochemistry, permeability, etc. was implemented as precisely as possible. Then, unknown parameters biodegradation rate constants and vertical dispersivity were adjusted. Based on the best fitting simulations, an estimation of total contaminant mass balance as well as mass transport to groundwater was obtained. That way, assessment of groundwater vulnerability for the given scenario was aimed for.

5.2 Description of site and experimental setup

The field experiment was conducted at Airbase Værløse, Denmark, in July 2001 to July 2002. The site location and characterisation was described in detail in (Christophersen et al., 2003). An overview of the site and its location is given in Fig. 5.1. The monitoring network in the near source area is illustrated in a N-S vertical cross-section in Figure 5.2.

Fig. 5.1 Location of the field experiment site Værløse airforce base in Denmark and overview of the experimental setup. Groundwater flow direction to the south west is followed by the multilevel groundwater sampling systems (Christophersen et al., 2003).

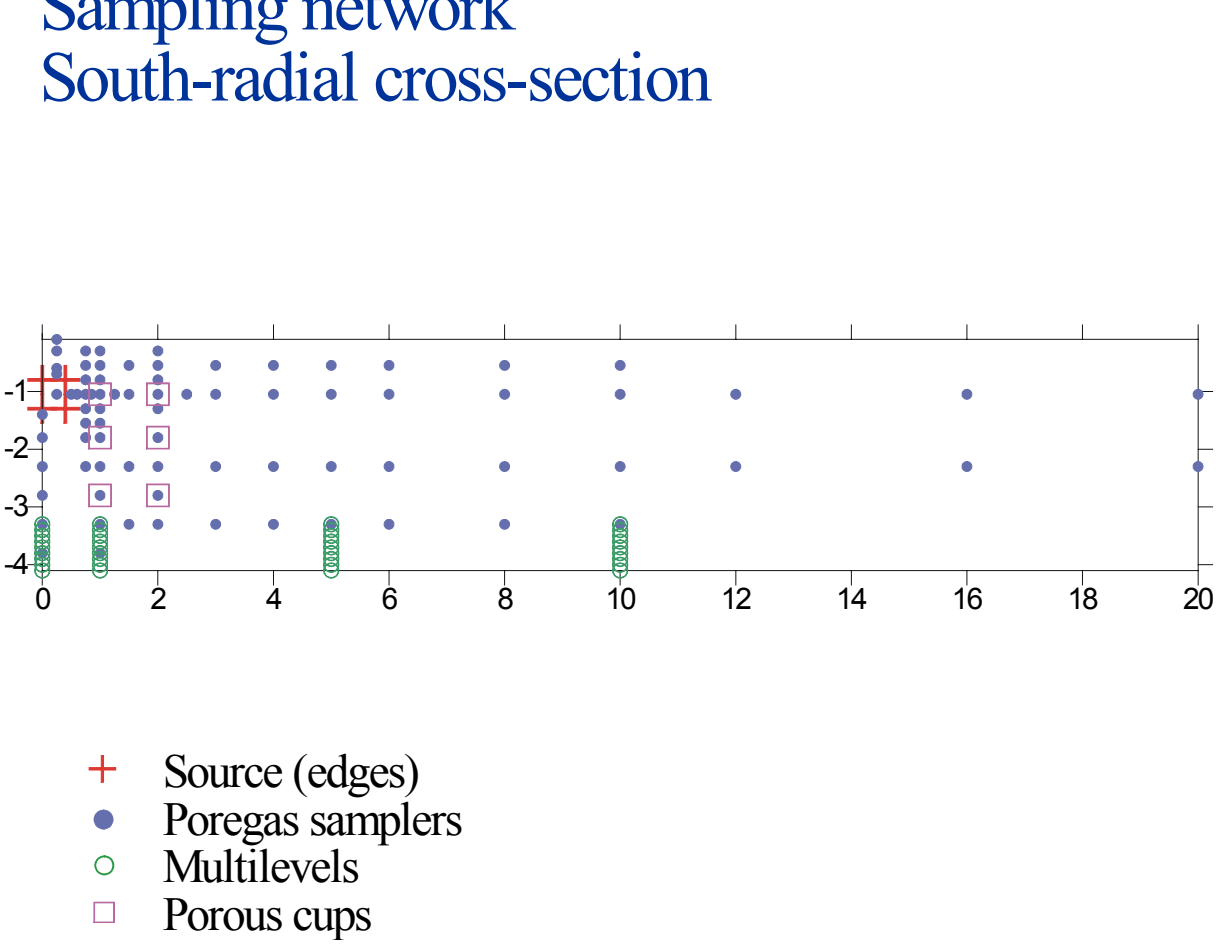

Fig. 5.2 Vertical cross-section and sampling network design of the Værløse airforce base test site (Christophersen et al., 2003).

A synthetic hydrocarbon mixture resembling jet-fuel mixed with sand was emplaced in the vadose zone (0.8-1.3 m bgs.) to form a cylindrical source of hydrocarbons. Rainwater infiltration directly above the source was prevented by a lid, in order to avoid mobilisation of the NAPL by percolating water.

Commercially available gasoline, diesel or kerosene contains several hundreds of different compounds in small percentages which are hard to determine (Gustafson, 1997). Therefore, a synthetic hydrocarbon mixture was decided on rather than a commercial product, such as, gasoline, kerosene, jet-fuel, diesel, etc. This facilitates quantitative analysis of the individual components. Commercial product compositions were reviewed, and a composition representative of kerosene or a mix of gasoline and kerosene, which would resemble aviation fuel JP4, was chosen based on a set of criteria. These included duration of the source and individual components prior to depletion, chromatographic separation, and quantification levels for individual components. Compounds representative of predominant compounds and compound types of commercial products, compounds with a range of volatilities, solubilities, and degradation potentials, and compounds of special environmental interest were included in the hydrocarbon mixture (Broholm et al., 2004). Relevant chemical and physical parameters for the kerosene compounds, selected for the hydrocarbon mixture, are given in Tab. 5.1. Henry enthalpies ΔH_{Henry} which define the temperature dependence of the

compounds were calculated from entries in the EPI-Suite database (USEPA, 1994) and are given in Tab. 5.2. 1,1,2-Trichloro-1,2,2-trifluoroethane (CFC-113) was added in a small amount as tracer known to be non-degradable under aerobic conditions (Höhener et al., 2002).

That way, the Værløse field experiment was conducted with an artificial kerosene mixture of 14 compounds in well defined composition. This provided the opportunity to build up a model accounting for the exact composition, which then could be used, as part of another study (Maier et al., 2003), to validate a grouping approach of compounds into clusters of similar physicochemical properties (Gaganis et al., 2002). Such simplification procedures are essential for modelling of realistic hydrocarbon spill scenarios.

The synthetic hydrocarbon mixture resembling jet-fuel mixed with sand was emplaced in the vadose zone (0.8-1.3 m bgs.) to form a cylindrical source of hydrocarbons. In total 10 kg (13.6 l, respectively) of NAPL were emplaced at the site. The composition of the mixture of 13 compounds and one non-degradable tracer (freon CF113) is also given in Tab. 5.1. Rainwater infiltration directly above the source was prevented, in order to avoid depletion of the most water-soluble components in the source by percolation. After termination of the measurement campaign the source was excavated in August 2002. Even though it was calculated to be at residual saturation, it had migrated downward by about 50 cm.

During the experiment the evolution in NAPL composition in the source was monitored, and pore-air, pore-water and groundwater hydrocarbon concentrations were monitored in an extensive sampling network. The dimensions of the field experiment and sampling network was designed according to previous numerical simulations using the USGS model R-UNSAT (Lahvis, 1997). The sampling strategy and network design as well as the analytical methods was described in (Christophersen et al., 2003).

Tab. 5.1. *Fuel mixture composition after source installation and physical-chemical properties of individual compounds, field experiment Værløse.*

	Compound	Weight fraction in source (%)	Density [g mL^{-1}]	Molecular Weight [g mol^{-1}]	Vapour Pressure of pure compound 25 ^{0}C [kPa]	Henrys law constant [-] 25^{0}C	Log K_{ow}	Water solubility [mg/l] 25°C
Aromatic	Benzene	1.02	0.8765	78.11	12.672[5]	0.217[3]	2.13[1]	1790[6]
	Toluene	2.93	0.8667	92.14	3.805[5]	0.244[3]	2.73[1]	556[5]
	m-Xylene	4.57	0.864	106.17	1.106[5]	0. 26[7]	3.20[1]	158[6]
	1,2,4 Trimethyl-benzene	10.99	0.8761	120.19	0.271[5]	0.28[8]	3.78[1]	57[4]
n-Alkanes	Hexane	7.26	0.660	86.17	20.20[9]	68.58[9]	4.11[11]	9.5[11]
	Octane	7.16	0.703	114.23	1.88[9]	121.0[9]	5.15[11]	0.66[11]
	Decane	15.99	0.730	148.28	0.175[9]	197.85[10]	6.25[11]	0.052[11]
	Dodecane	9.50	0.749	170.34	0.0157[9]	296.77[10]	7.24[11]	0.0037[11]
Cycloalkanes	Methyl-cyclo-pentane	5.79	0.7486	84.16	18.4[2,12]	14.8[12,17]	3.37[1]	42[15]
	Cyclo-pentane	1.59	0.7457	70.13	42.4[13]	7.6[4]	3.00[1]	156[15,16]
	Methyl-cyclohexane	10.23	0.7694	98.19	6.13[13]	17.6[14]	3.61[1]	14[16516]
Isoalkanes	Isooctane	15.36	0.692	114.2	6.56[11]	123.6[11]	4.20[19]	2.44[11]
	3-Methyl-pentane	7.45	0.664	84.16	25.3[11]	68.6[11]	3.60[11]	12.8[11]
Freon	CFC-113	0.16	1.575	187.38	44.67[17]	14.20[18]	3.16[8]	170[28]

[1] Hansch et al. (1995); [2] USEPA (1994); [3] Peng and Wan (1997); [4] Verschueren (1983); [5] Shiu and Ma (2000); [6] Montgomery and Welcom (1990); [7] Dewulf et al. (1995); [8] Hansen et al. (1995); [9] Mackay and Shiu (1981); [10] Yaws and Yang (1992); [11] Mackay et al. (1993); [12] Boublik et al. (1984); [13]Daubert and Danner (1989); [14] Hine and Mookerjee (1975); [15] McAuliffe (1966); [16] Yalkowsky and Dannenfelser (1992); [17] Yaws (1999); [18] Bu and Warner (1995); [19] Meylan and Howard (1995); [20] Dean (1985); [21] USEPA (2000); [22] Staudinger and Roberts (2001); [23] Lide (1992); [24] Milazzo (1956); [25] Williamham (1945); [27] Downing (1988); [28]Horvath et al. (1999)

Tab. 5.2 Heat/enthalpy of phase transfer determining the temperature dependence of the 14 fuel constituents used in the field experiment, obtained from EPISuite-database (USEPA, 1994). ΔH_{Henry} in [kJ/mol] and [kcal/mol] for calculation of Henry's law constant using the Van't Hoff equation.

Compound	ΔH_{Henry} [kJ/mol]	ΔH_{Henry} [kcal/mol]
Benzene	31.72	7.58
Toluene	29.94	7.16
M-Xylene	38.18	9.13
1,2,4-trimethyl-Benzene	37.85	9.05
Hexane	36.19	8.65
Octane	36.18	8.65
Decane	36.17	8.64
Dodecane	36.17	8.64
3-methyl-Pentane	36.19	8.65
iso.Octane	36.18	8.65
Cyclopentane	36.18	8.65
methyl-Cyclopentane,	36.17	8.65
methyl-Cyclohexane,	36.20	8.65
CF113	36.17	8.64

5.3 Implementation of the field parameters

The volatilisation of the kerosene source, transport and biodegradation of the compounds in the unsaturated zone was simulated using the reactive transport model MIN3P (Mayer, 1999). A pseudo-first order kinetic approach was used with respect to substrate concentration.

A number of simplifying assumptions had to be met. Microbial growth and lag time for biodegradation was not considered. Density driven gas advection and sorption was neglected in the simulations using MIN3P. Pressure gradient driven gas phase advection may be a significant transport process for compounds with high vapour pressures (early times of the experiment) in highly permeable materials such as coarse sand or gravel. Sorption was considered to be of minor relevance because the site consisted of sandy material with low f_{OC}, only the uppermost 15 cm of the soil showed higher organic fraction (Kjeldsen, 2003).

For sensitivity analysis on k, H, T, θ, groundwater recharge and transverse vertical dispersivity α_t, 1D and 2D simulations were performed and discussed in § 5.4 and 5.5. The results for the field site model discussed in § 5.6, however, were obtained by 3D simulations. For sensitivity analyses, a constant water table and steady state conditions of precipitation and temperature were assumed. In the 3D model which was used to reproduce the field measurements, all the transient data available were implemented (see § 5.6).

5.3.1 Geology

The field site has a relatively thin vadose zone consisting of 2 – 3 m glacial melt water sand with 0.3 - 0.5 m sandy mould topsoil. The

melt-water sand is underlain by 0.5 – 1 m sand till followed by a clayey till aquitard about 4 m below ground surface (m bgs.). The secondary groundwater table was located about 3 m below ground surface (Broholm et al., 2004). Site characterisation with respect to grain size distribution, geochemistry, permeability, etc. was implemented in the model as precisely as possible. The soil profile was divided into vertical layers. Approximately 50 cm of organic rich top soil showed generally higher water contents than the underlying sand. Soil physical parameters in soil samples such as the Van-Genuchten coefficients for unsaturated flow were measured at the university of Hohenheim by (LANGE, 2002). Soil properties for the model are given in Tab. 5.3, vertical cross sections of the model domains are given in Fig. 5.3.

Table 5.3 Property values assigned to the five zones of different soil types used in the field site model.

Property, model MIN3P (elevation [m] above aquifer bottom)	**Aquifer** 0 –1.8	**Soil D** 1.8 – 2.7	**Soil C** 2.7 – 3.5	**Soil B** 3.5 – 3.9	**Soil A** 3.9 - 4.0
Saturated hydraulic conductivity [ms^{-1}]	$1.2\ 10^{-4}$	$9.54\ 10^{-5}$	$9.54\ 10^{-5}$	$3.5\ 10^{-5}$	$3.5\ 10^{-5}$
Porosity [-]	0.35	0.35	0.34	0.39	0.4
van Genuchten parameters: θ_{res} [-]	0.028	0.026	0.255	0.0351	0.036
α [m^{-1}]	3.2	3.2	3.2	2.9	2.9
n	2.97	2.97	2.97	1.84	1.84

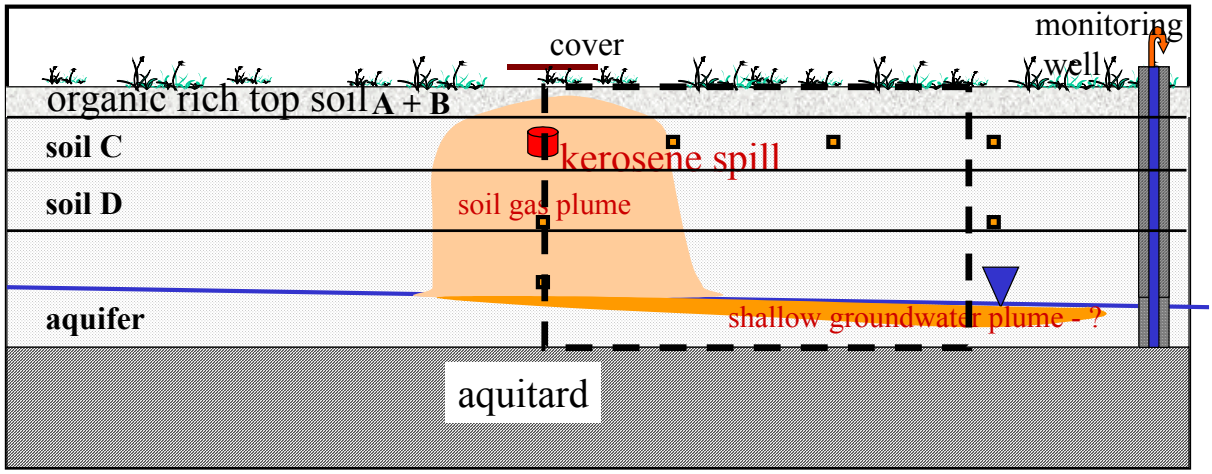

Figure 5.3 Conceptual model for the Værløse field site, Denmark, using MIN3P. Dashed line marks the extent of the 3D model domain.

5.3.2 Flow model

The hydraulic conductivity of the aquifer is $1.2{\cdot}10^{-4}$ m s^{-1} which results in groundwater flow velocities of 0.2 to 0.3 m day^{-1}. Water table fluctuations were implemented according to measured hydraulic heads. As outflux boundary condition a time-dependent constant head corresponding to a linear interpolation of a well downgradient was applied. The also transient influx boundary condition was implemented as Darcy flux calculated from the hydraulic gradient such as

$$q = K_f \, i \qquad [\text{m/s}] \qquad \text{eq. 5.1}$$

with q as the darcy flux [m/s] and i as the hydraulic gradient calculated from adjacent piezometers in flow direction. Watertable heads and gradients measured at the field site during the experiment from July 2001 to July 2002 are shown in Fig. 5.4 and 5.5.

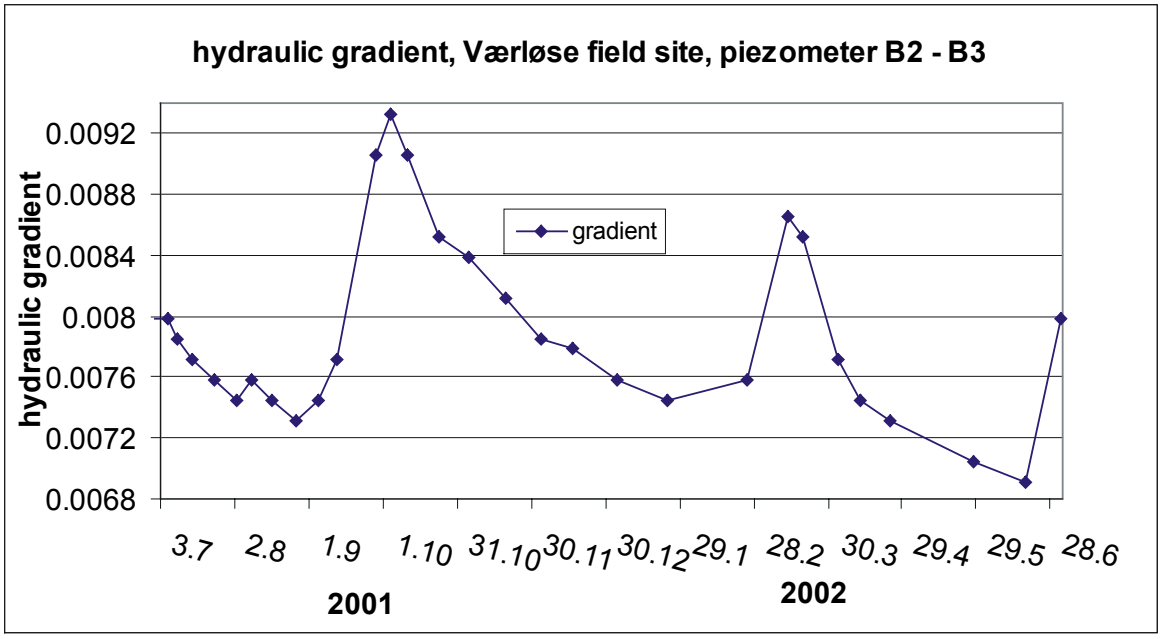

Fig. 5.4 Hydraulic gradients measured at Værløse field site from July 2001 until July 2002.

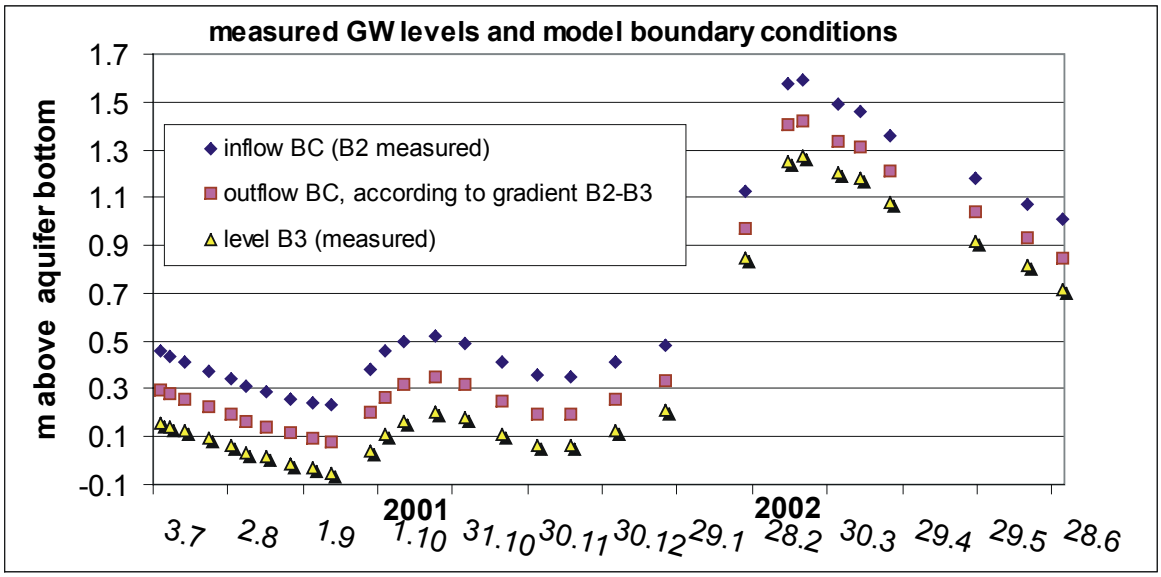

Fig. 5.5 Water table elevations measured at Værløse field site, implemented as boundary conditions into the model.

5.3.3 Climatic conditions

Henry's law constant H is defined as a temperature dependent variable in the external database of MIN3P, in a thermodynamic approach using the Van't Hoff equation (Atkins, 1990). Time and depth dependent temperature profiles can be implemented by an external input file. As daily measured

temperature and precipitation data from a meteorological station at the site as well as from a temperature datalogger in the source centre were available, one day was chosen as averaging interval for temperature T, precipitation P and evapotranspiration ET. Temperature profiles from ground surface to 3.7 m depth were also measured at the site close to the NAPL source, about 50 times during the period of investigation. Those values were interpolated to obtain daily values using the 1D finite difference diffusion model DR (§ 3.3). Measured temperatures were implemented in the 1D model as time-dependent boundary conditions for interpolation. That was possible because the process of heat conduction is analogous to diffusion and is described by the same kind of differential equations (Häfner et al., 1992). Heat conduction in soil is described by (Schachtschnabel et al., 1992)

$$\frac{\partial T}{\partial t} = \frac{\lambda}{c\rho}\frac{\partial^2 T}{\partial z^2} \qquad \text{eq. 5.2}$$

Where the lumped parameter $\lambda c^{-1}\rho^{-1}$ is refereed to as thermal diffusivity and is analogous to a diffusion coefficient. A soil typical value of $\lambda c^{-1}\rho^{-1} = 2\ 10^{-7}\ m^2s^{-1}$ was used, which provided relatively smooth curves. Temperature curves will be shown with the results in Fig. 5.21.

As intraday fluctuations in the soil are insignificant below 1 m depth (Schachtschnabel et al., 1992), one day was chosen as the averaging interval. Influence of soil temperature was investigated in 1D and 2D in a first cycle neglecting temperature dependence of biodegradation. In a second approach, the rate constant was doubled with an increase in 10°C as a rough estimate of temperature dependence. However, for 3D modelling of Værløse field experiment, the dependency of biodegradation on a time- and space-dependent soil temperature field could not be considered. The field site model provides comparability to measured data and was chosen to assess the influence of temporal variability of meteorological parameters.

Precipitation and evapotranspiration were implemented as transient boundary conditions with daily average values in MIN3P. That way, infiltration and soil water contents were calculated by the model using the Van-Genuchten approach for variably saturated flow. Potential evapotranspiration ET_{Pot} was calculated according to Haude (Hölting, 1992), using the equation

$$ET_{Pot} = x\ P_{14}\ (1-F_{14}/100) \text{ in [mm/day]} \qquad \text{eq. 5.3}$$

Where x is a tabulated monthly coefficient, P_{14} is the saturated water vapour pressure at 2 p.m., and F_{14} is the relative humidity at 2 p.m. If potential evapotranspiration would exceed the actual soil water content, the model does not converge. In such cases, the ET applied was corrected to account for actual evapotranspiration. Transient behaviour of soil water content calculated that way agreed to TDR measurements close to the site (Fig. 5.6), which were calibrated using gravimetric soil water contents. Water mass and water balance during the 350 day simulation in the 3D field site domain are shown in Fig. 5.7. Periods of longer groundwater recharge during the winter is indicated as continuous outflux, whereas the more discrete outflux events are attributed to significant evapotranspiration in the summer months.

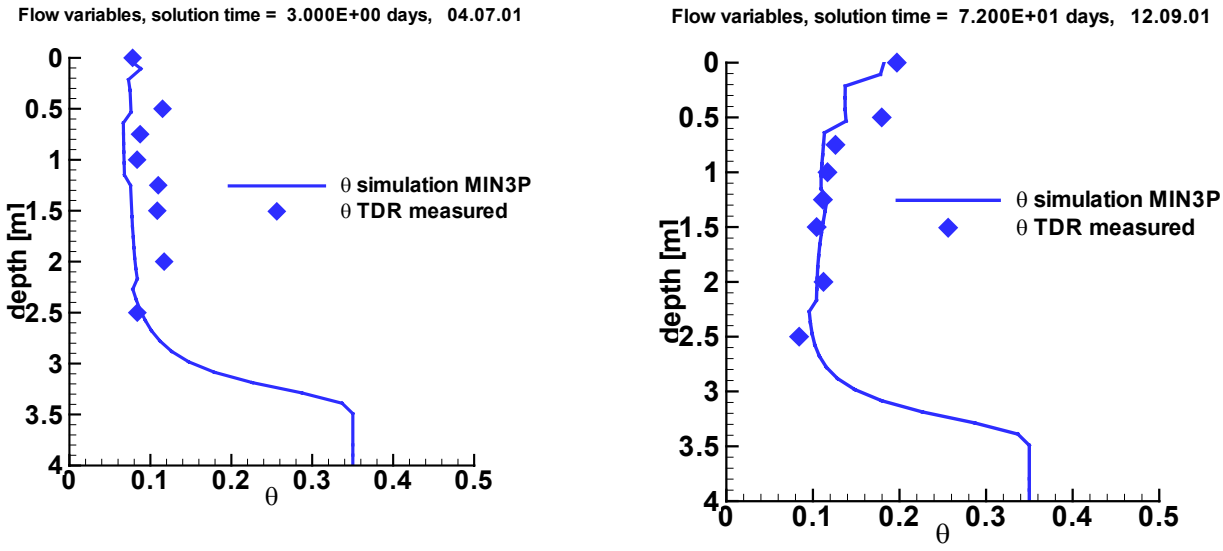

Figure 5.6 Soil moisture profile at day 3 and at day 72 of the experiment, simulated using MIN3P and experimentally determined from TDR measurements.

.

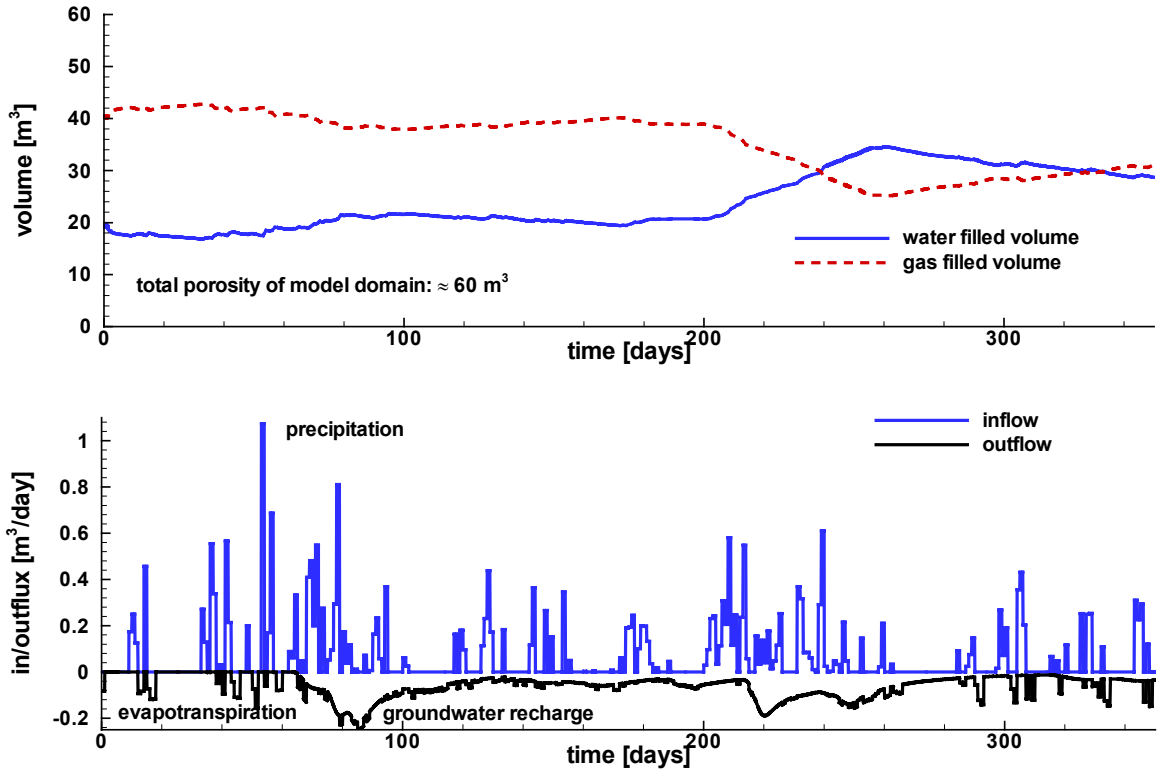

Fig. 5.7 Water and air filled pore volume during the 350 day 3D simulation and water balance contributions of precipitation (influx), evapotranspiration and groundwater recharge (outflux). The discrete outflux events are evapotranspiration, the continuous periods are due to groundwater outflux caused by recharge.

5.3.4 Geochemical system

Vapour phase diffusion acts as the most important transport process in the unsaturated zone. Diffusion coefficients used were $8 \cdot 10^{-10}$ m^2 s^{-1} in the aqueous phase and $7.3 \cdot 10^{-6}$ m^2 s^{-1} in the gaseous phase. The hydrogeochemical system of volatilisation and biodegradation of fuel phase in the unsaturated soil zone includes dissolution-volatilisation reactions of the fuel constituents, air-water partitioning, acid-base reactions due to infiltration of rainwater and production of carbon dioxide (equilibrium reactions) and the microbially driven redox reactions of the hydrocarbon degradation which require a kinetical formulation. All the compound specific parameters used in the caculations (Tab. 5.1) are defined in the external database of MIN3P. As Henry's law constant *H* is temperature dependent, also the enthalpies of phase transfer (Tab. 5.2) are defined in the database and will be automatically updated by the model according to the Van't Hoff equation (eq. 2.24) whenever temperature *T* changes at a certain location. Reaction kinetics were defined as quasi first order with a fractional order term of order one with respect to the substrate. Threshold values for oxygen below which the aerobic reactions cease were 10^{-6} mol/l, or 0.03 mg/l, respectively. The reaction equations were derived for implementation in the database of the numerical model MIN3P. The equations for aerobic degradation of the 14 fuel constituents are for:

Benzene:

$C_6H_6 + 7.5\ O_2 + 3\ H_2O \rightarrow 6\ CO_3^{2-} + 12\ H^+$

Toluene:

$C_7H_8 + 9\ O_2 + 3\ H_2O \rightarrow 7\ CO_3^{2-} + 14\ H^+$

m-Xylene:

$C_8H_{10} + 10.5\ O_2 + 3\ H_2O \rightarrow 8\ CO_3^{2-} + 16\ H^+$

1,2,4-tri-methyl-Benzene:

$C_9H_{12} + 12\ O_2 + 3\ H_2O \rightarrow 9\ CO_3^{2-} + 18\ H^+$

Hexane:

$C_6H_{14} + 9.5\ O_2 + H_2O \rightarrow 6\ CO_3^{2-} + 12\ H^+$

Octane:

$C_8H_{18} + 12.5\ O_2 + H_2O \rightarrow 8\ CO_3^{2-} + 16\ H^+$

Decane:

$C_{10}H_{22} + 15.5\ O_2 + H_2O \rightarrow 10\ CO_3^{2-} + 20\ H^+$

Dodecane:

$C_{12}H_{26} + 18.5\ O_2 + H_2O \rightarrow 12\ CO_3^{2-} + 24\ H^+$

3-methyl-Pentane (iso-Hexane): (equals Hexane)

Iso-Octane: (equals Octane)

Cyclo-Pentane:

$C_5H_{10} + 7.5\ O_2 \rightarrow 5\ CO_3^{2-} + 10\ H^+$

Methyl-cyclo-Pentane:

$C_6H_{12} + 9\ O_2 \rightarrow 6\ CO_3^{2-} + 12\ H^+$

Methyl-cyclo-Hexane:

$C_7H_{14} + 10.5\ O_2 \rightarrow 7\ CO_3^{2-} + 14\ H^+$

The freon CF113 was considered as a non reactive tracer and no reaction was defined. Carbonate speciation equilibrium of H_2CO_3, HCO_3^- and CO_3^{2-} are considered as seconary aqueous species depending on pH in the model.

Considering potential anaerobic scenarios, nitrate and sulphate could be neglected as electron acceptors due to the small equivalent mass input from the atmosphere, mainly due to acid rain and agricultural input (Scheffer & Schachtschnabel, 1992). Reduction of iron (III) requires the presence of a high fraction of iron oxide in the soil, which can be depleted for longer lasting sources. Methanogenetic biotransformations, however, are independent of external supply of electron acceptors. Thus, the conditions required for methanogenesis at Værløse field site were evaluated.

For anaerobic degradation the example of benzene is described here briefly. Anaerobic reactions of other compounds were not considered after it was proven to be not very significant as evaluated for benzene. Benzene oxidation by denitrification proceeds:

$C_6H_6 + 6\ NO_3^- \rightarrow 6\ CO_3^{2-} + 3\ N_2 + 6\ H^+$

Benzene oxidation by manganese oxide (Pyrolusite) dissolution is given by:

$C_6H_6 + 15\ MnO_2 + 18\ H^+ \rightarrow$

$6\ CO_3^{2-} + 15\ Mn^{2+}\ 12\ H_2O$

Benzene oxidation by iron oxide dissolution (Goethite) is denominated by:

$C_6H_6 + 30\ FeOOH + 48\ H^+ \rightarrow$

$6\ CO_3^{2-} + 30\ Fe^{2+}\ 42\ H_2O$

Benzene oxidation by sulphate reduction is:

$C_6H_6 + 3.75\ SO_4^{2-} + 3\ H_2O \rightarrow$

$6\ CO_3^{2-} + 3.75\ HS^- + 8.25\ H^+$

Methanogenesis from benzene proceeds according to:

$C_6H_6 + 6.75\ H_2O \rightarrow$

$2.25\ CO_3^{2-} + 3.75\ CH_4 + 4.5\ H^+$

Oxidation of methane is formulated:

$CH_4 + 2\ O_2 \rightarrow H_2O + CO_3^{2-} + 2\ H^+$

5.3.5 Numerics

The numerical model MIN3P (Mayer et al., 2002) was used for sensitivity analyses as well as for reproduction of the measured vapour phase plume and source evolution at Værløse field site in 3D. The code allows for the calculation of vapour phase transport, using the approach of Millington (1959), and unsaturated flow in the vadose zone (Richard's equation). The dissolution or degassing an organic compound mixture is simulated applying Raoult's law. Equilibrium partitioning between aqueous and gas phase is implemented according to Henry's law. Biogeochemical reactions and transport processes are coupled by a global implicit solution method and solved using a finite volume algorithm. A variable number of geochemical compounds and reactions, such as biodegradation processes, can be handled based on an external database derived from the geochemical equilibrium model MINTEQ (Allison et al., 1991). Transient boundary conditions and time and depth dependent soil temperature profiles can be applied in the simulations. That way, data measured at the site could be directly implemented in the model. A short overview of model capabilities and computational properties of the field site model using MIN3P is presented in Tab. 5.4.

Table 5.4. Compilation of model and numerical parameters of MIN3P.

Item	MIN3P
Solution method	Finite Volume Method
3D realisation	Full 3D cartesian
Transition from unsaturated to saturated zone	Full 3D
Number of compounds	Variable, limited by RAM
Computation requirements	1 Gbyte RAM, runtime several days (1.3 GHz CPU)
Mobile phases	Aqueous phase
3D domain dimension	6.5 m

The model was run accounting for 17 chemical compounds (13 kerosene constituents, the tracer CFC-113, and biodegradation reactants CO_2, O_2 and H^+). A vertical discretisation of $\Delta z = 10$ cm was used. In the sensitivity analyses a 20 extension of the model domain in flow direction was applied, with the kerosene source in the center, using a horizontal discretisation of $\Delta x = 20$ cm. For this grid spacing, accuracy was proven. Maximum extension of the 3D domain in flow (x) and y direction was 6.5 m. A 40 x 17 x 17 block grid was used. Grid size was constrained by the memory limitation of one Giga-Byte on the available PC, thus a compromise between accuracy and computational capability had to be found. Although the global implicit coupling of transport and reaction PDE's in MIN3P is responsible for the memory limitation, it maintains accuracy of transport even for longer timesteps and allows for still acceptable run-times. In times of increasing

computational power and memory capacity, however, the given restrictions will lose their relevance in the near future (Mayer, 1999). CPU times for the 3D model were between 40 hours for a system with steady state water table and 120 hours with water table fluctuations included.

It could be shown by variation of boundary conditions, that the domain extent was sufficient to account for the unsaturated zone mass balance and for the accuracy of concentrations at the sampling ports one and two meters lateral from the source. Variation of boundary conditions means that the model was run with a atmospheric concentration boundary and zero gradient, respectively, at the lateral boundaries. The results of the two simulations with otherwise same conditions were compared and yielded sufficient agreement

To further reduce required memory, the domain was split into four different parts by applying symmetry boundary conditions (zero gradient) through the source centre in x- and y-direction. Then, for only one of the parts the simulation was run. This strictly applicable to the unsaturated zone only. Possible deviations concerning groundwater and transport, which are not symmetrical in flow- (x) direction are discussed with the results for groundwater.

Biodegradation rate constants (pseudo first order with respect to the substrate concentration) were used as the only adjustable parameter in the unsaturated zone. Transverse vertical dispersivity α_t was adjusted to approach groundwater concentrations realistically. Due to long CPU run times of several days, simple eyeball fitting was applied comparing measured and simulated concentration time series at sampling ports below and one and two meters laterally from the kerosene source in a trial and error procedure. In total, about 15 runs were performed for the unsaturated zone and 5 for groundwater. Main focus was drawn on fitting the early 100 days (peak concentrations). Only simulations that fitted well in the beginning were continued.

5.4 Results of the sensitivity analyses – unsaturated zone

5.4.1 Sensitivity on biodegradation rate constant

Sensitivity analysis on k was performed in 2D using uniform rate constants of pseudo first order with respect to the substrate (contaminant) concentrations, for all the compounds between 10^{-3} and 10^{-6} per second (86 and 0.086 day^{-1}, respectively). A run with $k = 0$ was performed as well.

Significant differences between the compounds with respect to mass balance contributions could be observed. Sensitivity on k depends strongly on Henry's law constant H. For the kerosene compounds H ranges between 0.1 and 0.3 for BTEX, between 4 and 15 for the cyclo-alkanes and above 100 for most of the n- and iso- alkanes. High H compounds require very high k to become efficiently degraded (see alkanes, Fig. 5.8), whereas low H compounds like BTEX (see BTEX in Fig. 5.8), show a high percentage of depletion for much lower k. Volatilisation to the atmosphere is inversely correlated to biodegradation as indicated in Fig. 5.9. Both together, flux to the atmosphere and biodegradation make up the great majority of contaminant mass fate.

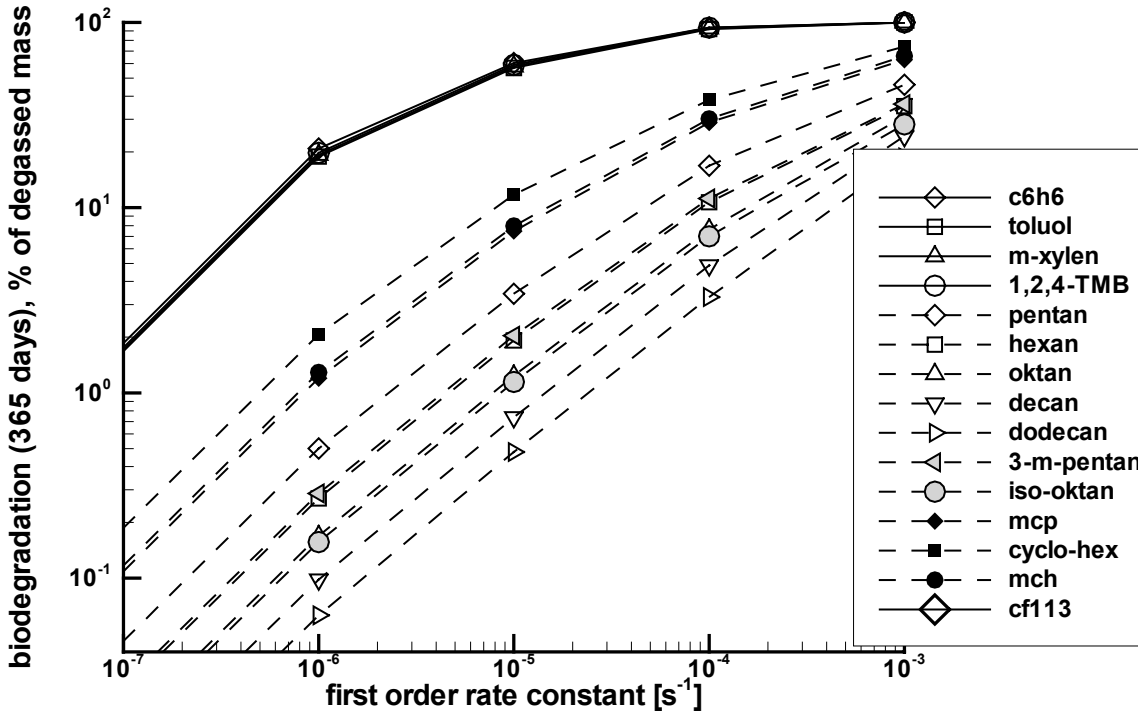

Fig. 5.8 Sensitivity of overall biodegradation rates after one year on biodegradation rate constant in terms of cumulated biodegradation (B) in % of mass volatilised from the NAPL source.

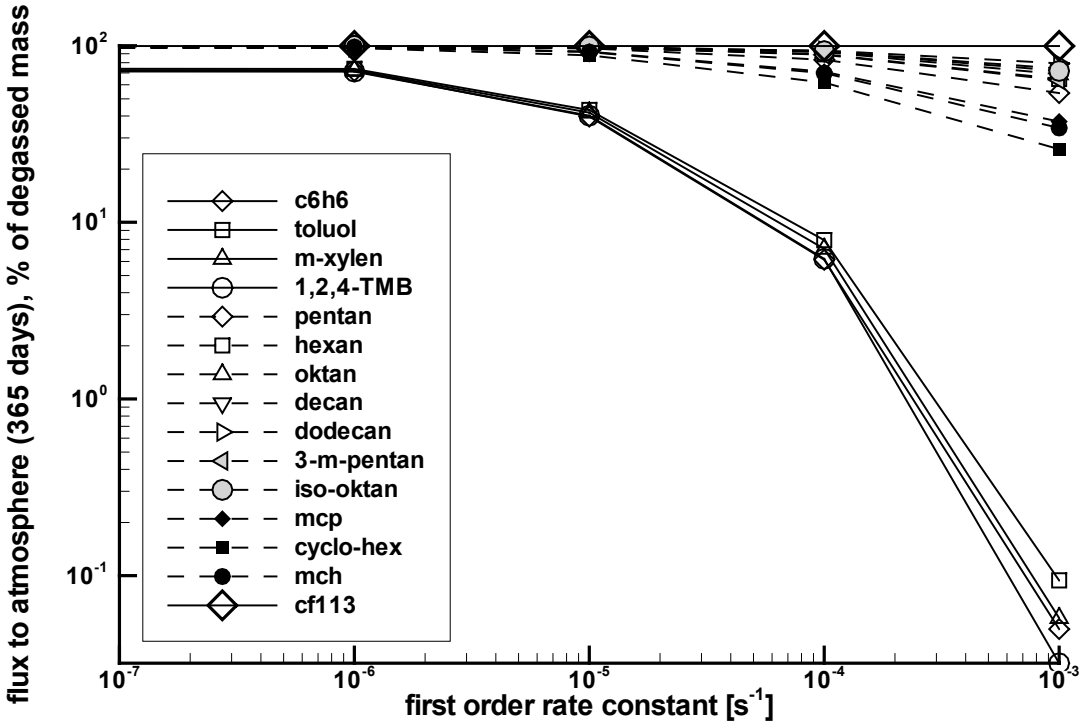

Fig. 5.9 Sensitivity of volatilisation to the atmosphere after one year on biodegradation rate constant in terms of cumulated flux to the atmosphere (A) in % of mass volatilised from the NAPL source.

Depletion of NAPL phase mass was completed for high volatile compounds before the time span of one year. Bioenhanced phase depletion is therefore especially interesting for the lower volatile compounds. For these, assuming a constant *k*, also low *H* compounds, such as xylene and tri-methyl-benzene, show most effective enhancement. Intermediate enhancement is observed for iso-octane, octane and methyl-cyclo-hexane, smaller enhancement for decane and dodecane (Fig. 5.10). The bioenhancement of NAPL-phase depletion at the field scale for Værløse field experiment is discussed in Broholm et al, 2003.

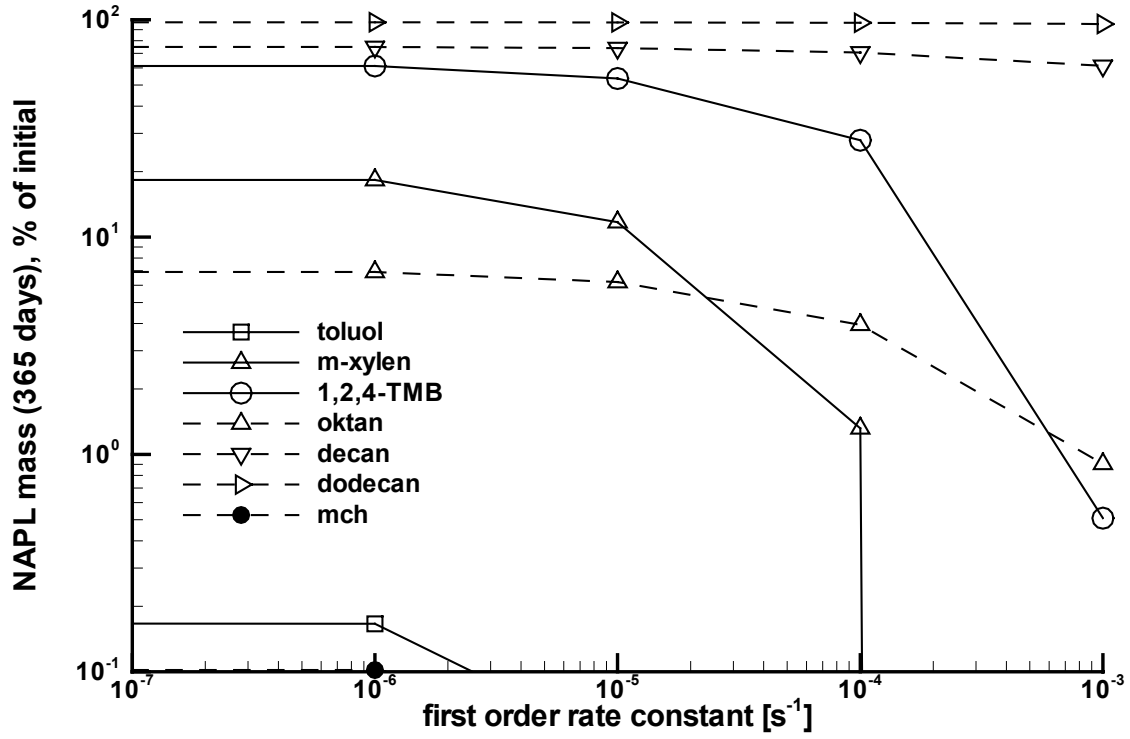

Fig. 5.10 Sensitivity of NAPL mass after one year on first order biodegradation rate constant in terms of mass left in NAPL phase (N) in % of initial mass in the NAPL source.

5.4.2 Sensitivity on Henry's law constant

The ratio of volatilisation to the atmosphere to biodegraded mass versus *H* at a constant degradation rate constant (pseudo first order) of 10^{-5} and 10^{-6} s^{-1} (0.86 and 0.086 day^{-1}, respectively) is shown in Fig. 5.11. It emphasises the observation described above, that low *H* compounds degrade more efficiently. This can be explained by the greater amount of the compound remaining in the aqueous phase for low *H*, which enhances the exposure of the compound to the biodegrading community. At the same time diffusive transport in the gaseous phase will be retarded. In the multiphase system of the soil, biodegradation is considered to take place only in the aqueous phase.

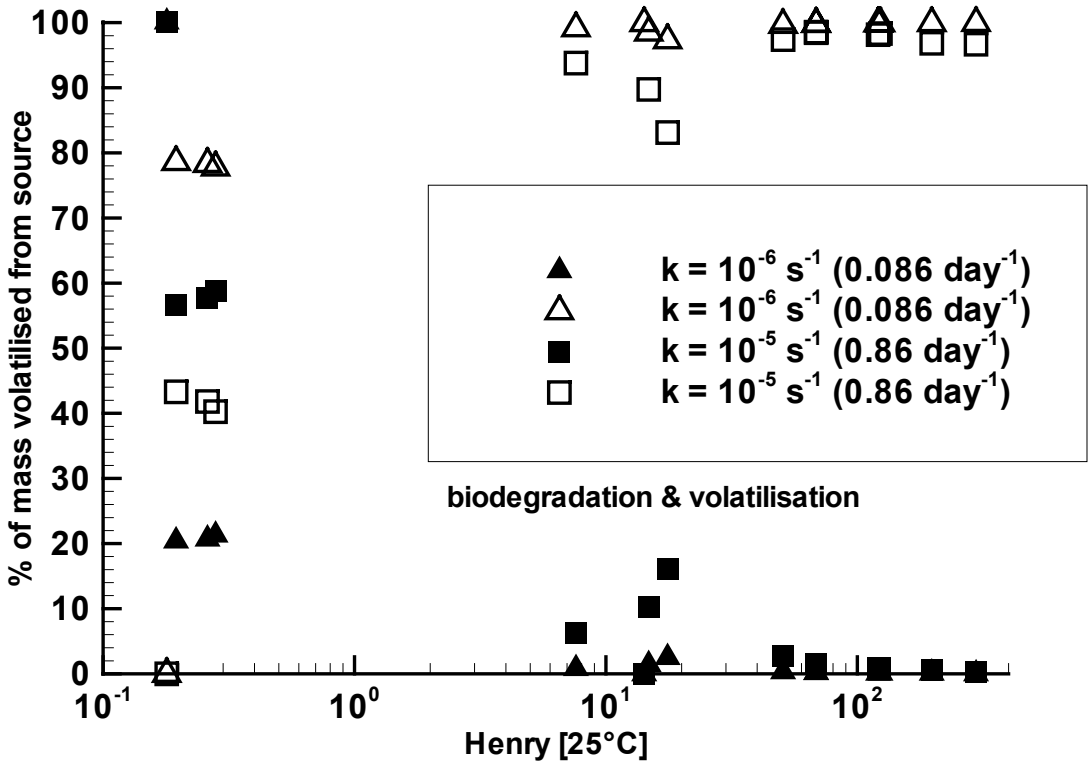

Fig. 5.11 Ratios of total volatilisation to the atmosphere (A, open symbols) and biodegradation (B, full symbols) depending on Henry's law constant H for two different rate constants.

5.4.3 Temperature

If only temperature dependency of vapour pressure and diffusion coefficients are considered, higher temperatures enhance the volatilisation of the NAPL phase and lead to more rapid degassing to the atmosphere. Biodegraded fraction of the already degassed compound (B) in that case, however, decreased with increasing temperature for all the compounds and can be halved for the very volatile compounds if T increases from 5 to 25°C. A steep decrease in remaining NAPL phase could be observed for most compounds, except the very low volatile ones. For three compounds (MCH, toluene and iso.octane) which would remain within the NAPL phase to more than 10 % of their initial mass at 5°C, a temperature of 25°C results in efficient depletion.

If k is a function of T, temperature dependence of B becomes weaker, but still showing slightly decreasing net biodegradation (B) with increasing T between 5 and 25°C for most compounds. This indicates that the relative fraction of B versus A remains relatively constant as a function of T. On the other hand, the total contaminant mass consumption due to both, A and B increases significantly with temperature. Thus, phase depletion is accelerated at higher temperature. Fig. 5.12 shows N as a function of temperature using k = 2.0, 1.0 and 0.5 10^{-5} s^{-1}, respectively.

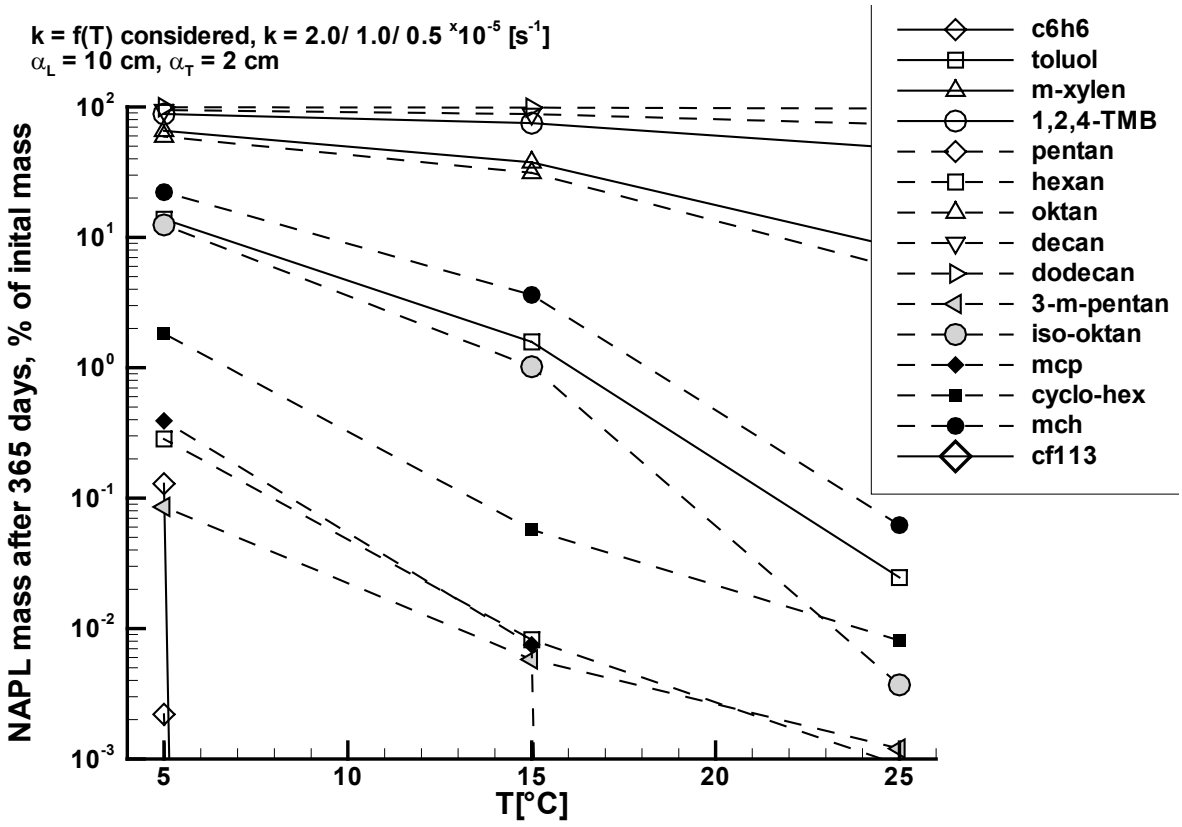

Fig. 5.12 Sensitivity of NAPL mass after one year on tempertature in terms of mass left in NAPL phase (N) in % of initial mass in the NAPL source.

5.4.4 Soil water content

As long there is no oxygen limitation, increasing soil water contents increased biodegradation on the expense of degassing to the atmosphere (Fig. 5.13). This effect was found to be emphasised for compounds with intermediate Henry's law constants, such as cyclo-alkanes or iso-alkanes, but also the light n-alkanes, which, for low water saturation, undergo only minor biodegradation. The maximum increase was found for 3-methyl-pentane with 7-fold (1.5-11 %), pentane and hexane 6-fold (2.5-16 and 1.5-10 %, respectively), methyl-cyclo-pentane 5-fold (6-30 %) and cyclo-hexane 4-fold (from 10-40%), for an increase in water saturation from 8.5 to 40 %. The biodegradation of very high H compounds does not respond on θ very much, whereas low H compounds are efficiently degraded even at low θ. This is caused by the larger fraction of mass present in the pore water for high θ as well as for low H.

High soil water content prolongs the time of NAPL depletion. An increase of soil water saturation from 20 to 40 % doubled the time until depletion of the nondegradable tracer CF113 in the source because of lower effective diffusion coefficients in the gaseous phase.

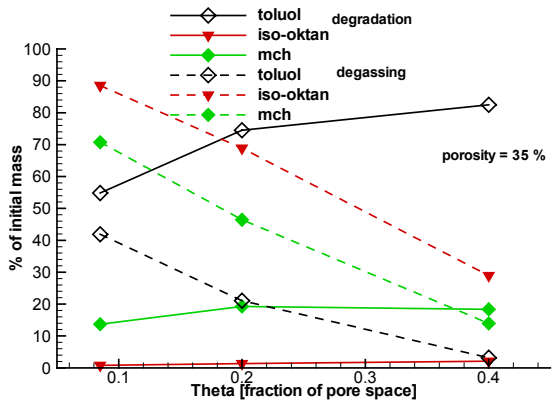

Fig. 5.13 Sensitivity of biodegradation (B) and volatilisation to the atmosphere (A) on biodegradation rate constant.

For compounds, which are also subject to biodegradation, oxygen availability also has to be considered. Once high water saturations impede oxygen delivery and anaerobic conditions establish, the situation becomes more complex, because anaerobic biodegradation is much less efficient.

5.4.5 Oxygen limitation

The conditions for which an anaerobic subsurface environment would establish at the Værløse field experiment were evaluated.

In a 1D scenario there is no lateral possibility for oxygen supply and anaerobic conditions can develop quickly, but this scenario is not very realistic. For a 2D model, the values required for methanogenesis at the field site are constant volumetric water content θ greater 14 % (with n = 35 %, a benzene fermentation rate constant of $7.8^{x}10^{-6}$ mg $l^{-1}s^{-1}$ zeroth order, a methane oxidation rate constant of 10^{-5} s^{-1} pseudo first order, and an inhibition threshold of 0.03 mg/l oxygen). The NAPL source in this scenario contained only benzene, which is relatively water soluble and fast degassing i.e. rapidly consuming oxygen. For this condition, small concentrations of methane (< 1 % Vol.) develop at the capillary fringe below the NAPL source (Fig. 5.14). If the soil water content is increased even higher, the zone of methane formation moves closer up to the NAPL source due to faster oxygen depletion and restricted diffusive transport.

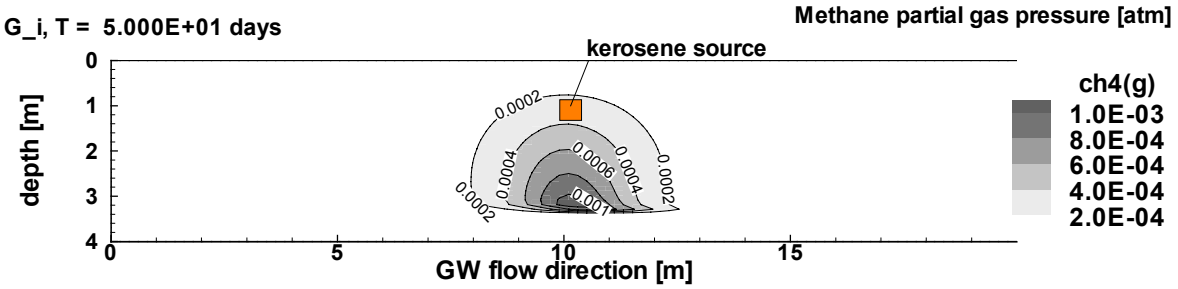

Fig. 5.14 Methane partial gas pressure in a 2D model with elevated θ of 14 %. Maximum concentrations were simulated about 50 days after source installation.

For the kerosene composition used in the experiment, however, oxygen depletion could not be achieved in the model for realistic water contents. Field data from Værløse site also showed no significant oxygen depletion at the NAPL source. Thus, anaerobic conditions can be excluded for the Værløse field experiment.

5.4.6 Groundwater recharge

The biodegraded fraction remains almost unaffected by groundwater recharge. NAPL depletion is somewhat enhanced by higher groundwater recharge with a maximum of 2 – 3 % stronger depletion after one year for the

lower volatile compounds. The volatilisation to the atmosphere is diminished between 1 and 2 % for alkanes if groundwater recharge rises from zero to 720 mm/year. The BTEX compounds show a little more emphasised response, A is decreased less than 10 % for the given difference in groundwater recharge. Comparing all the mass balance contributions, groundwater recharge is a minor factor for groundwater risk assessment regarding VOC's.

5.5 Results of the sensitivity analyses – transport to groundwater

5.5.1 Biodegradation rate constant and Henry's law constant

There is a very strong influence of *k* on the mass transport to groundwater. For the compounds with lowest *H*, the BTEX, a decrease in *k* from 10^{-3} to 10^{-6} per second, lead to an increase in contaminant outflux in groundwater by eight orders of magnitude (for α_t = 0.1 mm), even though the maximum values are only several percent of the total volatilised mass. Although a rate constant of 10^{-3} s^{-1} is a very high value (~ 100 day^{-1}), this emphasises the importance to quantify biodegradation. In the same setup, groundwater outflux increased by 6 orders of magnitude for cyclo-alkanes, by 4.5 orders of magnitude for average n-alkanes with an minimum for dodecane of 3.5 orders of magnitude (Fig. 5.15). Whereas BTEX have a maximum sensitivity already at small *k* around one per day, cyclo-alkanes reach their maximum sensitivity at about 10^{-4} s^{-1} and the n- and iso-alkanes become only sensitive for very high *k* above 10^{-3} s^{-1}. Biodegradation, thus, efficiently prevents transport to groundwater, especially for compounds with low *H*.

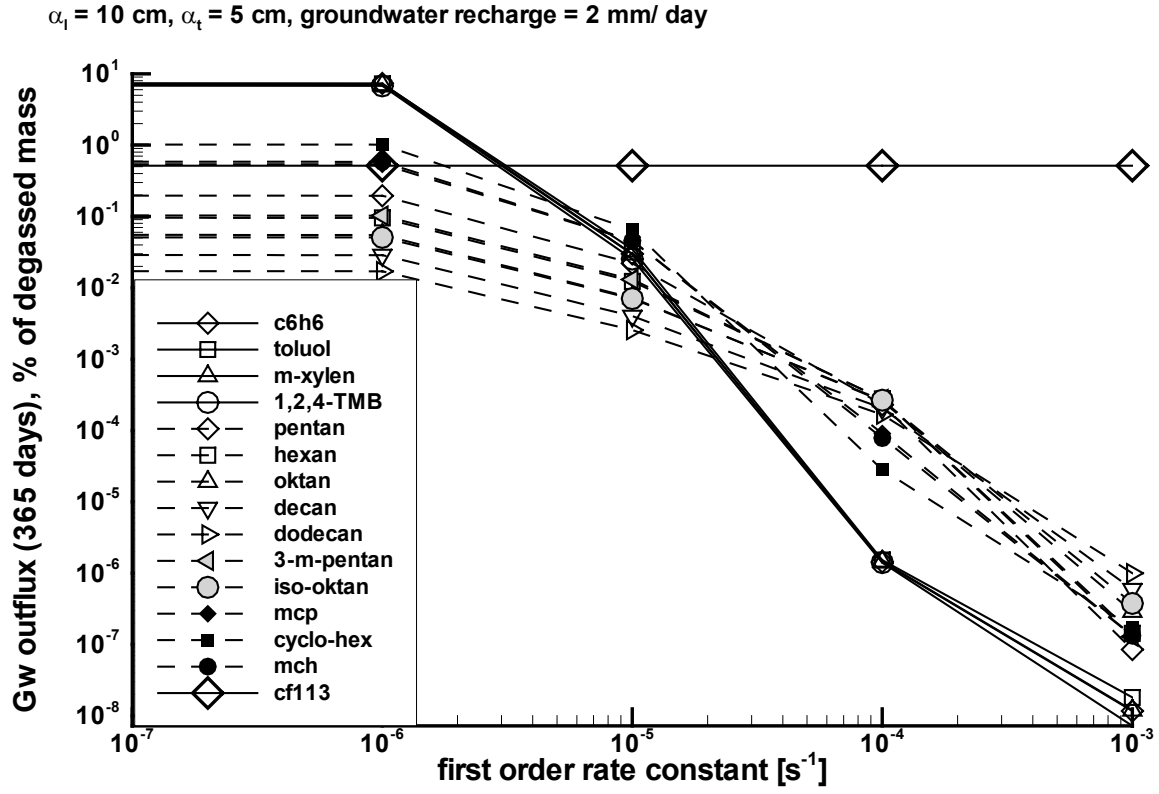

Fig. 5.15 Sensitivity of contaminant transport to groundwater on biodegradation rate constant in terms of cumulated flux out of the model domain (G) in % of mass volatilised from the NAPL source.

5.5.2 Temperature

Regarding the non-degradable (but also highly volatile) tracer CF113 as a reference, contaminant transport to groundwater will be diminished by a factor of about 2, if temperature rises from 5 to 25 °C, probably due to faster degassing to the atmosphere. If diffusion coefficient and vapour pressure only are affected by temperature, groundwater contamination decreases even less for most of the other compounds. The cyclo-pentanes, then remain almost unaffected. For BTEX, in contrast, G is enhanced by a factor between 10 and 15 for rising temperature (Fig. 5.16).

If biodegradation rate constant is doubled by temperature increase of 10°C, the situation changes totally (Fig. 5.17). For most alkanes, G decreases by one order of magnitude, but for BTEX even by 3 orders of magnitude if temperature rises from 5 to 25 °C. Considering that the latter scenario is more realistic, groundwater will be generally less vulnerable at higher temperature, i.e. during the summer months. On the other hand this result also emphasises the role of biodegradation as a factor to be quantified in the vadose zone.

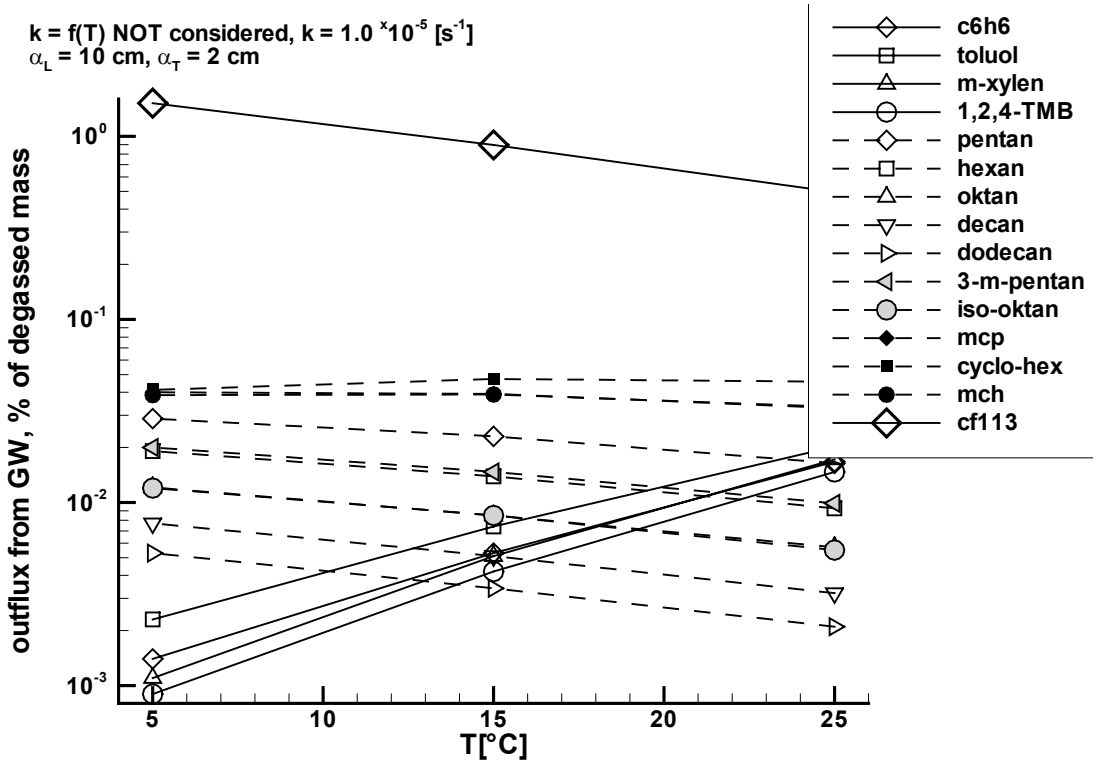

Fig. 5.16 Sensitivity of contaminant transport to groundwater on tempertature in terms of cumulated flux out of the model domain (G) in % of mass volatilised from the NAPL source. Biodegradation as function of temperature.

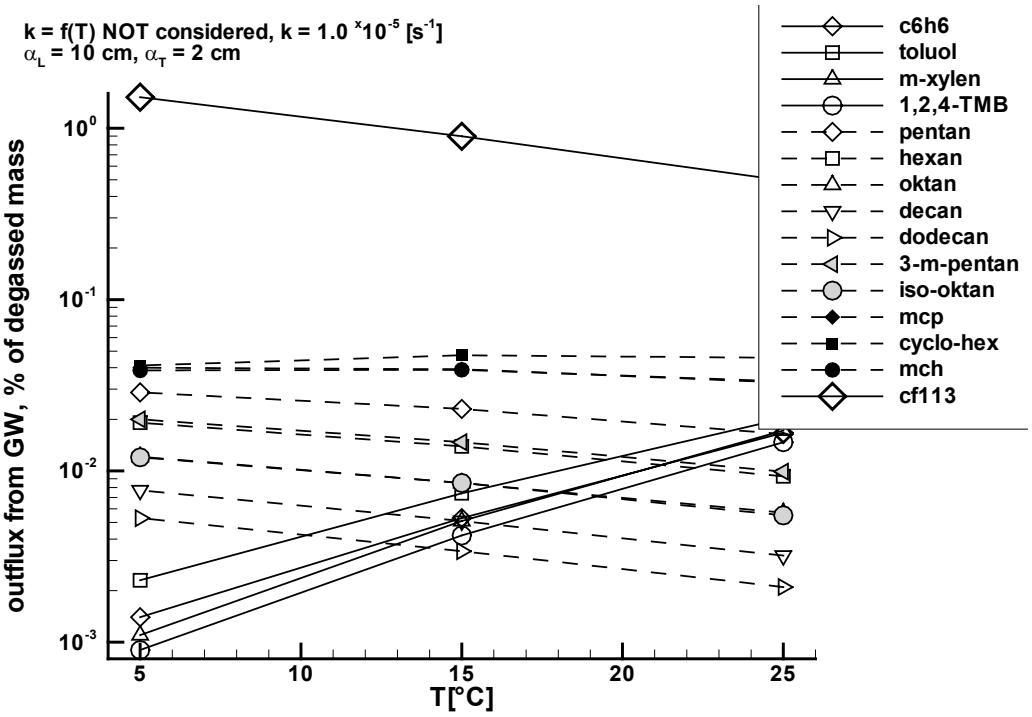

Fig. 5.17 Sensitivity of contaminant transport to groundwater on tempertature in terms of cumulated flux out of the model domain (G) in % of mass volatilised from the NAPL source. Biodegradation independent of temperature.

5.5.3 Soil water content

For the nondegradable tracer CF113, an increase in θ from 8.5 to 40 % aqueous saturation leads to a 4 fold increase in G (from 0.03 to 0.12 %). In contrast, the cyclo-pentanes as well as BTEX show a 3-5 fold decrease in G. The decrease for BTEX is especially emphasised between S = 0.85 and 0.2. N-alkanes and iso-octane show only weak sensitivity on θ in this range. These findings can be explained by the different sensitivity of the compounds on biodegradation. The BTEX and also cyclo-alkanes have low or intermediate *H* and therefore become efficiently captured in the pore water if the moisture content rises, which again enhances their biodegraded portion. High *H* compounds remain mostly unaffected. For low or intermediate H compounds which are not biodegraded, such as the tracer, the presence in the pore water results in the opposite effect as for the BTEX and leads to enhanced transport to groundwater. Again, Henry's law constant and its interaction with biodegradation reveals a crucial coherence.

5.5.4 Groundwater recharge

For all the volatile compounds, groundwater recharge was found to have only minor influence on the percentage transported to the saturated zone. An increase in infiltration from zero to 720 mm/year enhanced the transport to groundwater only by 10 to 25 % for most of the compounds (Fig. 5.18). It should be noted that this amount is within the sampling and analytical error or uncertainty of parameters. The low *H* compounds such as BTEX, which were suspected to be more sensitive on that, were more efficiently degraded due to slightly higher soil water contents and transport to groundwater was therefore also only slightly enhanced. Consistent with previous studies (Klenk and Grathwohl, 2002,Pasteris et al.,

2002), groundwater recharge is a significant contaminant pathway only in soils with high water content and for compounds with low Henry's Law constants (e.g. MTBE in silt or clay).

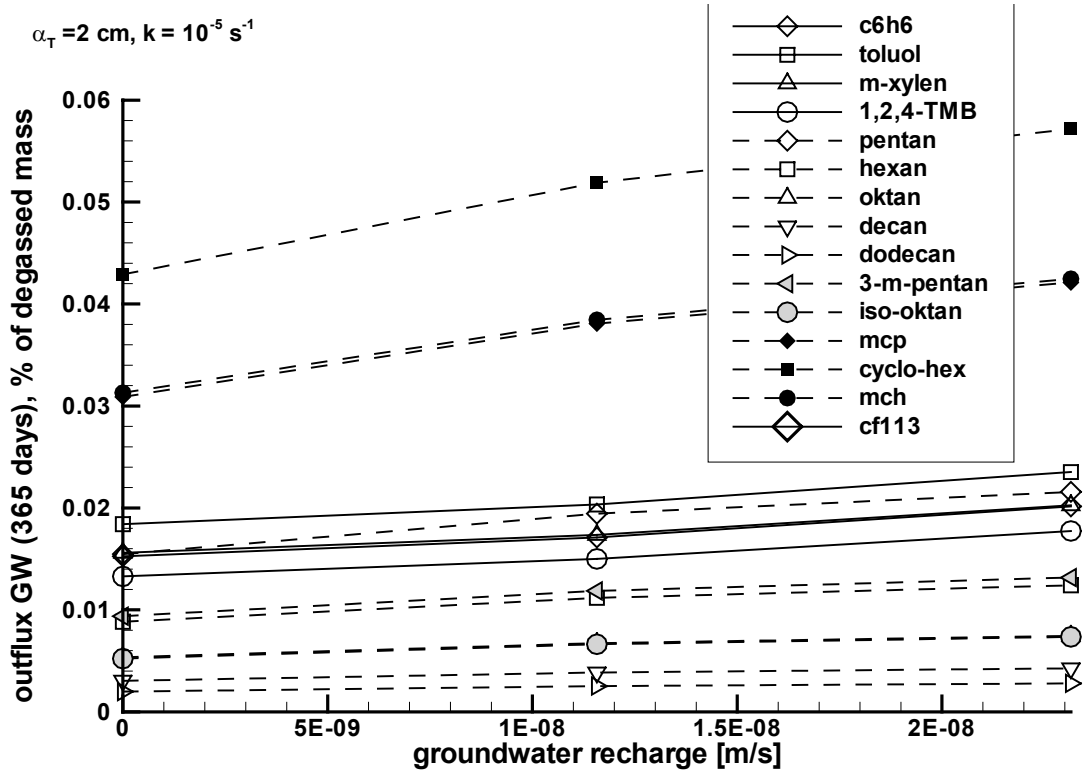

Fig. 5.18 Sensitivity of contaminant transport to groundwater on groundwater recharge in terms of cumulated flux out of the model domain (G) in % of mass volatilised from the NAPL source.

5.5.5 Transverse vertical dispersivity

The sensitivity analyses on the unsaturated zone behaviour indicate that some of the parameters that control mass balance the vadose zone also have a strong influence on mass flux to groundwater. Vertical dispersivity, in contrary, controls mixing in flowing groundwater and is negligible to unsaturated zone transport. Contaminant mass transfer to groundwater was compared between values of transverse vertical dispersivity α_t of 0.1 mm and 10 cm using the model MIN3P.

For the hypothetical case of no biodegradation, the groundwater mass outflux from the model domain was uniformly increased about 3-fold for all the compounds for the increases in α_t of four orders of magnitude and reached maximum levels above 10 % of degassed mass for the BTEX compounds (Fig. 5.19). For the alkanes, the outflux from groundwater starts to drop again if α_t > 2 cm. This is attributed to backward volatilisation of the compounds into the unsaturated zone downgradient of the source zone. For compounds with lower H this effect does not occur in the given ranges of α_t.

If a uniform biodegradation rate constant of 10^{-5} s^{-1} (little less than 1 day^{-1}) was applied for all the compounds, mass outflux from groundwater (G) was significantly enhanced for higher α_t. It should be noted, however, that G generally remained on a low level of below one per mil of the total degassed mass. G was increased for the BTEX by a factor of 20-30,

but only about 4-fold for the alkanes, and between 5-7-fold for cyclo-alkanes and the freon. This indicates that sensitivity on vertical dispersivity is enhanced especially for low *H* compounds, when biodegradation applies.

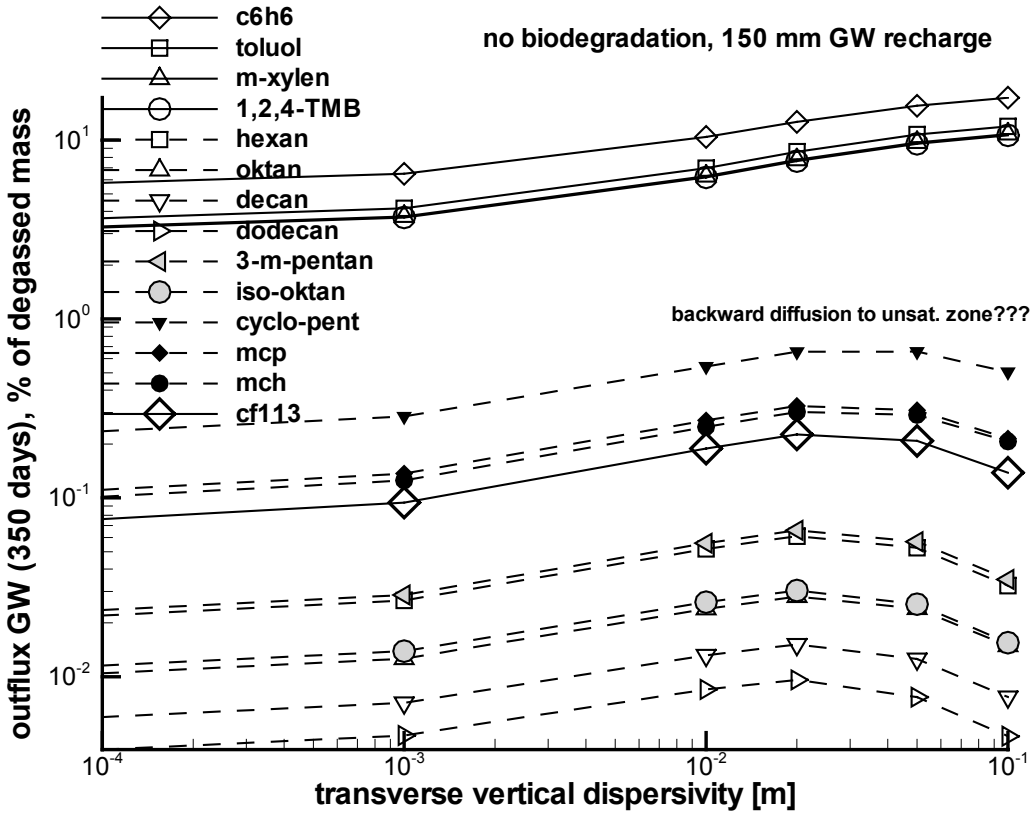

Fig. 5.19 Sensitivity of contaminant transport to groundwater on transverse vertical dispersivity α_t in terms of cumulated flux out of the model domain (G) in % of mass volatilised from the NAPL source.

In a second set of simulations, lower, nonuniform biodegradation rate constants were applied (but higher than one day^{-1} for the heavier n-alkanes), the situation changes somewhat. Maximum G is in the range of one percent, for benzene, toluene and cyclo-pentane. Mass in groundwater was found to be 3-5 fold increased by stronger dispersion for BTEX compounds and the freon, around doubled for iso- and cyclo-alkanes, but only weakly enhanced for the n-alkanes. The latter have the highest Henry's law constant but also in this case high biodegradation rate constants. The nondegradable tracer CF113 has an intermediate *H*, but its transfer to groundwater is also enhanced 5-fold.

This complex behaviour suggests that biodegradation rate strongly influences transport to groundwater and superimposes the effect of dispersion in the capillary fringe. Thus, as a requirement for risk assessment, it seems to be crucial to quantify the unsaturated zone mass balance before estimates of groundwater contamination can be met.

5.6 Results of the field site model

Delineating shape and propagation of vapour phase plume as contour plots serves well to provide a first intuitive understanding of the site situation.

Vertical cross-sections show rapid spreading across the unsaturated zone for the concentration of alkanes like iso-octane, which

is initially the main compound in the NAPL source. At 50 days, iso-octane reaches its maximum concentration around the source location (see Fig. 5.20 of a 2D simulation). Nearly no transport into groundwater can be observed. The soil gas plumes of aromatic compounds like benzene or toluene are much more restricted to the vicinity of the source and somewhat retarded, toluene shows its maximum spreading around 120 days (Fig. 3). At this time, significant transport to groundwater occurs. Minimum concentrations of O_2 of 17 Vol. % were observed, even at the source location there was no strong depletion of oxygen. The emplaced source was also surrounded by an anomaly of elevated CO_2 concentrations due to ongoing biodegradation. Maxima were calculated between 1.5 and 2 Vol. % at the source location and below after two longer periods of rainfall. At the capillary fringe below the source, CO_2 concentration gets even higher and is also dissolved in groundwater. These general findings coincide well with the field measurements.

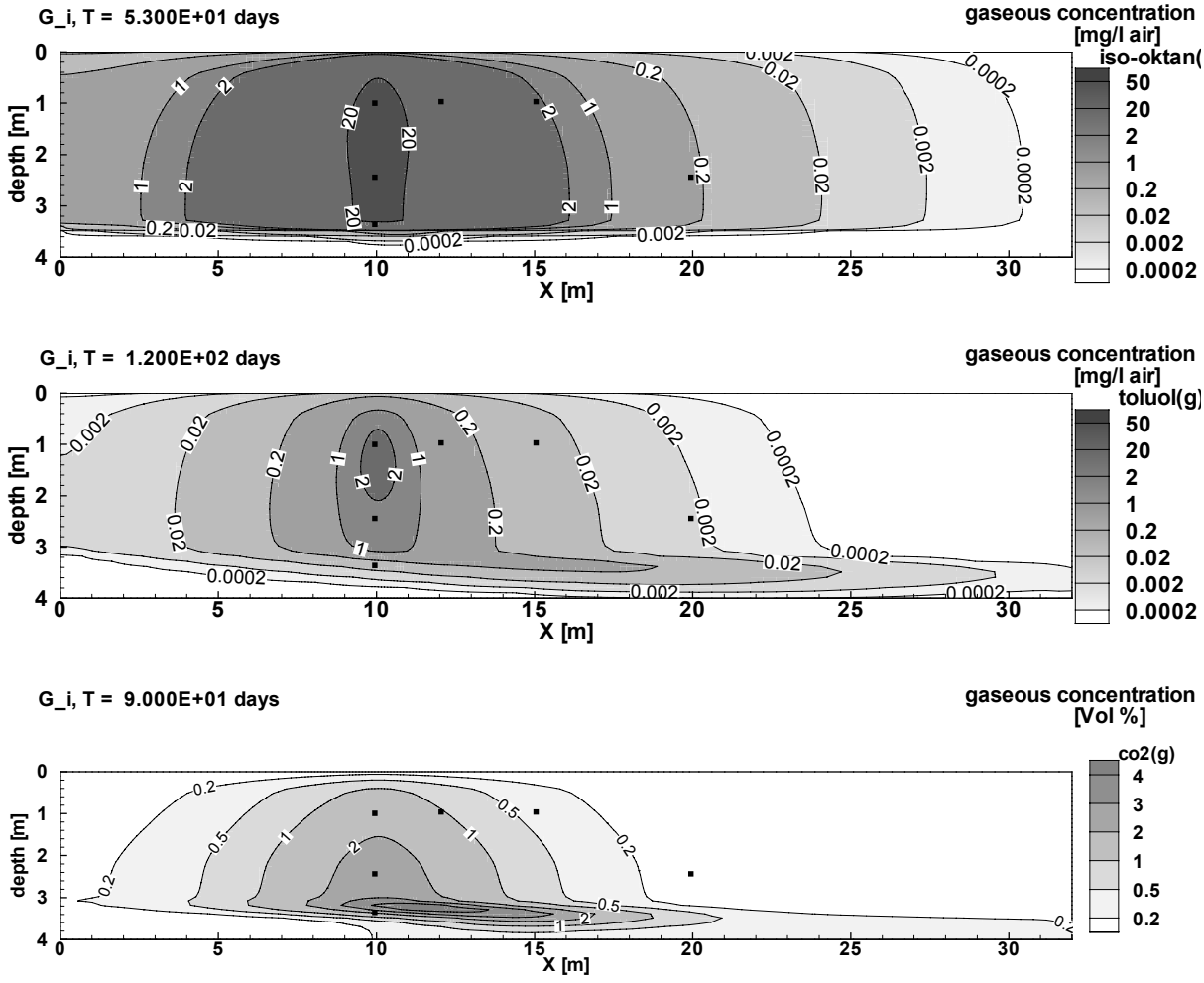

Fig. 5.20 Contour diagrams of 2D model results for the Værløse field site of iso-octane (upper), toluene (middle) and CO_2 (lower), at the time of maximum spreading.

Concentrations of compounds that are not sensitive to biodegradation like the non-degradable tracer CFC-113 could be reproduced reasonably well by the non-calibrated model already, simply applying compound, soil and weather characteristics determined at the field site.

5.6.1 Influence of transient temperature and soil water content

Implementing a depth and time-dependent temperature field as described in § 2.2.1, that accounts for the lower vapour pressures in the winter months, enhances the agreement to the measured concentrations significantly compared to constant temperatures. The example of toluene is given in Fig. 5.21. A temporily variable unsaturated flow field due to infiltration events, however, does not affect the kerosene vapour concentrations remarkably, but reproduces the elevated concentrations of CO_2 during longer precipitation periods significantly better. These rises in CO_2 levels can be explained by higher pore water saturation in the top soil which diminishes the diffusive transport of the biodegradation product to the atmosphere (Fig. 5.22).

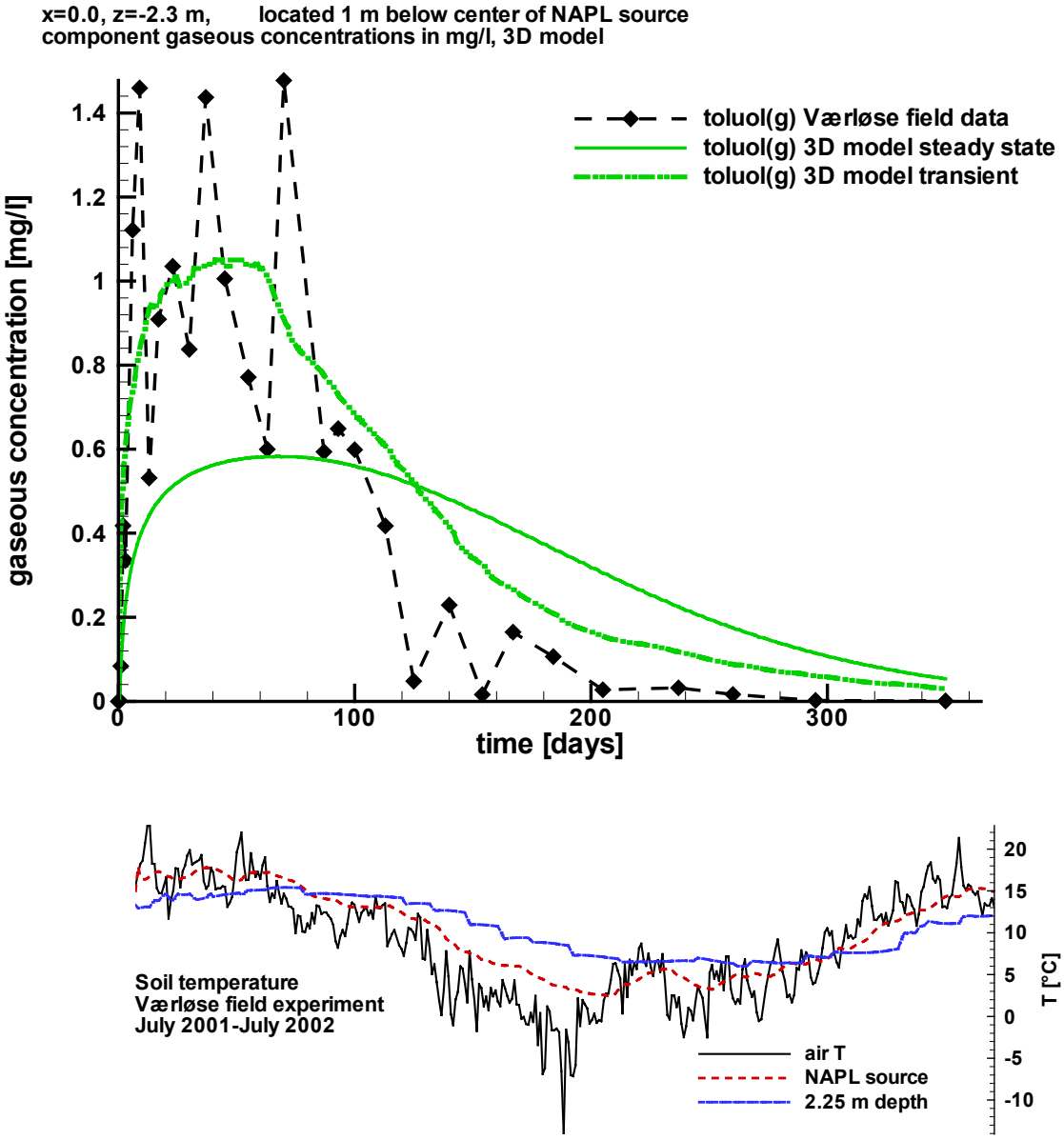

Figure 5.21 Influence of transient depth dependent temperature profiles on the model results using MIN3P for the compounds toluene. Much better agreement can be achieved if daily measured temperatures from the site are implemented.

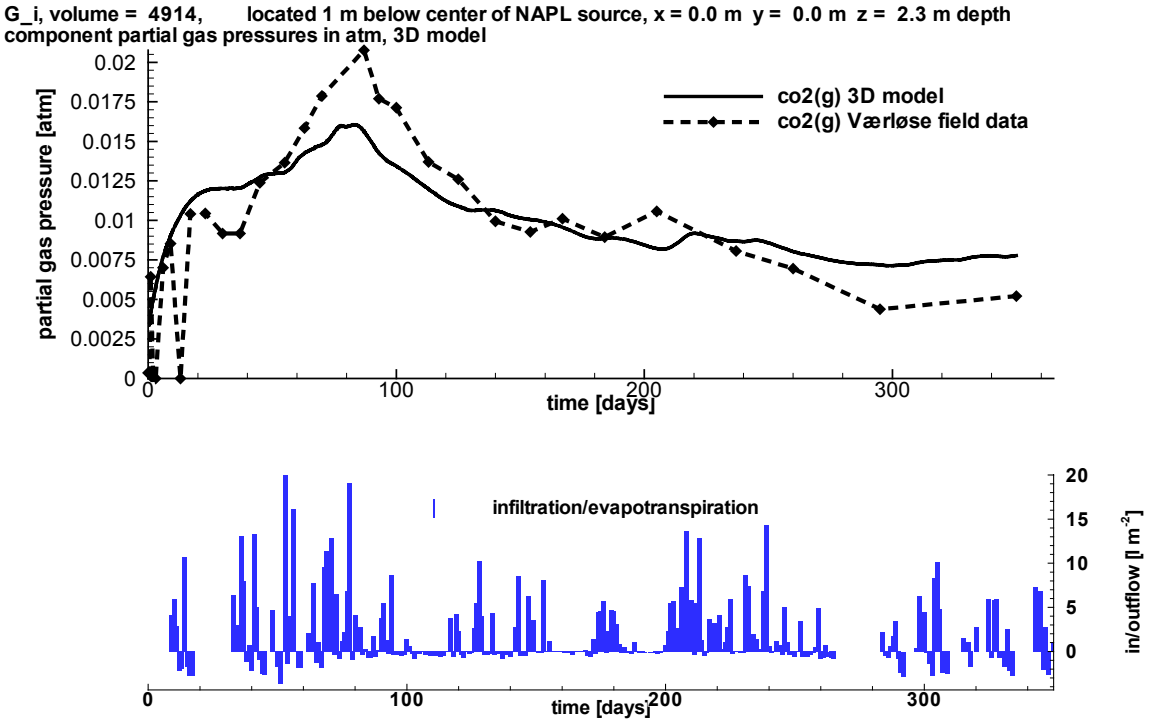

Figure 5.22 Comparison of measured and simulated CO_2 concentrations at a sampling port 1 m below the centre of the kerosene source and its correlation to measured infiltration and evapotranspiration.

5.6.2 Reproduction of measured field data – unsaturated zone

Biodegradation rate constants were identified as the only fitting parameters which could not be derived from measured data from the site for the unsaturated zone. To reproduce measured vapour phase concentrations at sampling ports in the unsaturated zone simulated data were compared as 'breakthrough curves' at seven different sampling locations (at the source location, 1 m below, 2 m below, 0.5 m above the source as well as 1 and 2 m laterally, respectively). Modelled concentrations and the measured field data show good agreement for the sampling ports in the vicinity of the NAPL source. Fig. 5.23 shows four selected compounds at the sampling location 1 m below the centre of the NAPL source. Toluene and CO_2 were already shown in Fig. 5.21 and Fig. 5.22. The model misses high concentration peaks of the most volatile compounds (benzene, hexane, cyclo-pentane and methyl-cyclo-pentane) at early times during the first 3 –5 days. A possible explanation is a lag time of microbial growth and biodegradation, as evidence of microbial activity (CO_2-production) in the field was observed only 2 weeks after the start of the experiment, which was not accounted for in the model. Other possible reasons for deviation are density driven flow for compounds with high vapour pressure at the beginning of the experiment or activity coefficients greater than one for highly volatile compounds (Broholm et al., 2004).

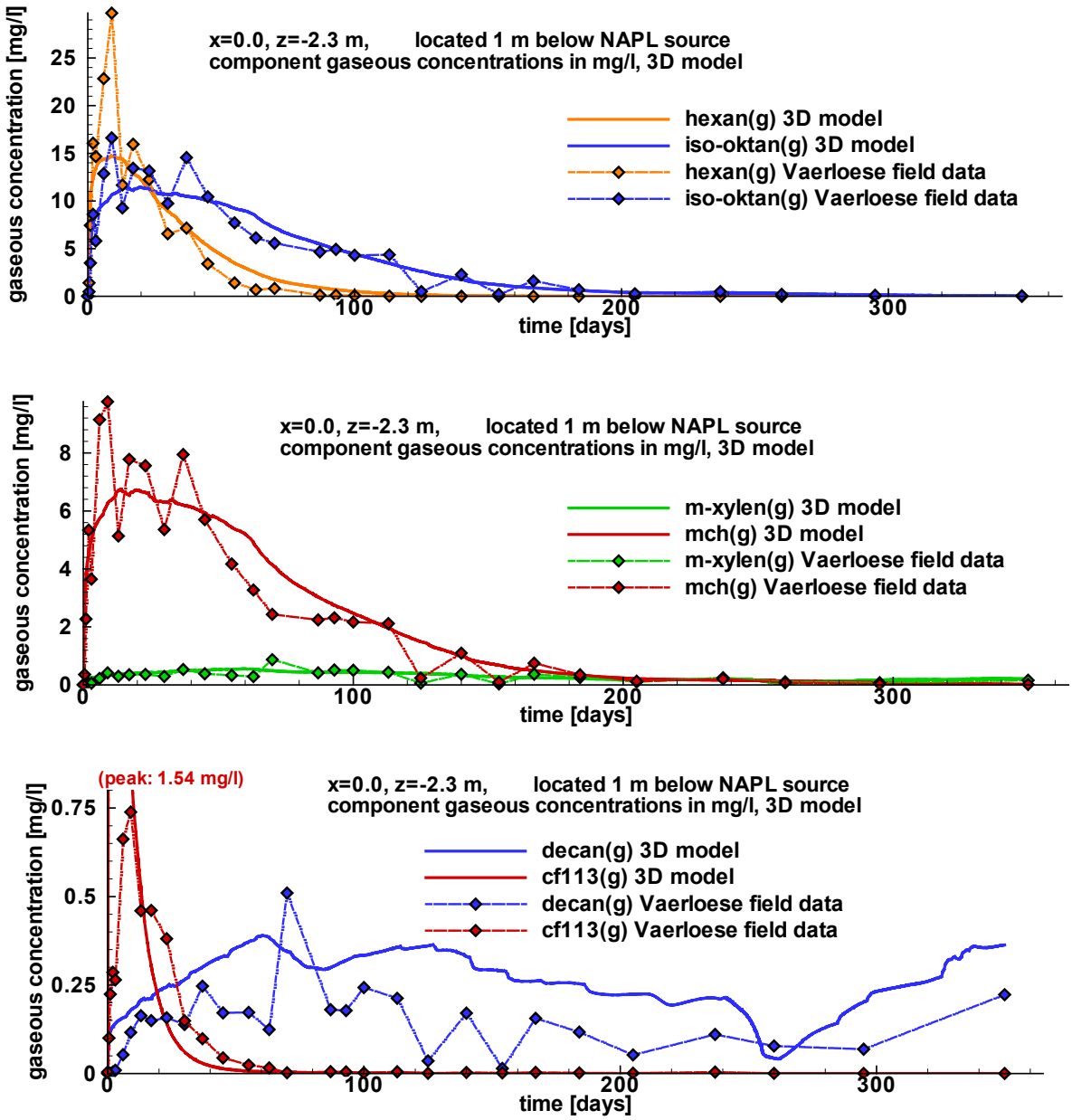

Fig. 5.23 Comparison of measured and simulated concentrations at a sampling port 1 m below the centre of the kerosene source for the selected compounds hexane, iso-octane, m-xylene, methyl-cyclo-hexane, decane and the tracer CF113.

The biodegradation rate constants in the aqueous phase (pseudo first order) obtained by fitting the model to the field site are given in Tab. 5.5 (right column). The aqueous phase rate constants divided by *H* to account for the gaseous phase (center column) can be compared to values measured in soil air at the lab scale using material excavated at Værløse field site (left column) (Pasteris et al., 2002,Christophersen et al., 2003). Gaseous phase biodegradation rate constants were generally below one per day, but two classes of compounds had to be assigned high rate constants: the aromatic compounds (except toluene) and the heavy n-alkanes from octane to dodecane. The latter ones were assigned very high biodegradation rate constants of more than 100 with respect to the aqueous phase, which appear below 5 per day when transformed to rate constants with respect to the gaseous phase. These high rate constants can be explained by their good bioavailability

(Pasteris et al., 2002). Whether high biodegradation rates suffice to explain the low vapour concentrations of the least volatile compounds can only be speculated on. Considering that the least volatile compounds are also the most hydrophobic ones, sorption to soil organic matter may help to explain their low gaseous concentrations. A possible adsorption of organic compounds to the water/air-interface could provide a higher availability of the compound to the microbial community than indicted by pure aqueous solubility alone. Low volatile hydrocarbon degradaing bacteria may as well concentrate themselves at the soil water interface where the substrate has a maximum availability, keeping gradients steep at this particular place and preventing complete partitioning into the aqueous phase that way.

Light n-alkanes, cyclo-alkanes and iso-alkanes were found to have low biodegradation rate constants and are only subject to minor net biodegradation due to their high volatility (short residence time in the soil) and their suspected toxicity for microorganisms. The agreement to the values measured in the lab (Christophersen et al., 2003) is good for all compounds except benzene, which shows an about 10 times higher rate constant in the field site model. Surprisingly, toluene was observed to have a lower biodegradation rate constant than the other BTEX constituents.

*Table 5.5 first order biodegradation rate constant estimates k_{air} for the **gas phase** from lab experiments (Christophersen et al., 2004, left column) and transferred from 3D model (using MIN3P, middle) in [d^{-1}]. Corresponding k_{aq} accounting for the aqueous phase (raw data obtained by model fitting) are given in the right column (see also text).*

Compound	**Column experiment**	**Calibration MIN3P**	**MIN3P k_{aq} (aq. phase)**
Benzene	0.21 ± 0.12	1.95	0.43
Toluene	0.7 ± 0.2	0.27	0.069
m-Xylene	1.65 ±0.6	1.65	0.43
1,2,4- Trimethyl-Benzene	3.7 ±0.4	2.56	0.69 *
n-Hexane	0.1 ±0.04	0.004 1)	0.26
n-Octane	1.23 ±0.2	1.08	130 *
n-Decane	5.83 ±1.1	3.53	691 *
n-Dodecane	-	1.12	1037 *
3-Methyl-Pentane	0.06 ±0.02	0.01 1)	0.43
Iso-Octane	0.2 ±0.010	0.01 1)	1.73
Cyclo-Pentane	0.04 ±0.04	0.02	0.17
Methyl-Cyclo-Pentane	0.12 ±0.08	0.18	2.59
Methyl-Cyclo-Hexane	0.31 ±0.08	0.1	1.73
CFC-113	-	0	0

1) quasi non-sensitive to k * possibly affected by sorption

It should be noted that concentrations of compounds that are non-degradable like the tracer CFC-113 or weakly sensitive to biodegradation could be reproduced well by the non-calibrated model already, simply applying compound-, soil- and weather

characteristics determined at the field site. That means unsaturated zone concentrations for compounds with no or weak sensitivity on biodegradation rate constants can be regarded as reproduceable by pure forward modelling. As the reproduction of measured vapour phase concentrations at sampling ports in the unsaturated zone by adjusting biodegradation rate constants could provide good agreement, it can be regarded as validation of the models to unsaturated zone processes. That way, the fate of the contaminants in the unsaturated zone with respect to mass balance could be quantified (§ 4.23).

5.6.3 Reproduction of measured field data – groundwater

In a second step, starting from determined unsaturated zone situation, transverse vertical dispersivity α_t was adjusted to approach measured groundwater concentrations using the model MIN3P. Qualitative agreement was achieved and an estimation of contaminant mass transported to groundwater and groundwater vulnerability for the given scenario could be obtained.

Reproduction of measured groundwater concentrations by the model was found to be subject to a greater uncertainty than in the unsaturated zone. The best approach to measured concentrations of VOC in groundwater could be achieved applying a transverse vertical dispersivity α_t of 2 cm. In the capillary fringe directly below the source zone, a small zone developed where oxygen was slightly depleted (8 mg/l). This zone was dragged several meters downgradient with groundwater flow. Here, maximum CO_2 concentrations of 0.6 Vol. % (30 mg/l TIC, respectively) were calculated by the model. Restricted to this area, the model resulted in concentrations greater than 1 µg/l for 11 of the 14 fuel constituents. All BTEX compounds were present as well as cyclo- and iso- alkanes and Cf113. The compound with highest concentration was toluene with more than 100 µg/l, the most critical compound benzene showed a maximum concentration of 8 µg/l. Only n-octane, n-decane and n-dodecane were found in very low concentrations far below 1 µg/l. At the outflow boundary condition, toluene still exceeded the trigger value according to German law (sum of BTEX: 20 µg/l] (BBodSchV, 1999)(§2.1.1).

The implementation of water table fluctuations was found to be essential to reproduce measured groundwater concentrations. Even without regarding the effect of vertical advection of both, soil air and pore water within the funicular zone, the distance for diffusive transport though water saturated soil from the vadose zone to a sampling port in shallow groundwater is changing concentrations by several orders of magnitude and is therefore crucial to consider.

Possible explanations for the lesser agreement of the model to measured groundwater concentrations are the intrinsic heterogeneity and hysteresis of the capillary fringe which is a strong source of uncertainty and possible numerical dispersion to the model. Unlike in the unsaturated zone, a sufficient spatial discretisation for this small scale process could not be achieved. The approximation of the "symmetry boundary condition" at the source centre in flow direction which was essential to satisfy memory restrictions but is strictly valid only in the unsaturated zone. The neglection of gas phase advection as one possibly important process may disregard effects of soil air pumping above a fluctuating water table. Entrapped air bubbles in the capillary fringe may not only serve as 'mixing chambers' due to their high diffusion coefficients, but also increase flow tortuosity and enhance VOC dispersion significantly (Klenk and Grathwohl, 2002). The model cannot account for these local scale processes. It should be noted that such small scale heterogeneities in a zone of very steep concentration gradients like the capillary fringe pose a serious challenge to

numerical modelling and require further research and uncertainty analyses.

5.6.4 Mass balance for the field site

From the model calibrated by using best fitting biodegradation rate constants *k* and transverse vertical dispersivities α_t, a mass balance for Værløse field experiment was compiled (Tab. 5.6). The model calculated that a total mass of 5 kg O_2 was consumed by biodegradation during one year of the experiment and a little less CO_2 was produced. The discrepancy is because oxygen is also being used up for oxidation of hydrogen contained in the hydrocarbons. In the best fit, about 1.5 kg of VOC were bio-transformed to CO_2 in 1 year. The 5 lowest volatile organic compounds (xylene, TMB, n-octane, n-decane and n-dodecane) remained in the NAPL source in significant amounts for longer than the duration of the experiment.

Mass balance contributions of flux to the atmosphere (A), groundwater (G) and biodegradation (B) showed significant differences for the groups of compounds involved. The flux to the atmosphere was pronounced for the tracer freon 113 (99%) and the light alkanes (n-, and iso-alkanes) due to their low to mediate biodegradation rate constants and high *H*. The situation for the cyclo-alkanes is similar, but due to low or intermediate *H* they showed a potential for groundwater pollution, as pointed out by the example of cyclo-pentane. The highest volatile compounds, generally, are being transported too fast to be readily biodegraded. Additionally toxicity for microorganisms is presumably high for alkanes of short chain length (Höhener, 2002). Thus, these will be transported either to groundwater or the atmosphere, depending also on the site conditions.

*Table 5.6 Modelled mass balance contributions for the 14 different compounds using the best fit biodegradation rate constants (see Tab.6), at Værløse field site, after the duration of one year. Contaminant mass in [g] for O_2 and CO_2, in % of evaporated mass for biodegradation, flux to the atmosphere and groundwater, and in % of initial mass for NAPL, respectively). [1] net outflux, * possibly affected b sorption.*

Compound	Atmosphere	Biodegradation	GW outflux	In NAPL [%]
Benzene [%]	18.72	81.40	0.01	0.00
Toluene [%]	36.34	59.64	3.12	3.13
m-Xylene [%]	10.34	88.77	0.01	29.17
1,2,4-TMB [%]	6.18	92.92 *	0.00	61.39
Hexane [%]	97.78	2.16	0.08	0.03
Octane [%]	18.41	81.36 *	0.00	12.38
Decane [%]	4.26	95.49 *	0.00	73.63
Dodecane [%]	4.04	95.65 *	0.00	97.04
3-Meth-Pent [%]	96.84	3.13	0.05	0.01
iso-Octane [%]	91.58	8.33	0.02	0.29
Cyclo-Pent. [%]	90.93	8.70	0.40	0.00
MCP [%]	64.86	35.14	0.01	0.02
MCH [%]	67.11	32.81	0.03	0.32
CF113 [%]	99.38	0.00	0.64	0.00
O_2 [g]	11290 (influx)	5130	169.80 [1]	
CO_2 [g]	4900 (outflux)	4850	55.00 [1]	

Biodegradation was most important for the aromatic compounds (low Henry's law constant) and the heavier n-alkanes. For the latter ones very high biodegradation rate constants were applied to fit the low measured concentrations. For these compounds, however, low concentrations may be partially due to sorption to soil organic matter (see also § 5.6.2). Nevertheless, heavier n-alkanes are unlikely to reach groundwater due to high *H* and additionally due to high bioavailability.

The maximum transport to groundwater was found for the 3 most volatile and soluble compounds toluene (3 %), CF113 (0.6 %) and cyclo-pentane (0.4 % of the volatilised mass, respectively). It should be noted that these are also the ones that are most sensitive to biodegradation, thus the quantification of biodegradation rate for these compounds is very crucial for groundwater risk assessment.

As shown by the simulations above, the greatest amount of VOC mass will remain in the unsaturated zone, either be transported to the atmosphere and be subject to biodegradation and only a smaller amount will reach the groundwater.

5.6.5 The effect of biodegradation on source component depletion

NAPL source mass and composition in the calibrated 3D model was compared to measurements from the field site. To evaluate the impact of biodegradation on the depletion of the fuel phase, the calibrated model was compared to a simulation without biodegradation. Figure 5.24 shows the modelled composition of the NAPL during the time span of the field experiment. After one year only 5 components remain present in the phase in significant amounts: xylene, trimethylbenzene, n-octane, n-decane and n-dodecane. This is consistent with the experimental data (Broholm et al., 2004). A fast depletion due to high temperatures in the summer months and high initial contents of the most volatile compounds in the NAPL can be observed in the early times (steep slope) followed by slower volatilisation during the winter.

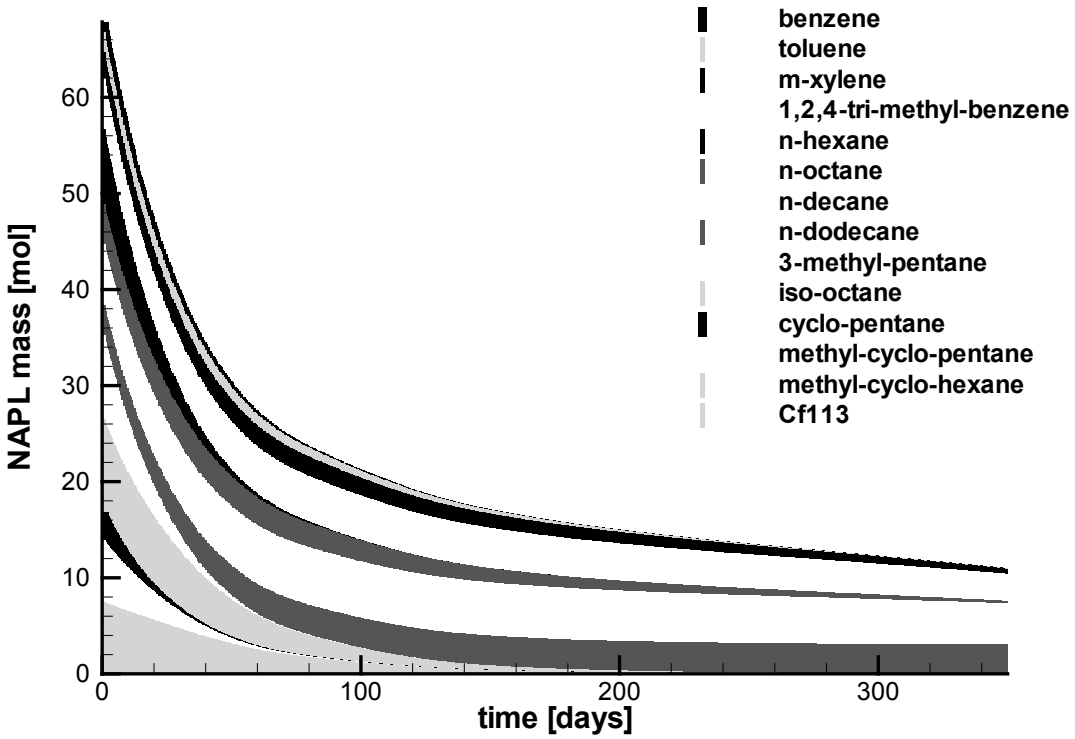

Fig. 5.24 The mass of the kerosene compounds remaining in the NAPL during the first year in a 3D model (in moles) assuming transient conditions of T and θ. Sorted in compound classes (see Fig. above).

The mole fractions of the compounds in the NAPL were compared to measured mole fractions from the field. All the compounds show reasonably good agreement (Figure 8). n-Hexane disappears during the first 100 days, iso-octane volatilises slower, whereas n-decane shows a constant increase in mole fraction of the residual phase. Initially n-hexane decreases faster and n-decane increases faster than indicated by the model (Figure 5.25). Benzene and toluene decrease faster than indicated by the model, toluene does not show the initial increase indicated by the model, m-xylene and 1,2,4-trimethylbenzene initially increase faster than indicated by the model, at later times (>120 days) m-xylene decreases faster than indicated by the model (Figure 5.26). The faster decrease in the mole-fractions of the aromatic compounds in the NAPL than indicated by the model is likely – at least partially, a result of the non-ideality of the mixture (Broholm et al., 2004). Faster decrease of some compounds naturally results in faster increase of other less volatile compounds, such as decane.

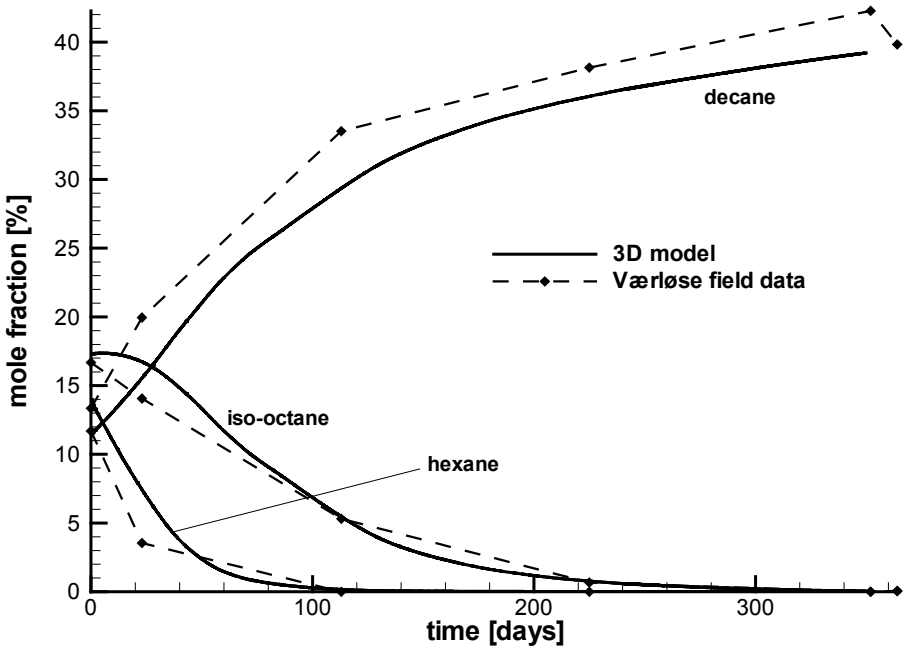

Fig. 5.25 The mole fractions in the NAPL during the first year, NAPL mole fractions in 3D model compared to field data for the compounds hexane, iso-octane and decane.

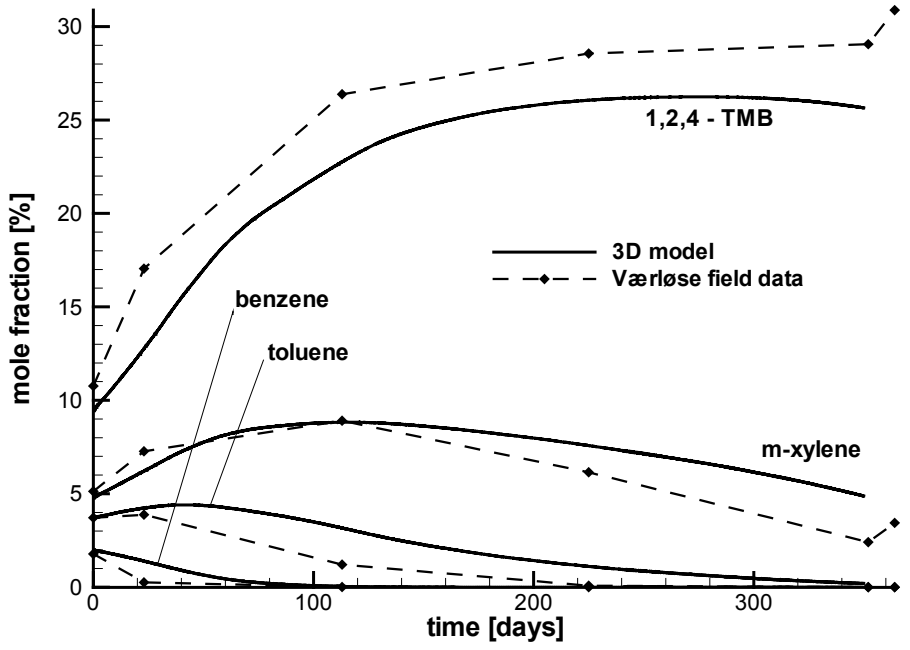

Fig. 5.26 The mole fractions in the NAPL during the first year, NAPL mole fractions in 3D model compared to field data for the compounds benzene, toluene, m-xylene and 1,2,4 TMB.

To assess the possibility of bio-enhanced volatilisation in the vadose zone for the Værløse field experiment, in a first step sensitivity analyses on biodegradation rate

constant were performed in 2D simulations. The result in terms of the mass balance is shown in Figure 5.27 and clearly indicates an influence of high rate biodegradation on phase depletion for the example of 1,2,4-trimethylbenzene (TMB). However, even for this compound of relatively low vapour pressure, NAPL mass leftover is only sensitive on biodegradation at relatively high rates. Otherwise, biodegradation predominantly results in lower diffusive flux to the atmosphere. For more volatile compounds, even at high biodegradation rates, little effect will be observed on the NAPL depletion. Hence, for very volatile compounds even low values of the enhancement factor (*ef*) may well reflect great biodegradation.

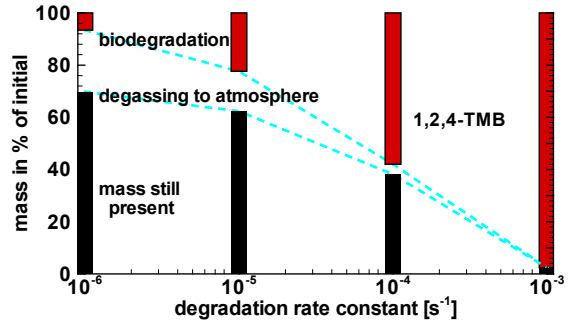

Fig. 5.27 Fate of 1,2,4-tri-methyl-benzene mass(percent of initially present in NAPL) after one year in relation to the pseudo first order biodegradation rate constant. GRACOS- Værløse 2D scenario (14 compound mixture), depth of contaminant source one m.

To reproduce the field results by a 3D model, the biodegradation rate constants were adapted to fit concentration time series at 3 different sampling ports in a trial and error procedure (§ 4.3). The so obtained rate constants can be regarded as a rough estimate for biodegradation at the field site. In the best fit, about 1.5 kg of VOC were bio-transformed to CO_2 in 1 year. To assess the enhancement of NAPL depletion driven by microbial activity, the model was run again without biodegradation but otherwise same conditions. The depletion enhancement factor ef was calculated as

$$ef = \left(\frac{1-m_{bio}}{1-m_{no}} - 1\right)\cdot 100 \qquad [\%] \qquad \text{eq. 5.4}$$

where m_{bio} and m_{no} are the compound mass' in the NAPL after a given time if biodegradation occurs and for no biodegradation, respectively.

The comparison is shown in Table 5.7. Bio-enhancement of depletion after 60 days and 350 days was evident especially for the low volatile compounds. n-decane showed the maximum *ef* after 350 days with more than 50 % stronger depletion. The higher volatile compounds such as toluene or cyclo-pentane had almost completely disappeared after 350 days in both scenarios, but were subject to minor bio-enhancement during early times of the experiment, 60 days. In total, the model comparison yielded an about 5 % (300 g) stronger depletion of the NAPL than it would have been without biodegradation after 350 days. The actual depletion of mass based on the analysis of source samples at the end of the experiment was even greater, suggesting even greater bio-enhancement for the compounds still present in the source (Broholm et al., 2004).

Comparison of the enhancement factors with vapour pressures indicates strongly increasing effect of degradation with decreasing volatility. As mentioned previously for the more volatile compounds, biodegradation will predominantly influence the loss by diffusion to the atmosphere rather than the depletion of the source-NAPL. A greater effect on aromatic relative to aliphatic compounds is observed after 60 days, but it is small relative to the apparent increase with decreasing volatility. However, this implies that the faster depletion of the aromatic relative to the aliphatic compounds in the source-NAPL is partially a result of bio-enhancement.

The biodegradation rates for the least volatile compounds are very high. Note that the stated rates are aqueous phase rates and therefore appear lower for the more soluble aromatic compounds. The concentrations of the lowest

volatile compounds TMB, n-octane, n-decane and n-dodecane are supected to be lowered by soprtion to soil organic matter, which then would superimpose the effect of biodegradation to some extent. Other explanations are discussed in § 5.6.2.

Table 5.7 Comparison of model runs with and without biodegradation: NAPL mass [moles] in percent of initial mass, after 60 and 350 days., and bio-enhancement of NAPL depletion after 60 days and 1 year (350 days, respectively). Also included are pseudo first order degradation rate constants (aqueous phase) used in the model (corresponding k with respect to the gaseous phase see Tab. 5.5).

Compound	Remaining without biodegradation [%]		Remaining with biodegradation [%]		Depletion – Bio-enhancement *ef* [%]		Aqueous phase rate constant [day^{-1}]
(After time:)	**60 days**	**350 days**	**60 days**	**350 days**	**60 days**	**350 days**	
Benzene	16.13	0.00	10.82	0.00	6.34		0.43
Toluene	55.08	2.45	53.58	1.03	3.35	1.45	0.069
m-Xylene	79.61	32.53	77.33	18.94	11.11	20.14	0.43
1,2,4-TMB	88.80	64.13	87.57	50.07	10.91	39.18	0.69 *
n-Hexane	5.55	0.03	5.39	0.03	0.17	-	0.26
n-Octane	70.28	14.00	67.23	6.13	10.28	9.15	130 *
n-Decane	91.34	75.99	90.38	63.39	11.15	52.48	691 *
n-Dodecane	94.44	92.76	94.35	91.00	1.65	24.28	1037 *
3-Meth-Pent.	2.38	0.01	2.28	0.01	0.10	-	0.43
iso-Octane	32.87	0.11	32.37	0.06	0.75	0.05	1.73
Cyclo-Pent.	0.40	0.00	0.35	0.00	(0.05)	-	0.17
MCP	5.76	0.02	4.84	0.02	0.98	-	2.59
MCH	35.48	0.18	34.30	0.09	1.84	0.10	1.73
CFC-113	0.0	0.0	0.0	0.0	-	-	0
total	41.26	20.05	40.32	16.37	1.61	4.60	

- already totally depleted, () remaining mole fraction below 1 %, * possibly affected by sorption.

5.6.6 Summary

The quantification of the actual mass fluxes between saturated and unsaturated zone in the model is nontrivial. An equivalent and easy to determine measure of groundwater contamination, therefore, is the bulk mass outflux from the model domain in groundwater. In the 3D model, the outflux boundaray is 6.5 m downgradient of the source. Tab. 5.8 compares the groundwater mass outflux from the model domain between the calibrated field site model and the simulation without biodegradation. Overall, the mass fluxes are several orders of magnitude higher if there is no biodegradation. Especially for the BTEX compounds this would cause a serious risk for groundwater quality.

Interestingly, even for compounds with low biodegradation, mass flux to groundwater is enhanced. For the nondegradable tracer CF113, this can only be explained by the slower depletion from the kerosene source, which leads to a longer residence time of the compound in the unsaturated zone. That provides a longer potential of transport to groundwater instead of degassing to the atmosphere. Indeed, CF113 shows a higher flux to the saturated zone in the first 30 days after installation relative to the case with biodegradation due to stronger initial phase depletion. The higher initial flux then decreases faster if there is biodegradation. This longer residence time indeed causes a significantly higher flux to groundwater (~10 fold) for the time of one year. This may be additionally enhanced by the circumstance that the experiment started in summer, and a longer tailing in volatilisation coincides with the winter months. It was shown in the sensitivity analyses, that at lower temperature, partitioning into water increases and volatilisation to the atmosphere is decelerated. That way, low *T* can lead to higher fluxes to groundwater. After all, model results for the mass balance and groundwater fluxes emphasize that the behaviour of a fuel mixture under transient climatic conditions in the unsaturated zone is highly nonlinear and biodegradation of specific compound also affect the mass balance of other consituents.

In order to set site specific conditions into relation to the efficiency of Natural Attenuation, Damköhler numbers were defined. These account for the sensitivity analyses performed, using first and zeroth order kinetics. Sensitivity on biodegradation described in § 5.4 was performed in a first order kinetic approach with respect to substrate. This was repeated for zeroth order degradation to compare the different approaches.

Certainly, simplifying assumptions had to be met to express complex sites characteristics by a few dimensionless numbers. So, the Damköhler number is generally formulated for a one dimensional, homogeneous and steady state medium. Thus, it should be noted that this quantification represents only a rough estimation of the situation and is not able to substitute detailed investigation and modelling. However, it may be useful to gain a quick overview of a given situation.

Table 5.8. Simulated groundwater contamination of the 14 kerosene compounds, for two different scenarios: field site model Værløse including best fit biodegradtion rate constants (see Tab.6) and hypothetical case without biodegradation, using the model MIN3P. Cumulative flux out of the model domain after one year in [mg].

Compound	with biodegradation	no biodegradation
Benzene [mg]	0.23	6177
Toluene [mg]	120.47	13020
m-Xylene [mg]	0.33	10490
1,2,4-TMB [mg]	0.23	10197
Hexane [mg]	15.85	331.6
Octane [mg]	3.01E-03	171.0
Decane [mg]	1.90E-04	49.8
Dodecane [mg]	1.73E-05	2.32
3-Meth-Pent [mg]	15.35	335.5
iso-Octane [mg]	3.11	414.5
Cyclo-Pent. [mg]	98.91	680.7
MCP [mg]	0.29	1197
MCH [mg]	1.84	1712
CF113 [mg]	3.80	33.7

The Damköhler number is defined as

$$Da = \frac{t_T}{t_R} \qquad \text{eq. 5.5}$$

in the first order approach concentration cancels out and *Da* equals

$$Da = L^2 D_{app}^{-1} (C R^{-1}) = L^2 D_{app}^{-1} k_{app} \qquad \text{eq. 5.6}$$

and for zeroth order kinetics:

$$Da = L^2 D_{app}^{-1} (C R^{-1}) = L^2 D_{app}^{-1} (C K_{app}^{-1})$$ eq. 5.7

Where D denotes the apparent diffusion coefficient in soil air, R the total reaction rate and k and K the apparent reaction rate constant for first and zeroth order degradation. As volatilisation to the atmosphere was found to be the main transport process out of the model domain for VOC, the distance from the NAPL source to ground surface was chosen as the characteristic length L to the point of interest. Including partitioning between all the phases in the soil, the apparent diffusion coefficient is defined by

$$D_{app} = \frac{D_{eff}}{\alpha} = \frac{D_{air}}{\tau} f_T = \frac{D_{air}}{\tau} \frac{n_g}{n_g + \theta / H + K_d \rho / H},$$ eq. 5.8

the apparent degradation rate constant by

$$k_{app} = k_W f_R = k_W \frac{\theta / H}{n_g + \theta / H + K_d \rho / H}$$ eq. 5.9

where f_T and f_R denote the mobile and reactive fractions of the compound in the soil, with f_T representing the gaseous phase where diffusion takes place and f_R representing the aqueous phase where biotransformations take place. As sorption was neglected in the simulations, the term $K_d \rho/H$ can be omitted in the equations and the Damköhler numbers are given by:

$$Da = \frac{L^2 k_W \theta n^2}{D_{air} (n-\theta)^{3.1} H \alpha}$$ (first order), eq. 5.10

and

$$Da = \frac{L^2 k_W \theta n^2}{D_{air} (n-\theta)^{3.1} H \alpha C_W^{Sat} \chi \gamma}$$ (zeroth order) eq. 5.11

Fig. 5.28 shows the results. As expected, the results are scattered, but give a clear trend of increasingly significant attenuation with increasing Damköhler numbers. The whole range from very insignificant to complete degradation is represented. Zeroth order shows much more efficient degradation for lower Da, but, as indicated by the analytical considerations in § 2.3.6, this can be attributed mainly to the different kind of formulation of the kinetics. For Damköhler numbers above 10 (zeroth order) and 100 (first order), respectively, total depletion of the compound before reaching the given point of interest can be assumed. Unlike the situation in groundwater, where natural attenuation often proves to be mixing limited (§ 4.2.1), biodegradation kinetics play a major role in the unsaturated zone at sufficiently high gas permeabilities.

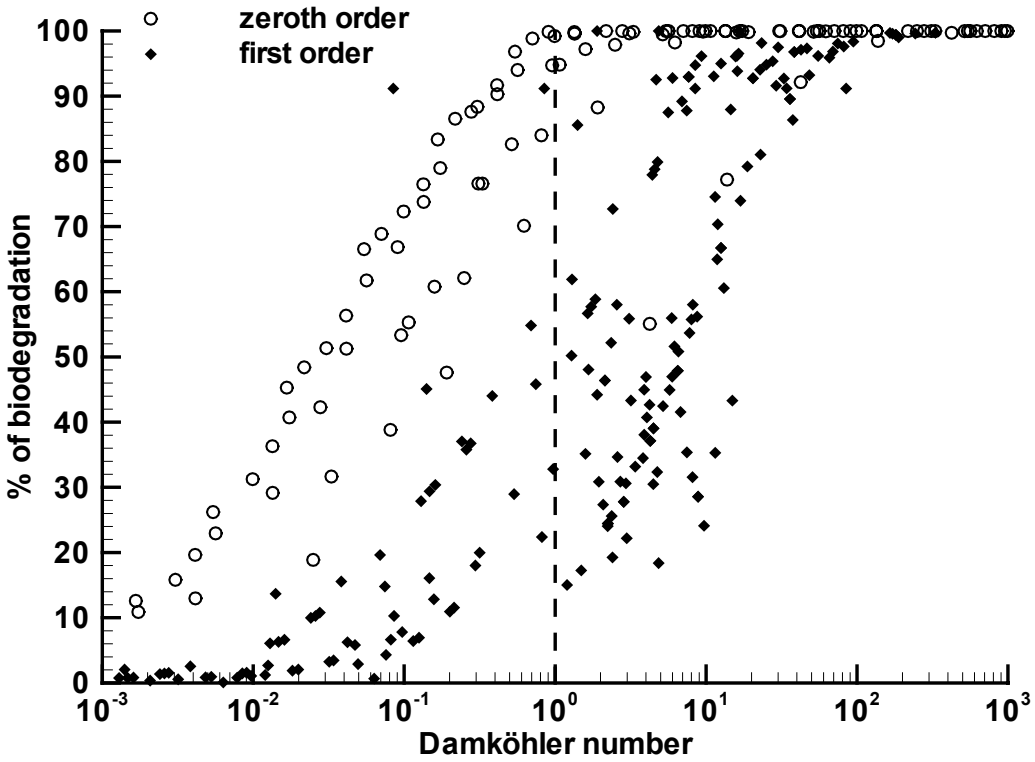

Fig. 5.28 Damköhler number derived in eq. 5.10 and 5.11 and its correlation to mass balance contribution of biodegradation.

6 Conclusions

As active remediation is not feasible for the great number of locations with contaminated groundwater in the industrialised countries, the prediction of Natural Attenuation capabilities of aquifers is an important task. Crucial for groundwater risk assessment is dispersion that leads to mixing of electron acceptors into contaminant plumes and that way allows for biodegradation. Transverse dispersivities measured in the lab or field scale (Garabedian, 1991,Gelhar, 1992,Rivett et al., 2001,Klenk and Grathwohl, 2002,Olsson et al., 2003,Cirpka et al., 2004) are usually very small and imply that they can be limiting factors for Natural Attenuation rather than biodegradation kinetics for aerobically well degradable compounds. Combination of numerical modelling and geostatistical evaluations provide measures to estimate the average dispersivities at the aquifer scale and allow for scenario specific modelling using quasi homogeneous domains (Cirpka and Kitanidis, 2000,Cirpka, 2003). Numerical experiments in this study provided estimation functions for steady state plume sizes for readily degradable contaminants under aerobic conditions in a base case scenario when the whole aquifer thickness is contaminated. If the aquifer is only partly contaminated, significantly shorter plumes establish when a second reactive fringe supports attenuation. For that case, qualitative relationships were delineated.

By careful evaluation of the grid spacing and model setup artificial mixing could be minimised and assured not to affect results. Sensitivity analysis and theoretical considerations (Cirpka, 2002,Ham et al., 2004) suggest that, for the given conditions, longitudinal dispersion is of minor importance for mixing of biogeochemical reactants. In that case, besides plume geometry, transverse dispersivity α_t remains the crucial factor for Natural Attenuation.

For simple geometry – a quasi homogeneous subsurface with a uniform steady state flow field, and if mixing due to longitudinal dispersion is of minor importance, the reduction of the 2D model to a 1D problem was derived. This helps to reduce computation time in groundwater risk assessment.

To evaluate the ratio of mixing and reaction rate, a Damköhler number *Da* is defined. For *Da* > about 10, mixing rather than reaction kinetics are the limiting factors. In the field this can be attributed to readily biodegradable compounds and at sufficiently large scales, e.g. distances greater than dm and low or intermediate groundwater flow velocities.

The size of steady state plumes in the given base case scenario can be predicted by numerical modelling and depends on the reciprocal of transverse dispersivity (α_t^{-1}), the contaminated aquifer thickness in a squared relationship (M^2) and the reaction stoichiometry in a non-linear correlation, for the ratios expected in groundwater plumes considered here with an exponent of about 0.3. An empirical relationship to predict the plume size was provided. It should be noted that these plume sizes are minimum values that would be exceeded if other factors than mixing limit biotransformation processes. The example of the partly contaminated aquifer emphasises that further investigation for other scenarios are promising tasks.

The methodology developed was applied to the field site “Osterhofen” in south west Germany and contributed to prove applicability of

Natural Attenuation as remediation strategy for an already steady state ammonium plume *(Rügner et al., 2004)*. Calibration of the model to the field case resulted in a plume length of 570 m and a transverse vertical dispersivity α_t of 3.2 cm.

The dispersivities are crucial for groundwater risk assessment, because they determine the length of steady state groundwater plumes if biodegradation is limited by the supply rate of external electron acceptors or donors. This implies that, under such conditions, the rate of mixing will be the limiting factor for Natural Attenuation. Once the transverse dispersivity α_t, the reaction stoichiometry and aquifer geometry are known, the size of steady state plumes of easily biodegradable contaminants can be predicted. Scenario specific modelling, therefore, serves as an important tool to asses risks of groundwater pollution, classify contaminated sites and predict Natural Attenuation perspectives.

Transport and biodegradation of VOC in the unsaturated zone could be simulated realistically using a highly sophisticated numerical model for a field site with a well controlled aviation fuel spill of known extent and composition. Comparing simulated concentration from the numerical models to measured field data provided a good opportunity for validation of the model under complex field scale conditions. The fate of the contaminants in the unsaturated zone could be quantified and an estimation of groundwater vulnerability for the given scenario could be obtained.

The validation of the models also confirms the underlying assumptions of NAPL phase volatilisation (Raoult's law) and diffusion coefficient type empirical relationships according to Millington-Quirk. The assumptions of equilibrium mass partitioning (Henry's and Roult's law) were proven to be valid for transfer between gaseous, aqueous and NAPL phase. First order degradation kinetics were found to be a reasonable approximation for the biodegradation process of VOCs in the vadose zone. However, the biodegradation rate is, typically, a highly uncertain quantity even when experimental laboratory measurements are available.

Risk assessment for Værløse field site was approached by evaluation of the relevance of parameters by means of sensitivity analyses. Adjustment of biodegradation rate constants to fit measured soil gas concentration could provide a mass balance for the unsaturated zone. Underlying the determined vadose zone situation, groundwater contamination could be assessed by adjusting transverse vertical dispersivity to reproduce groundwater concentrations. Experience of modelling on the current subject confirms that there is an advantage of carrying out early sensitivity studies with smaller dimension to gain more detailed understanding about process and parameter sensitivity to base 3D modelling on.

Sensitivity analyses illustrate that the behaviour of VOC in the unsaturated zone depend mainly on distribution parameters such as Henry's Law constant of the fuel constituents, on the biological degradation rate constant, and to a lesser extent on soil water content and temperature. Gas phase diffusion was confirmed to be the major transport process in the vadose zone. Infiltration rate and groundwater recharge is of minor importance for volatile compounds with low aqueous solubility. The emission into groundwater is considered as a dispersive-diffusive process and can be determined once the processes in the unsaturated zone are quantified.

Careful evaluation of the environmental preconditions for the development of anaerobic zones showed that these are not likely to be expected for small, shallow kerosene spills. However, anaerobic environments can be expected for fine grained material and very wet conditions or very strong, extended sources, especially if they are close to or floating on the water table.

Biodegradation can enhance depletion of contaminant source zones (see also Broholm et al., 2003). Temporal changes in soil

temperature can affect VOC concentrations significantly and should be accounted for in modelling to reproduce field data. Temporal changes in infiltration was of minor influence on VOC behaviour but changed concentrations of the biodegradation product CO_2 remarkably. Regarding the fate of total contaminant mass released in the unsaturated zone, characteristic groups of the compounds involved could be identified and their behaviour and risk potential was evaluated. The mass balance shows that highly volatile organic contaminants predominantly degas to the atmosphere, water soluble compounds are mainly degraded and a smaller fraction is transported to groundwater. Unfortunately, however, even small percentages of contaminant mass reaching the water table can exceed the legal limit locally. Further on, as a requirement for risk assessment, it seems to be crucial to quantify the unsaturated zone mass balance before estimates of groundwater contamination can be met.

Mass transfer across the capillary fringe still remains a challenge for groundwater risk assessment. This can be explained by the inherently heterogeneous and under transient conditions highly dynamic and hysteretic spatial distribution of water flow and saturation, which produce very steep small scales concentration gradients if applied to contaminant transport. Therefore, further investigation, using modelling approaches with higher spatial resolution and minimised numerical dispersion as well as stochastic approaches to quantify mass transfer in the capillary fringe are deemed to be essential. Modelling of contaminant concentrations at the capillary fringe could as well be potentially improved by implementing gas phase advection induced by water table fluctuations.

Further enhancement of reproducibility of field data by modelling can be expected from implementation of microbial growth and population dynamics in biodegradation kinetics as a more realistic approach. Field scale model fitting to biodegradation parameters in the unsaturated zone, in combination with lab experiments, that way can serve to improve the estimation of the overall biodegradation rates for specific groups of compounds at contaminated sites. These overall rates have been shown to be one of the most relevant paramters for risk assessment.

As the final objective, results of the field investigation could be used for the validation of the model MIN3P, which will allow to quantify the risk of groundwater contamination for a variety of different scenarios in the future. General patterns of contaminant behaviour from a hydrocarbon source in the shallow unsaturated zone could be provided and contributed to the compilation of a compliance scheme (Grathwohl et al., 2003). Improvement of modelling tools and capabilities is supported by growing computational capacities and optimisation of software and can help to predict risks of environmental pollution and to assess the potential of Natural Attenuation. Therefore, numerical modelling, which is growing in capability and applicability, has become an indispensable tool for groundwater risk assessment.

Evaluation of the Damköhler numbers emphasises an important difference between unsaturated and saturated zone risk assessment. Whereas biodegradation rates were shown not to be the limiting factor for Natural Attenuation of aerobically degradable compounds in groundwater ($Da >> 1$), aerobic biodegradation rate constants are very sensitive in the unsaturated zone, ranging from compounds almost unaffected by degradation to total depletion for others, depending on the compound and site characteristics. Here, Damköhler numbers range from low to high values. This is caused by the rapid, overall dominating transport process of vapour phase diffusion in the vadose zone. Therefore, quantification of field scale biodegradation rates and kinetics appears to be crucial for unsaturated zone risk assessment.

7 References

Allison, J. D., Brown, D. S. and Novvo-Gradac, K. J. (1991). MINTEQA2/PRODEFA2, A geochemical assessment model for environmental systems: Version 3.0 User's Manual., Environmental research laboratory, U.S.Environmental Protection Agency.

Atkins, P.W. (1990). Physical Chemistry. Weinheim, VCH.

Bayer-Raich, M., Jarsjö, J., Liedl, R., Ptak, T. and Teutsch, G. (2004). "Average contaminant concentration and mass flow in aquifers from temporal pumping well data: Analytical framework." Water Resour. Res. submitted.

BBodSchV (1999). Federal Soil Protection and Contaminated Sites Ordinance. Bundesgesetzblatt. Part I**:** 1554- 1582.

Broholm, M.M., Christophersen, M., Maier, U., Stenby, E.H. and Kjeldsen, P. (2004). "Compositional evolution of the emplaced fuel source in the vadose zone field experiment at Airbase Værløse, Denmark." Environmental Science and Technology submitted.

CARACAS (1998). Risk Assessment for Contaminated Sites in Europe. Nottingham, European Commission**:** 170.

Carvalho, J.R.F. and Delgado, J.M.P.Q. (2000). "Lateral dispersion in liquid flow through packed beds at Pem < 1400." American Institute for Chemical Engineering 46(5): 1089-1095.

Christophersen, M., Broholm, M.M., Mosbæk, H., Karapanagioti, H. and Kjeldsen, P. (2003). "Emplaced fuel source experiment in the vadose zone at Airbase Værløse, Denmark. Site characterisation and hydrocarbon migration." J. Contam. Hydrol. submitted.

Cirpka, O. A. (2002). "Choice of dispersion coefficients in reactive transport calculations on smoothed fields." Journal of Contaminant Hydrology 58(3-4): 261-282.

Cirpka, O. A., Frind, E. O. and Helmig, R. (1999). "Numerical simulation of biodegradation controlled by transverse mixing." Journal of Contaminant Hydrology 40(2): 159-182.

Cirpka, O. A. and Kitanidis, P. K. (2000). "Characterization of mixing and dilution in heterogeneous aquifers by means of local temporal moments." Water Resources Research 36(5): 1221-1236.

Cirpka, O. A., Olsson, Å. H., Qiongsong, J., Rahman, M. A. and Grathwohl, P. (2004). "Length of Reactive Plumes Controlled by Transverse Dispersion." Environ. Sci. Technol. submitted.

Cirpka, O.A. (1997). Numerische Methoden zur Simulation des reaktiven Mehrkomponententransports im Grundwasser. Institut für Wasserbau. Stuttgart, Universität Stuttgart.

Cirpka, O.A. (2002). Dispersion, Dilution and Reactive Mixing in Heterogeneous Aquifers. Stanford.

Cirpka, O.A. (2003). "Choice of coefficients for dispersive mixing in heterogeneous formations." Geophysical Research Abstracts 5(01502).

Dagan, G. (1989). Flow and transport in porous formations. New York, Springer.

Dagan, G. (1990). "Transport in heterogeneous porous formations: spatial moments, ergodicity, and effective dispersion." Water Resour. Res. 26(6): 1281-1290.

Damköhler, G. (1936). "Einflüsse der Strömung, Diffusion und des Wärmeübergangs auf die Leistung von Reaktionsöfen." Zeitschrift Elektrochemie 42(12): 846-862.

De Josselin de Jong, G. (1958). "Longitudinal and transverse diffusion in granular deposits, Transactions." American Geophysical Union 39: 67-74.

Domenico, P.A. and Schwartz, F.W. (1998). Physical and Chemical Hydrogeology. New York, John Wiley & Sons.

Eberhardt, C. and Grathwohl, P. (2002). "Time scales of organic contaminant dissolution from complex source zones: coal tar pools vs. blobs." Journal of Contaminant Hydrology 59(1-2): 45-66.

Feeney, R., Schmidt, S.L, Strickholm, P., Chadam, J. and Ortoleva, P. (1983). "Periodic precipitation and coarsening waves: Applicaions of the competitive particle growth model." J. Chem. Phys. 78(3): 1293-1311.

Fick, A. (1855). "Über Diffusion." Annalen der Physik, Hg: Poggendroff 170: 59-86.

Frind, E. O. (1999). Groundwater Modelling (Numerical Methods). Lecture Note Earth 456/656. University of Waterloo, Ontario.

Frind, E. O., Molson, J. W., Schirmer, M. and Guiguer, N. (1999). "Dissolution and mass transfer of multiple organics under field conditions: The Borden emplaced source." Water Resources Research 35(3): 683-694.

Gaganis, P., Karapanagioti, H. K. and Burganos, V. N. (2002). "Modeling multicomponent NAPL transport in the unsaturated zone with the constituent averaging technique." Advances in Water Resources 25(7): 723-732.

Garabedian, S. P., LeBlanc, D. R., Gelhar, L. W., Celia, M. A. (1991). "Large Scale Natural Tracer Test in Sand and Gravel, Cape Cod, Massachusetts. - 2. Analysis of Spatial Moments for a nonreactive Tracer." Water Resources Research 27(5): 911 - 924.

Gelhar, L. W., Welty, C., Rehfeldt, K. R. (1992). "A Critical Review of Data on Field Scale Dispersion in Aquifers." Water Resource Research 28(7): 1955 - 1974.

Gnedenko, B.V and Kolmogorov, A.N. (1968). Limit distributions for sums of independent random variables. Reading, Massachusetts, Addison-Wesley.

Grathwohl, P. (1998). Diffusion in Natural Porous Media. Dordrecht, Netherlands, Kluwer Academic.

Grathwohl, P., Halm, D., Bonilla, A., Broholm, M., Burganos, V., Christophersen, M., Comanys, R., Gaganis, P., Gorostiza, I., Höhener, P., Kjeldsen, P. and Van der Sloot, H. (2003). Guideline for Groundwater Risk Assessment at COntaminated Sites (GRACOS). Tübingen, GRACOS-Consortium, funded by EU-Commission**:** 66.

Grathwohl, P., Klenk, .I.D., Eberhardt, C. and Maier, U. (2000). Steady State Plumes: Mechanisms of Transverse Mixing in Aquifers. Contaminated Site Remediation Conference: From Source Zones to Ecosystemes, Melbourne, Vic., CSRC, Melbourne.

Griebler, C. and Mösslacher, F. (2003). Grundwasserökologie. Weinheim und Basel, UTB.

Gustafson, J.B., Tell, J.G., Orem, D. (1997). Selection of Representative TPH Fractions Based on Fate and Transport Considerations. Total Petroleum Hydrocarbon Criteria Working Group Series, Vol. 3**:** 109.

Häfner, F., Sames, D. and Voigt, H:D. (1992). Wärme- und Stofftransport. Mathematische Methoden, Springer.

Ham, P., Schotting, R. and Prommer, H. (2004). "A reactive solute transport model for the determination of plume lengths." Journal of Contaminant Hydrology submitted.

Höhener, P. (2002). Bioavailability of hydrocarbons. U. M. Patras.

Höhener, P., Werner, D., Balsiger, C. and Pasteris, G. (2002). "Worldwide occurrence and fate of volatile fluorinated organic compounds in groundwater." Crit. Rev. Env. Sci. Technol accepted.

Hölting, B. (1992). Hydrogeologie. Stuttgart, Enke.

Hughes-Conant, B., Gillham, R.W., Mendoza, C.A. (1996). "Vapor transport of trichloroethylene in the unsaturated zone: Field and numerical modeling investigations." Water Resour. Res. 32(1): 9-22.

Jellali, S., Benremita, H., Muntzer, P., Razakarisoa, O. and Schafer, G. (2003). "A large-scale experiment on mass transfer of trichloroethylene from the unsaturated zone of a sandy aquifer to its interfaces." Journal of Contaminant Hydrology 60(1-2): 31-53.

Jennings, A.A. and Kirkner, D.J. (1984). "Instantaneous equilibrium approximation analysis." Journal of Hydraulic Engineering 110(12): 1700-1717.

Karapanagioti, H. K., Gaganis, P. and Burganos, V. N. (2003). "Modeling attenuation of volatile organic mixtures in the unsaturated zone: codes and usage." Environmental Modelling & Software 18(4): 329-337.

Kjeldsen, P., Christophersen, M., Broholm, M., Höhener, P., Aravena, R., Hunkeler, D. (2003). Biodegradation of fuel vapours in the vadose zone at Airbase Værløese, Denmark. Proceedings of the 2nd International workshop on Groundwater Risk Assessment at COntaminated Sites (GRACOS) and Integrated Soil and Water Protection (SOWA), Tübingen, TGA.

Klenk, I. D. and Grathwohl, P. (2002). "Transverse vertical dispersion in groundwater and the capillary fringe." Journal of Contaminant Hydrology 58(1-2): 111-128.
Koussis, A. D., Pesmajoglou, S. and Syriopoulou, D. (2003). "Modelling biodegradation of hydrocarbons in aquifers: when is the use of the instantaneous reaction approximation justified?" Journal of Contaminant Hydrology 60(3-4): 287-305.
Lahvis, M. A., Baehr, A. L. (1996). "Estimation of rates of aerobic hydrocarbon degradation by simulations of gas transport in the unsaturated zone." Water Resour. Res. 32(7): 2231-2249.
Lahvis, M.A., and Baehr, A.L., (1997). Documentation of R-UNSAT, a computer model for the simulation of reactive, multispecies transport in the unsaturated zone**:** 104.
LANGE, FRANK-MICHAEL (2002). Physical properties and estimation of van Genuchten parameters from soil samples of the Airbase Værløse/DK. Hohenheim.
LeBlanc, D.; Garabedian, S. P.; Hess, K. M., Gelhar, L. W.; Quadri, R. D.; Stollenwerk, K. G.; Wood, W. W. (1991). "Large Scale Natural Tracer Test in Sand and Gravel, Cape Cod, Massachusetts. - 1. Experimental Design and Observed Tracer Movement." Water Resources Research 27(5): 895 - 910.
Maier, U. (1998). Schadensherderkundung anhand von Bodenluftanomalien - Feldmessungen und numerische Modellierung. Diplomarbeit am Lehrstuhl für Angewandte Geologie. Tübingen, Universität Tübingen**:** 96.
Maier, U., Gaganis, P., Christophersen, M., Mayer, U. , Grathwohl, P. and Burganos, V.N. (2003). "Fate and transport modelling of fuel compounds in the vadose zone at the emplaced fuel source experiment, Airbase Værløse, Denmark." in preparation.
Marrin, K.L., Kerfoot, H.B. (1988). "Soil-gas surveying techniques, a new way to detect volatile organic contaminants in the subsurface." Environmental Sciene & Technology 22: 740-745.
Mayer, K.U. (1999). A multicomponent reactive transport model for variably saturated media. Department of Earth Sciences. Waterloo, Ontario, Canada, University of Waterloo.
Mayer, K.U., Frind, E. O. and Blowes, D.W. (2002). "Multicomponent reactive transport modeling in variably saturated porous media using a generalized formulation for kinetically controlled reactions." Water Resources Research 38(9): 1174-1195.
McCarthy, K.A. Johnson, R.L. (1993). "Transport of volatile organic compounds across the capillary fringe." Water Resource Research 29(6): 1675 - 1683.
Meckenstock, R. U. (2001). Microbial population dynamics and biodegradation rates. U. Maier. Tübingen.
Millington, R. J. (1959). "Gas diffusion in porous media." Science 130: 100-102.
Molson, J. W. (2000). Numerical Simulation of Hydrocarbon Fuel Dissolution and Biodegradation in Groundwater. Department of Earth Sciences. Waterloo, University of Waterloo.
Molson, J. W., Barker, J. F., Frind, E. O. and Schirmer, M. (2002). "Modeling the impact of ethanol on the persistence of benzene in gasoline-contaminated groundwater." Water Resources Research 38(1): art. no.-1003.
Molson, J. W., Frind, E. O., Van Stempvoort, D. R. and Lesage, S. (2002). "Humic acid enhanced remediation of an emplaced diesel source in groundwater. 2. Numerical model development and application." Journal of Contaminant Hydrology 54(3-4): 277-305.
Nielsen, P. and Perrochet, P. (2000). "Watertable dynamics under capillary fringes: experiments and modelling." Advances in Water Resources 23(5): 503-515.
Olsson, Å.H., Piepenbrink, M., Ptak, T. and Grathwohl, P. (2003). Determination of transverse dispersivities at lab scale: conservative transport and steady state reactive plumes. Proceedings of AGU fall meeting, San Fransisco.
Orientierungswerte, VwV (1993). Umwelt- und Verkehrministerium/ Sozialministerium Baden-Württemberg. AZ: 32-8984.00 (UM), 57-8490.1.40 (SM).
Ortoleva, P. (1994). Geochemical Self-Organisation, Oxford University Press.
Pasteris, G., Werner, D., Kaufmann, K. and Hohener, P. (2002). "Vapor phase transport and biodegradation of volatile fuel compounds in the unsaturated zone: A large scale lysimeter experiment." Environmental Science & Technology 36(1): 30-39.
Pasteris, G., Werner, D., Kaufmann, K. and Höhener, P. (2002). "Vapor phase transport and biodegradation of volatile fuel compounds in the unsaturated zone: a large scale lysimeter experiment." Environmental Science & Technology 36((1)): 30-39.

Prommer, H., Barry, D. A. and Davis, G. B. (2000). "Numerical modelling for design and evaluation of groundwater remediation schemes." Ecological Modelling 128(2-3): 181-195.
Prommer, H., Barry, D. A. and Davis, G. B. (2002). "Modelling of physical and reactive processes during biodegradation of a hydrocarbon plume under transient groundwater flow conditions." Journal of Contaminant Hydrology 59(1-2): 113-131.
Prommer, H., Barry, D. A. and Zheng, C. (2003). "MODFLOW/MT3DMS-based reactive multicomponent transport modeling." Ground Water 41(2): 247-257.
Prommer, H., Davis, GB, Barry, DA and Miller, CT. (2003). Modelling the fate of petroleum hydrocarbons in groundwater, in Health and Environmental Assessment of Site Contamination. Proceedings of the Fifth National Workshop on the Assessment of Site Contamination, Adelaide, Australian Environmental Protection and Heritage Council (EPHC) incorporating the National Environmental Protection Council (NEPC).
Reisinger, C. and Grathwohl, P. (1996). Formulierung einer Verfahrensempfehlung zur Bestimmung organischer Schadstoffe (LCKW, BTEX etc.) aus kontaminierten Böden. Tübingen, Lehrstuhl für Angewandte Geologie.
Reitsma, S., Dai, Q.L. (2001). "Reaction-enhanced mass transfer and transport from non-aqueous phase liquid source zones." JOURNAL OF CONTAMINANT HYDROLOGY 49: 49-66.
Rivett, M. O. (1995). "Soil-gas signatures from volatile chlorinated solvents: Borden Field Experiments." Ground Water 33(1): 84-98.
Rivett, M. O., Feenstra, S. and Cherry, J. A. (2001). "A controlled field experiment on groundwater contamination by a multicomponent DNAPL: creation of the emplaced-source and overview of dissolved plume development." Journal of Contaminant Hydrology 49(1-2): 111-149.
Rügner, H., Holder, T., Bayer-Raich, M., Maier, U. and Teutsch, G. (2004). "Natural Attenuation Referenzstandort "ehemalige Abfalldeponie Osterhofen": Quantifizierung des mikrobiologischen Abbaus von Ammonium." Grundwasser submitted.
Schachtschnabel, P., Blume, H.-P., Brümmer, G., Hartge, K.-H. and Schwertmann, U. (1992). Lehrbuch der Bodenkunde. Stuttgart, Enke.
Schiedek, T, Grathwohl, P., Teutsch, G. (1997). Literaturstudie zum natürlichen Rückhalt/ Abbau von Schadstoffen im Grundwasser. Im Auftrag der LfU Baden-Württemberg. Tübingen, Zentrum für Angewandte Geowissenschaften, Universität Tübingen**:** 53.
Schlender, M.H., Rowe, J. (1989). "Soil gas survey techniques for the investigation of underground storage tanks." Environmental Progress 8: 231-234.
Seagren, E. A., Rittmann, B. E. and Valocchi, A. J. (2002). "Bioenhancement of NAPL pool dissolution: experimental evaluation." Journal of Contaminant Hydrology 55(1-2): 57-85.
Steefel, C.I. (2000). "New directions in hydrogeochemical transport modelling: Incorporating multiple kinetic and equilibrium reaction pathways."
Susset, B. (1998). Quantifizierung des Stoffübergangs von leichtflüchtigen chlorierten Kohlenwasserstoffen (LCKW) im Kapillarsaum des Grundwassers. Geological Institute. Tübingen, University of Tübingen.
Trefry, M.G., Ruan, F.P. and McLaughlin, D. (2003). "Numerical Simulations of pre-asymptotic transport in heterogeneous porous media: Departures from the Gaussian limit." Water Resour. Res. revised.
Truesdale, G.A., Downing, A.L., Lowden, G.F. (1955). "The solubility of oxygen in pure water and the sea water." J. Appl. Chem. 5: 53-62.
Valocchi, A. J., Baveye, P., Clement, P. and Engesgaard, P. (2000). Transport and Biodegradation in Heterogeneous Groundwater Aquifers. DCAMM Ph.D. course. Lyngby, Denmark**:** 120.
Valsaraj, K. T. (1995). Elements of Environmental Engineering - Thermodynamics and Kinetics. Boca Raton, CRC Press.
Wang, G., Brederode F. Reckhorn, S., Grathwohl, P. (2003). "Volatile organic compounds volatilisation from multicomponent organic liquids and diffusion in unsaturated porous media." Vadose Zone Journal 2: 692-701.
Werner, D. (2002). Gaseous tracer diffusion from a point source as a site investigation method. Facultée Environnement Naturel, Architectural et Construit. Lausanne, École Polytechnique Fédérale de Lausanne**:** 98.

Werner, D., Höhener, P. (2002). The influence of water table fluctuations on the volatilisation of contaminants from groundwater. Groundwater Quality: Natural and enhanced restoration of groundwater polltuion, Sheffield, IAHS Publ. 275.

Wiedemeier, T.H., Rifai, H.S., Newell, C.J. and Wilson, J.T. (1999). Natural Attenuation of Fuels and Chlorinated Solvents in the Subsurface. New York, John Wiley and Sons.

Yang, Y, , McCarty, P.L. (2000). "Biologically Enhanced Dissolution of Tetrachloroethene DNAPL." ENVIRONMENTAL SCIENCE & TECHNOLOGY 34: 2979-2984.

In der Reihe C Hydro-, Ingenieur- und Umweltgeologie der Tübinger Geowissenschaftlichen Arbeiten (TGA) sind bisher erschienen:

Nr. 1: Grathwohl, Peter (1989): Verteilung unpolarer organischer Verbindungen in der wasserungesättigten Bodenzone am Beispiel der leichtflüchtigen aliphatischen Chlorkohlenwasserstoffe. 102 S.

Nr. 2: Eisele, Gerhard (1989): Labor- und Felduntersuchungen zur Ausbreitung und Verteilung leichtflüchtiger chlorierter Kohlenwasserstoffe (LCKW) im Übergangsbereich wasserungesättigte/wassergesättigte Zone. 84 S.

Nr. 3: Ehmann, Michael (1989): Auswirkungen atmogener Stoffeinträge auf Boden- und Grundwässer sowie Stoffbilanzierungen in drei bewaldeten Einzugsgebieten im Oberen Buntsandstein (Nordschwarzwald). 134 S.

Nr. 4: Irouschek, Thomas (1990): Hydrogeologie und Stoffumsatz im Buntsandstein des Nordschwarzwaldes. 144 S.

Nr. 5: Sanns, Matthias (1990): Experimentelle Untersuchungen zum Ausbreitungsverhalten von leichtflüchtigen Chlorkohlenwasserstoffen (LCKW) in der wassergesättigten Zone. 122 S. **(Vergriffen!)**

Nr. 6: Seeger, Thomas (1990): Abfluß- und Stofffrachtseparation im Buntsandstein des Nordschwarzwaldes. 154 S.

Nr. 7: Einsele, Gerhard & Pfeffer, Karl-Heinz (Hrsg.) (1990): Untersuchungen über die Auswirkungen des Reaktorunfalls von Tschernobyl auf Böden, Klärschlamm und Sickerwasser im Raum von Oberschwaben und Tübingen. 151 S.

Nr. 8: Douveas, Nikon G. (1990): Verwitterungstiefe und Untergrundabdichtung beim Talsperrenbau in dem verkarsteten Nord-Pindos-Flysch (Projekt Pigai-Aoos, NW-Griechenland). 165 S.

Nr. 9: Schlöser, Heike (1991): Quantifizierung der Silikatverwitterung in karbonatfreien Deckschichten des Mittleren Buntsandsteins im Nordschwarzwald. 93 S.

Nr. 10: Köhler, Wulf-Rainer (1992): Beschaffenheit ausgewählter, nicht direkt anthropogen beeinflußter oberflächennaher und tiefer Grundwasservorkommen in Baden-Württemberg. 144 S.

Nr. 11: Bundschuh, Jochen (1991): Der Aquifer als thermodynamisch offenes System. – Untersuchungen zum Wärmetransport in oberflächennahen Grundwasserleitern unter besonderer Berücksichtigung von Quellwassertemperaturen (Modellversuche und Geländebeispiele). 100 S. **(Vergriffen!)**

Nr. 12: Herbert, Mike (1992): Sorptions- und Desorptionsverhalten von ausgewählten polyzyklischen aromatischen Kohlenwasserstoffen (PAK) im Grundwasserbereich. 111 S.

Nr. 13: Sauter, Martin (1993): Quantification and forecasting of regional groundwater flow and transport in a karst aquifer (Gallusquelle, Malm, SW-Germany. 150 S.

Nr. 14: Bauer, Michael (1993): Wasserhaushalt, aktueller und holozäner Lösungsabtrag im Wutachgebiet (Südschwarzwald). 130 S.

Nr. 15: Einsele, Gerhard & Ricken, Werner (Hrsg.) (1993): Eintiefungsgeschichte und Stoffaustrag im Wutachgebiet (SW-Deutschland). 215 S.

Nr. 16: Jordan, Ulrich (1993): Die holozänen Massenverlagerungen des Wutachgebietes (Südschwarzwald). 132 S. **(Vergriffen!)**

Nr. 17: Krejci, Dieter (1994): Grundwasserchemismus im Umfeld der Sonderabfalldeponie Billigheim und Strategie zur Erkennung eines Deponiesickerwassereinflusses. 121 S.

Nr. 18: Hekel, Uwe (1994): Hydrogeologische Erkundung toniger Festgesteine am Beispiel des Opalinustons (Unteres Aalenium). 170 S. **(Vergriffen!)**

Nr. 19: Schüth, Christoph (1994): Sorptionskinetik und Transportverhalten von polyzyklischen aromatischen Kohlenwasserstoffen (PAK) im Grundwasser - Laborversuche. 80 S.

Nr. 20: Schlöser, Helmut (1994): Lösungsgleichgewichte im Mineralwasser des überdeckten Muschelkalks in Mittel-Württemberg. 76 S.

Nr. 21: Pyka, Wilhelm (1994): Freisetzung von Teerinhaltsstoffen aus residualer Teerphase in das Grundwasser: Laboruntersuchungen zur Lösungsrate und Lösungsvermittlung. 76 S.

Nr. 22: Biehler, Daniel (1995): Kluftgrundwässer im kristallinen Grundgebirge des Schwarzwaldes – Ergebnisse von Untersuchungen in Stollen. 103 S.

Nr. 23: Schmid, Thomas (1995): Wasserhaushalt und Stoffumsatz in Grünlandgebieten im württembergischen Allgäu. 145+ 92 S.

Nr. 24: Kretzschmar, Thomas (1995): Hydrochemische, petrographische und thermodynamische Untersuchungen zur Genese tiefer Buntsandsteinwässer in Baden-Württemberg. 142 S. **(Vergriffen!)**

Nr. 25: Hebestreit, Christoph (1995): Zur jungpleistozänen und holozänen Entwicklung der Wutach (SW-Deutschland). 88 S.

Nr. 26: Hinderer, Matthias (1995): Simulation langfristiger Trends der Boden- und Grundwasserversauerung im Buntsandstein-Schwarzwald auf der Grundlage langjähriger Stoffbilanzen. 175 S.

Nr. 27: Körner, Johannes (1996): Abflußbildung, Interflow und Stoffbilanz im Schönbuch Waldgebiet. 206 S.

Nr. 28: Gewald, Thomas (1996): Der Einfluß der Desorptionskinetik bei der Freisetzung von Trichlorethen (TCE) aus verschiedenen Aquifersanden. 67 S.

Nr. 29: Schanz, Ulrich (1996): Geophysikalische Untersuchungen im Nahbereich eines Karstsystems (westliche Schwäbische Alb). 114 S.

Nr. 30: Renner, Sven (1996): Wärmetransport in Einzelklüften und Kluftaquiferen – Untersuchungen und Modellrechnungen am Beispiel eines Karstaquifers. 89 S.

Nr. 31: Mohrlok, Ulf (1996): Parameter-Identifikation in Doppel-Kontinuum-Modellen am Beispiel von Karstaquiferen. 125 S.

Nr. 32: Merkel, Peter (1996): Desorption and Release of Polycyclic Aromatic Hydrocarbons (PAHs) from Contaminated Aquifer Materials. 76 S.

Nr. 33: Schiedek, Thomas (1996): Auftreten und Verhalten von ausgewählten Phthalaten in Wasser und Boden. 112 S.

Nr. 34: Herbert, Mike & Teutsch, Georg (Hrsg.) (1997): Aquifersysteme Südwestdeutschlands - Eine Vorlesungsreihe an der Eberhard-Karls-Universität Tübingen. 162 S.

Nr. 35: Schad, Hermann (1997): Variability of Hydraulic Parameters in Non-Uniform Porous Media: Experiments and Stochastic Modelling at Different Scales. 233 S.

Nr. 36: Herbert, Mike & Kovar, Karel (Eds.) (1998): GROUNDWATER QUALITY 1998: Remediation and Protection - Posters -.- Proceedings of the GQ'98 conference, Tübingen, Sept. 21-25, 1998, Poster Papers. 146 S.

Nr. 37: Klein, Rainer (1998): Mechanische Bodenbearbeitungsverfahren zur Verbesserung der Sanierungseffizienz bei In-situ-Maßnahmen. 106 S.

Nr. 38: Schollenberger, Uli (1998): Beschaffenheit und Dynamik des Kiesgrundwassers im Neckartal bei Tübingen. 74 S.

Nr. 39: Rügner, Hermann (1998): Einfluß der Aquiferlithologie des Neckartals auf die Sorption und Sorptionskinetik organischer Schadstoffe. 78 S.

Nr. 40: Fechner, Thomas (1998): Seismische Tomographie zur Beschreibung heterogener Grundwasserleiter. 113 S.

Nr. 41: Kleineidam, Sybille (1998): Der Einfluß von Sedimentologie und Sedimentpetrographie auf den Transport gelöster organischer Schadstoffe im Grundwasser. 82 S.

Nr. 42: Hückinghaus, Dirk (1998): Simulation der Aquifergenese und des Wärmetransports in Karstaquiferen. 124 S.

Nr. 43: Klingbeil, Ralf (1998): Outcrop Analogue Studies – Implications for Groundwater Flow and Contaminant Transport in Heterogeneous Glaciofluvial Quaternary Deposits. 111 S.

Nr. 44: Loyek, Diana (1998): Die Löslichkeit und Lösungskinetik von polyzyklischen aromatischen Kohlenwasserstoffen (PAK) aus der Teerphase. 81 S.

Nr. 45: Weiß, Hansjörg (1998): Säulenversuche zur Gefahrenbeurteilung für das Grundwasser an PAK-kontaminierten Standorten. 111 S.

Nr. 46: Jianping Yan (1998): Numerical Modeling of Topographically-closed Lakes: Impact of Climate on Lake Level, Hydrochemistry and Chemical Sedimentation. 144 S.

Nr. 47: Finkel, Michael (1999): Quantitative Beschreibung des Transports von polyzyklischen aromatischen Kohlenwasserstoffen (PAK) und Tensiden in porösen Medien. 98 S.

Nr. 48: Jaritz, Renate (1999): Quantifizierung der Heterogenität einer Sandsteinmatrix (Mittlerer Keuper, Württemberg). 106 S.

Nr. 49: Danzer, Jörg (1999): Surfactant Transport and Coupled Transport of Polycyclic Aromatic Hydrocarbons (PAHs) and Surfactants in Natural Aquifer Material - Laboratory Experiments. 75 S.

Nr. 50: Dietrich, Peter (1999): Konzeption und Auswertung gleichstromgeoelektrischer Tracerversuche unter Verwendung von Sensitivitätskoeffizienten. 130 S.

Nr. 51: Baraka-Lokmane, Salima (1999): Determination of Hydraulic Conductivities from Discrete Geometrical Characterisation of Fractured Sandstone Cores. 119 S.

Nr. 52: M^{c}Dermott, Christopher I. (1999): New Experimental and Modelling Techniques to Investigate the Fractured System. 170 S.

Nr. 53: Zamfirescu, Daniela (2000): Release and Fate of Specific Organic Contaminants at a Former Gasworks Site. 96 S.

Nr. 54: Herfort, Martin (2000): Reactive Transport of Organic Compounds Within a Heterogeneous Porous Aquifer. 76 S.

Nr. 55: Klenk, Ingo (2000): Transport of Volatile Organic Compounds (VOC's) From Soilgas to Groundwater. 70 S.

Nr. 56: Martin, Holger (2000): Entwicklung von Passivsammlern zum zeitlich integrierenden Depositions- und Grundwassermonitoring: Adsorberkartuschen und Keramikdosimeter. 84 S.

Nr. 57: Diallo, Mamadou Sanou (2000): Acoustic Waves Attenuation and Velocity Dispersion in Fluid-Filled Porous Media: Theoretical and Experimental Investigations. 101 S.

Nr. 58: Lörcher, Gerhard (2000): Verarbeitung und Auswertung hyperspektraler Fernerkundungsdaten für die Charakterisierung hydrothermaler Systeme (Goldfield/Cuprite, Yellowstone National Park). 158 S.

Nr. 59: Heinz, Jürgen (2001): Sedimentary Geology of Glacial and Periglacial Gravel Bodies (SW-Germany): Dynamic Stratigraphy and Aquifer Sedimentology. 102 S.

Nr. 60: Birk, Steffen (2002): Characterisation of Karst Systems by Simulating Aquifer Genesis and Spring Responses: Model Development and Application to Gypsum Karst. 122 S.

Nr. 61: Halm, Dietrich & Grathwohl, Peter (Eds.) (2002): Proceedings of the 1st International Workshop on Groundwater Risk Assessment at Contaminated Sites (GRACOS). 280 S.

Nr. 62: Bauer, Sebastian (2002): Simulation of the genesis of karst aquifers in carbonate rocks. 143 S.

Nr. 63: Rahman, Mokhlesur (2002): Sorption and Transport Behaviour of Hydrophobic Organic Compounds in Soils and Sediments of Bangladesh and their Impact on Groundwater Pollution – Laboratory Investigations and Model Simulations. 73 S.

Nr. 64: Peter, Anita (2002): Assessing natural attenuation at field scale by stochastic reactive transport modelling. 101 S.

Nr. 65: Leven-Pfister, Carsten (2002): Effects of Heterogeneous Parameter Distributions on Hydraulic Tests - Analysis and Assessment. 94 S.

Nr. 66: Schwarz, Rainer (2002): Grundwasser-Gefährdungsabschätzungen durch Emissions- und Immissionsmessungen an Deponien und Altlasten. 100 S.

Nr. 67: Abel, Thekla (2003): Untersuchungen zur Genese des Malmkarsts der Mittleren Schwäbischen Alb im Quartär und jüngeren Tertiär. 187 S.

Nr. 68: Prokop, Gundula & Bittens, Martin & Cofalka, Piotr & Roehl, Karl Ernst & Schamann, Martin & Younger, Paul (Eds.) (2003): Summary Report on the 1st IMAGE-TRAIN Advanced Study Course “Innovative Groundwater Management Technologies”. 119 S.

Nr. 69: Halm, Dietrich & Grathwohl, Peter (Eds.) (2003): Proceedings of the 2nd International Workshop on Groundwater Risk Assessment at Contaminated Sites (GRACOS) and Integrated Soil and Water Protection (SOWA). 260 S.

Nr. 70: Bayer, Peter (2004): Modelling, economic assessment and optimisation of in-situ groundwater remediation systems. 78 S.

Nr. 71: Kraft, Siegfried (2004): Untersuchungen zum Langzeiteinsatz der in-situ Aktivkohlefiltration zur Entfernung von organischen Schadstoffen aus Grundwasser. 64 S.

Nr. 72: Bold, Steffen (2004): Process-based prediction of the long-term risk of groundwater pollution by organic non-volatile contaminants. 76 S.

Nr. 73: Maier, Ulrich (2004): Modelling of Natural Attenuation in Soil and Groundwater. 81 S.

Nr. 74: Susset, Bernd (2004): Materialuntersuchungen und Modellierungen zur Unterscheidung Gleichgewicht / Ungleichgewicht in Säulenversuchen für die Sickerwasserprognose organischer Schadstoffe. 100 S. **– Im Druck.**

Nr. 75: Madlener, Iris (2004): Quantifizierung und Modellierung des PAK-Desorptionsverhaltens aus feinkörnigem Material mittels Säulenversuchen (DIN V 19736) und Hochdruck-Temperatur-Elution (ASE) – **Im Druck.**

Nr. 76: Henzler, Rainer (2004): Quantifizierung und Modellierung der PAK-Elution aus verfestigten und unverfestigten Abfallmaterialien **– Im Druck.**

Nr. 77: Valley, Stephan (2004): **– Im Druck.**

Nr. 78: Röttgen, Klaus Peter (2004): Kritische Analyse des Aufwandes zur Erkundung von Kontaminationen in niedersächsischen Grundwassergeringleitern.

Nr. 79: Gocht, Tilman (2004): Die vier Griechischen Elemente: Massenbilanzierung von polyzyklischen aromatischen Kohlenwasserstoffen (PAK) in Kleineinzugsgebieten des ländlichen Raumes. **– Im Druck.**

Nr. 80: Halm, Dietrich & Grathwohl, Peter (Eds.) (2004): Proceedings of the 2nd International Workshop on Integrated Soil and Water Protection (SOWA). 161 S.

Nr. 81: Prokop, Gundula, Bittens, Martin, Moraczewska-Maikut, Katarzyna, Roehl, Karl Ernst, Schamann, Martin & Younger, Paul (Eds.) (2004): Summary Report on the 3rd IMAGE-TRAIN Advanced Study Course "Quantitative Risk Assessment". 66 S.

Nr. 82: Hoffmann, Ruth (2004): Optimierungsansätze zur Datenerfassung und Interpretation von Multielektrodenmessungen**– Im Druck.**

Nr. 83: Kostic, Boris (2004): **– Im Druck.**

Nr. 84: Bayer-Raich, Marti (2004): **– Im Druck.**

Nr. 85: Piepenbrink, Matthias (2004): **– Im Druck.**